First Observation of a 5^- Resonance in ^{12}C; Evidence for Triangular $\mathcal{D}_{3h}$ Symmetry

by

Daniel José Marín Lámbarri

A thesis submitted to
The University of Birmingham
for the degree of
DOCTOR OF PHILOSOPHY

Nuclear Physics Group
School of Physics and Astronomy
College of Engineering and Physical Sciences
The University of Birmingham

February 12, 2015

Abstract

This thesis reports a measurement of the break-up reaction ^{12}C(^{4}He, ^{12}C*)^{4}He performed at the Birmingham MC40 cyclotron facility at a beam energy of 40 MeV. An array of four double-sided silicon-strip detectors was used to detect the final-state products of the reaction. Results from previous measurements of this reaction have shown that various excited states in ^{12}C can be populated. In the present study the 13.3 MeV and the 22.4 MeV resonances were, in particular, populated. The latter has been seen for the first time. The analysis for both resonances was performed using the angular correlations technique from which their spin and parity were determined with values of J^{π}=4^{+} and J^{π}=5^{-}, respectively. Monte-Carlo simulations were performed both before and after the experiment in order to have the optimal detector-array efficiency and normalise the results of the angular correlations analysis. The results have been compared to predictions of the algebraic cluster model, for which the J^{π}=4^{+} is thought to be related to a rotational band based on the Hoyle state and the J^{π}=5^{-} resonance is part of the ground-state band. This latter state provides strong evidence for triangular $\mathcal{D}_{3h}$ symmetry corresponding to an equilateral triangle structure, observed here for the first time in a nucleus.

To Araceli, my mother.

ACKNOWLEDGEMENTS

As with other cycles I have been through in this life, many people have been involved and crossed my path. With out them, my PhD cycle would have been different and I am completely grateful, without any regrets, for this amazing experience.

Firstly, I would like to thank my supervisor Martin Freer, the first person I contacted in the UK and the first who said "yes, you can come and do a PhD in my group". Thank you for your support along all these years, for sharing your knowledge and for your infinite patience.

I want to thank my supervisors (yes, I had three) Tzany Kokalova and Carl Wheldon, for helping me in many different aspects, not only the academic side, also for their support I have received in those cloudy moments.

I also want to thank Neil Curtis, who probably is more than happy I have left the office, so he does not have to explain Pssketch or Resolution8 every morning before the first tea.

Thank you very much all you guys from 319 and 320 (I always was confused in which one my desk was), Tanya, Joe, Sam, Robin, Jack, Mat, Jon as well as the "others" from the cold atoms group, Lyndsie, Andy, Rob, Jon and Kit (who disappeared the last half year). Also thank you all from the 3rd floor, Peter, Nick, Paul, Lee, Garry and the other nuclear guys I have only met at Staff House, Tom and Dave.

Thank you Dave and Dom, the first British friends ever. I am very grateful for your friendship (and the Newcastle Browns).

I would like to thank my family, my aunt and uncle Manola and José as well as my cousins Chris and Joxe for all the stability they have brought. Massive thanks to my “compadres“ César and Fily.

A big thanks to my siblings, Jaz, Daniela, Daniel, Erika and my father Daniel.

And last but not least, I would like to thank my three women, Araceli, Bibiana and Penélope. The first, my mother, who has given me the support and the love needed to grow as a human being and finish this cycle. The second, my grandma, who has taught me the most important values in my life (and for playing baseball with me when I was a kid) and the third, my love, my star, the light who has guided me the last twelve years (made out of carbon-12 also).

I am also grateful to CONACyT for funding my PhD.

CONTENTS

LIST OF FIGURES

LIST OF TABLES

CHAPTER 1

INTRODUCTION

1.1 The Nucleus

The nucleus is the central component of an atom and is composed of nucleons (Z protons and N neutrons), in which Z also defines the atomic number and is equal to the number of electrons in the neutral atom. The dimensions of nuclei are of the order of femtometres (10^{-15} m). Both protons and neutrons are fermions with intrinsic spin, s = $1/2$ which follow the Pauli Exclusion Principle, which means that only two protons or neutrons can occupy the same quantum state, one nucleon with spin projection $+1/2$ and the other with $-1/2$, often referred to spin up ($\uparrow$) and spin down ($\downarrow$) respectively. While neutrons have no electric charge, protons are positive charged particles with charge e ($= 1.6022 \times 10^{-19}$C) which is equal and opposite to the electron charge [13]. A general expression for a particular nucleus can be written as ${}^{A}_{Z}Z_N$, in which A is the mass number (*i.e* the total number of nucleons $= N + Z$) and Z defines the specific element. Nuclei can be classified in to three different series. Those nuclei which have the same Z number but different neutron number N are called *isotopes* and share the same chemical properties. *Isotones* are those which have an identical number of neutrons N but different number of protons Z and *isobars* are those with the same mass number A.

Neutrons and protons as well as protons and protons and neutrons and neutrons interact with each other within the nucleus through the attractive nuclear force (though which is repulsive at very short-range, < 0.5 fm) and protons with protons via the repulsive electromagnetic force. This gives rise to binding energy; the energy difference between a nucleus and its individual constituents. In general the binding energy of nuclei increases as the atomic number A increases. This is shown in Fig. 1.1 for light nuclei, expressed in the form of binding energy per nucleon. It is also important to comment on the presence of peaks, which appear below $A = 30$, corresponding to ^{4}He, ^{8}Be, ^{12}C, ^{16}O, ^{20}Ne, ^{24}Mg nuclei. These are multiples of $A = 4$, which corresponds to an α-particle (^{4}He nucleus); α-particles are highly stable due to the complete filling of the first quantum state for both protons and neutrons; a fact that is remarkably important for nucleon-nucleon correlations.

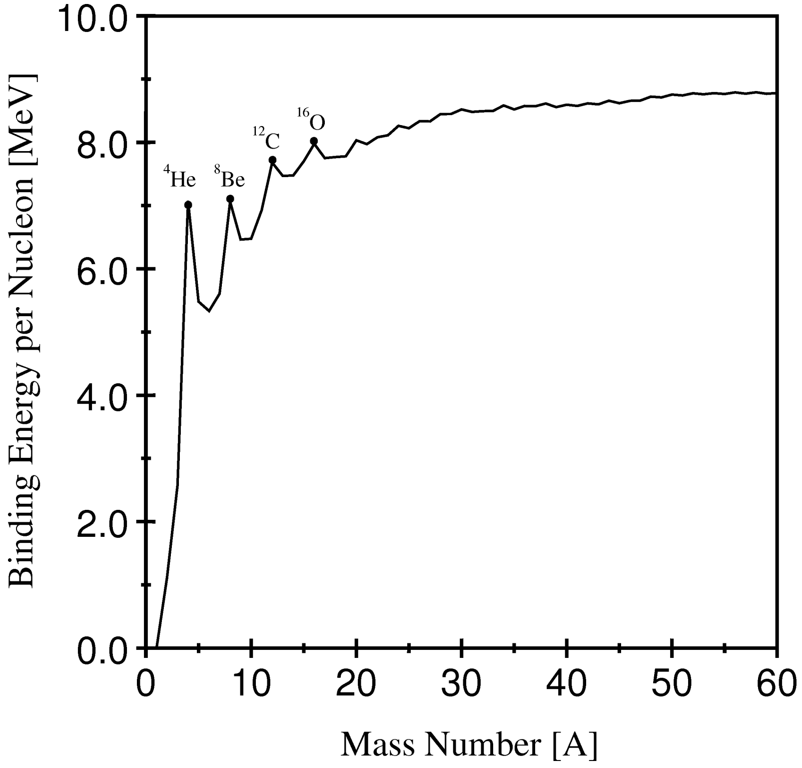

Figure 1.1: *Binding energy per nucleon versus the mass number for the most stable nuclei for a given A.*

Different configurations of the components of a nucleus gives rise to characteristic quantum energy levels. Each nucleus has its own energy-level spectrum in which each state is described by its total angular momentum quantum number (which is associated with the vector sum of the total angular momenta of all the nucleon components). For those nuclei with even numbers of neutrons and protons the total spin is zero due to the occupation of time-reversed orbits by equal numbers of identical nucleons as this results in the maximal overlap since for heavy nuclei, isotopes with more neutrons have increased stable due to the Coulomb repulsion from a large number of protons. Nuclei which are in an excited state decay towards stability which can proceed by different processes such as γ- and β-decays, or by the emission of light particles, such as neutrons, protons or α-particles. An example of the latter is the Hoyle state, which is the second excited state of ^{12}C lying 7.654 MeV above the ground state. This resonance decays most of the time through the emission of an α-particle leaving a residual nucleus of ^{8}Be, but occasionally it decays via γ-emission. This process of γ-decay is very important for nucleosynthesis and, therefore, for the formation of heavier elements in stars. This aspect is explained further in the following section.

1.2 Motivation

1.2.1 Nucleosynthesis in Stars; the Triple Alpha-Process

Stars are to first order massive spheres of plasma, which act as the cauldrons in our universe, and are formed by the coalescence of cosmic matter by the force of gravity. Particles start to get closer and closer and the temperature of the system increases and, therefore, the pressure increases, giving rise to a wide range of particle energies, characterised by Maxwell-Boltzman distributions. Charged particle reactions are the first to happen, especially those triggered by protons and helium nuclei and known as the proton-proton chain. This hydrogen burning process releases 26 MeV and comprises these reactions:

The proton-proton I branch:

- $\mathrm{p} + \mathrm{p} \rightarrow \mathrm{p} + \mathrm{n} + \mathrm{e}^{+} + \nu \rightarrow \mathrm{d} + \mathrm{e}^{+} + \nu_e$
- $\mathrm{d} + \mathrm{p} \rightarrow {}^{3}\mathrm{He} + \gamma$
- ${}^{3}\mathrm{He} + {}^{3}\mathrm{He} \rightarrow {}^{4}\mathrm{He} + 2\mathrm{p}$

The proton-proton II branch:

- ${}^{3}\mathrm{He} + {}^{4}\mathrm{He} \rightarrow {}^{7}\mathrm{Be} + \gamma$
- ${}^{7}\mathrm{Be} + \mathrm{e}^{-} \rightarrow {}^{7}\mathrm{Li} + \nu_e$
- ${}^{7}\mathrm{Li} + {}^{1}\mathrm{H} \rightarrow 2{}^{4}\mathrm{He}$

The proton-proton III branch:

- ${}^{7}\mathrm{Be} + {}^{1}\mathrm{H} \rightarrow {}^{8}\mathrm{B} + \gamma$
- ${}^{8}\mathrm{B} \rightarrow {}^{8}\mathrm{Be} + \mathrm{e}^{+} + \nu_e$
- ${}^{8}\mathrm{Be} \rightarrow 2{}^{4}\mathrm{He}$

Once the proton-proton chain has consumed the available fuel, the gravitational force will once again dominate, making the star collapse and raising the temperature until the point at which ^{4}He nuclei can fuse together, forming ^{8}Be nuclei, which requires 92 keV from the environment; these processes are present along the red giant stars phase. Öpik pointed out that high temperatures were possible in stars, particularly in the red giant phase [14]. Beryllium-8 is unstable in its ground state and has a very short lifetime of approximately 10^{-16} s, decaying back into two α-particles. This produces an equilibrium between the $\alpha + \alpha$ and ^{8}Be,

$$\alpha + \alpha \rightleftharpoons {}^{8}\text{Be} \tag{1.1}$$

which means that the latter is in an equilibrated concentration which is temperature dependent. In red giants this concentration is enough to permit a third α-particle to be captured as shown in Fig. 1.2.

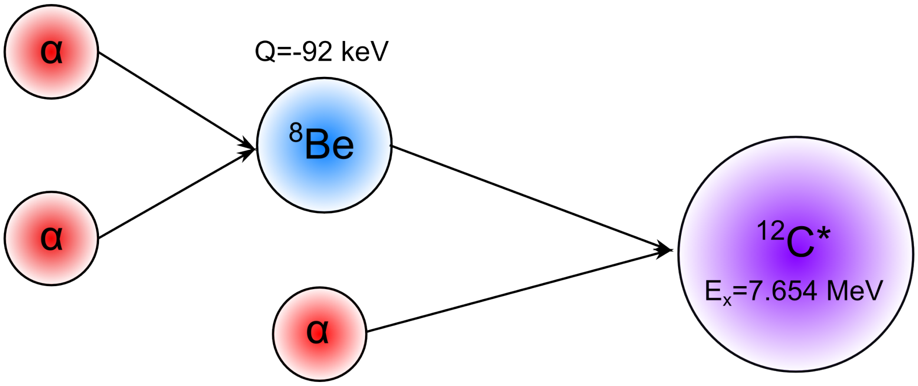

Figure 1.2: *Triple α-process in which ^{12}C is formed during the nucleosynthesis in stars. Firstly two α-particles fuse together to form a nucleus of ^{8}Be, subsequently a third α-particle is captured.*

1.2.2 Hoyle State

Sixty one years ago, in 1953, Fred Hoyle pointed out that the rate of these reactions is not enough to explain the amount of ^{12}C in the universe [15], so he proposed the existence of a specific resonance which increased the ^{8}Be + ^{4}He reaction cross section. It was at Kellogg Laboratory where a group measured the ^{14}N(d,α)^{12}C reaction using a high resolution spectrometer and found a resonance at 7.68 MeV [16]. W.A. Fowler and colleagues made a measurement of an exited state (0^+ state) in ^{12}C at 7.65 MeV, just above the triple-α threshold ($S_{3\alpha}$=7.274 MeV), which subsequently decays into three α-particles [17].

After this resonance is populated during the triple α-process, it decays predominantly into an α-particle and a ^{8}Be nucleus (with a branching ratio $\approx$ 100%), but a small amount (0.04%)

decays through γ-emission, to the first excited state in ^{12}C at 4.438 MeV. A competing process is pair production directly to the ground-state with a branching ratio of ${}^{\mathit{\Gamma}_{\pi}}\!/\mathit{\Gamma}$=6.7(6)$\times$10^{-6} [18]. When taken together with the destruction of ^{12}C, *e.g.* through photo-dissociation, these internal decays account for the abundance of ^{12}C in our universe, as well as heavier nuclei, formed through further reactions. The abundance in the universe of ^{16}O and ^{12}C is therefore a delicate balance between reaction rates and quantum states with precisely the right energy. Although the main decay process undergone by the Hoyle state is through the α+^{8}Be decay process, there is continued interest in the direct 3α-decay process which has a recently reported upper limit for the branching ration of $\sim$5$\times$10^{-3} [19, 20].

Despite the Hoyle state being discovered over 60 years ago, its precise structure has still not been determined. It is known to be composed of three α-particles, but the arrangement remains unclear. *Ab initio* calculations suggest the Hoyle state has a bent-arm configuration [21,22], in which the three α-particles are located at the vertices of an open triangle. Whereas other predictions suggest a Bose-Einstein Condensate [23, 24].

This resonance is of great importance, not only because it is the catalyst for creating the main elements for organic life, but also because it is a key step in the synthesis of the heavier elements. The present thesis is motivated by the idea to measure and characterise an excited state in ^{12}C at an energy of 13.3 MeV which had previously been observed by members of the Charissa collaboration. The earlier results did not provide conclusive measurements of the spin of this resonance [25, 26], but it is a candidate member of the Hoyle-state band. By characterising this resonance it will be possible to increase the information about the nature of the structure of the Hoyle state, and, ergo, how it rotates or vibrates. Recent measurements show the existence of a 2^{+} resonance at 9.8 MeV, which could be a collective rotational or vibrational excitation of the Hoyle state [27, 28], as well as the measurement of a resonance at 13.3 MeV, which has been suggested as the continuation of these collective excitations [25].

Nowadays, there are a wide range of models which explain some of the characteristics of the structure of the ^{12}C nucleus. However, despite their success in explaining some features, few of them can predict the existence of the Hoyle state at 7.654 MeV and its higher lying excitations.

The measurement and investigation of the ^{12}C(^{4}He, ^{12}C*)^{4}He reaction is presented in this thesis. By making precise measurements of the properties of excited states on ^{12}C, ultimately, the models may be refined and our understanding increased. The results and interpretation of such a measurement are presented in the subsequent chapters of this thesis.

CHAPTER 2

NUCLEAR STRUCTURE AND MODELS

2.1 Nuclear Clustering

It is remarkable that at different scales, nature always tends to congregate, probably because it tends to lead to a more stable state of equilibrium. It is possible to observe this sort of behaviour in galaxies, stars, solar systems and molecules. Therefore, it is not surprising to observe the existence of sub units (clusters) in nuclear structure. An easy way to picture the structure of an average nucleus is by means of its components, the nucleons (neutrons and protons), distributed within the nucleus in a homogeneous arrangement. However, the structure of light nuclei, since the beginning of nuclear physics, has been described to a good approximation through the arrangement of stable clusters.

The idea of clustering in nuclei started when α-decay was discovered; nucleons congregating in α-particles before the emission. If one examines the behaviour of binding energies for the very lightest nuclei, those with the same even number of neutrons and protons have the highest values. Examples of these nuclei are ^{4}He, ^{8}Be, ^{12}C... and such nuclei can be thought of as multiples of α-particles. In the early days of nuclear physics Hafstad and Teller's [29] work was crucial, in which they considered geometrical arrangements of α-particles and the bonds between them. They compared this to the binding energies for A = 4n (n=2, 3, 4,

...), $N = Z$ nuclei and found a close correspondence. In the 1950s, Morinaga [30] introduced the idea that the clusters have to be arranged in a linear shape, and also that the cluster structures should emerge when the internal energy of the nucleus is increased and not in the ground state as suggested by Hafstad and Teller. In the 1960s, it was understood that the cluster states emerge close to the decay-threshold energy; an idea that Ikeda [1] demonstrated in the well-known Ikeda diagram shown in Fig. 2.1. It is possible to observe that the double-α cluster is localised in the ground state of ^{8}Be with a half life of $\approx 10^{-16}$ s, and the triple-α cluster was expected to appear close to the α-decay threshold at 7.27 MeV in ^{12}C.

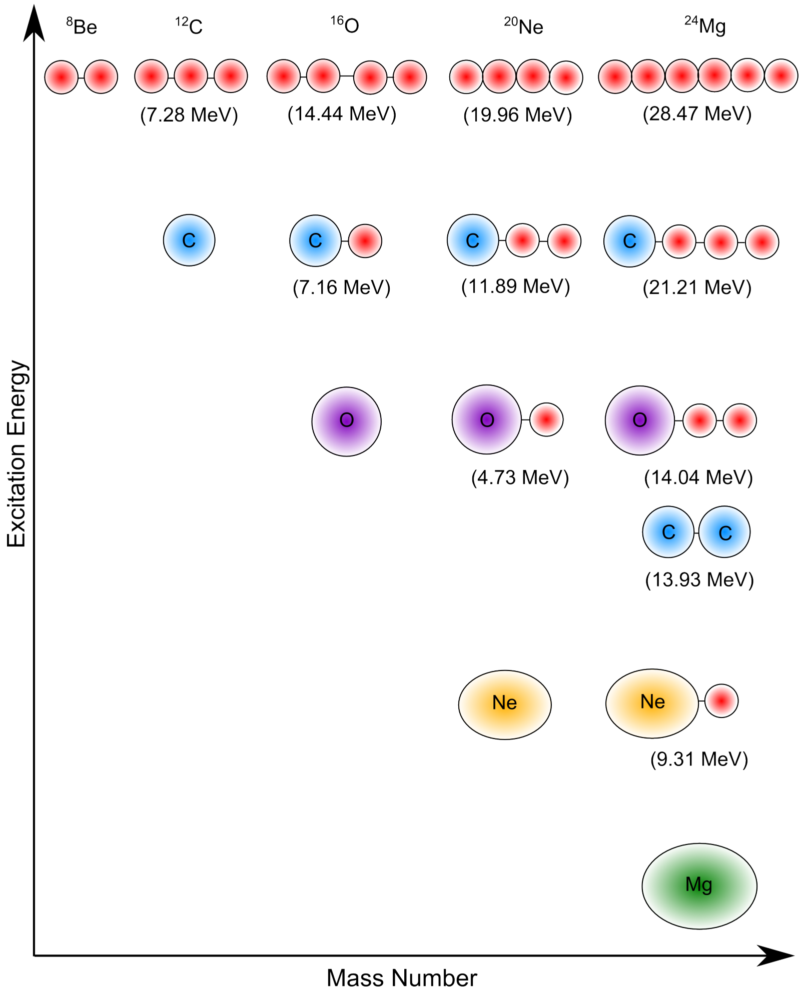

Figure 2.1: *Ikeda diagram for various possible cluster structures and their threshold energies in MeV. Alpha particles are shown in red, adapted from Ref. [1].*

Building on these ideas, the models describing nuclear clustering and other aspects of nuclear structure have been continually evolving. In the following sections, a brief overview of cluster models is given in chronological order.

2.1.1 The Liquid Drop Model

Modelling the nuclear structural shape and its behaviour over the years has been a challenge. Presently there is not a single model which fully describes the nucleus perfectly, but there are many which are very good approximations. One of the most general models describes the nucleus as an assemblage of neutrons and protons forming a drop-like incompressible fluid, acting with the same behaviour and same characteristics as a classical liquid drop. In 1935, based on this model, C.F. von Weizsäcker developed the Semi-Empirical Mass Formula (SEMF) with which it was able to represent the nuclear masses:

$$M = Zm_p + Nm_n - B.E. \tag{2.1}$$

For which the binding energy $B.E.$ of the nucleus is represented by:

$$B.E. = a_v A - a_s A^{\frac{2}{3}} - a_c \frac{Z^2}{A^{\frac{1}{3}}} - a_a \frac{(N-Z)^2}{A} \pm \Delta, \tag{2.2}$$

for which a_v, a_s, a_c, a_a and Δ are constants which are obtained by fitting experimental data. With the SEMF formula, it was possible to fit the known nuclear masses and also estimate unknown masses. The terms of Equation 2.2 are, from right to left, pairing, symmetry, Coulomb, surface and volume.

2.1.2 Nuclear Shell Model

The basis of this model is to describe the nuclear structure in terms of filling energy levels in a mean-field potential. With the aim of clarifying some nuclear properties, during the decade of the 40s, the nuclear shell model was developed. Nuclear physicists took inspiration from atomic theory, based on the electron shells to describe the characteristics of atomic structure. In the nuclear shell model, instead of filling the orbits with electrons to increase the energy, they are filled with nucleons, for which the Pauli exclusion principle is considered. A requirement for this model is that the potential under which the nucleons are moving is created by all of the nucleons, unlike the electrons in an atom, which move under a potential originating from the Coulomb field. Experiments showed evidence of the existence of nuclear shells, *e.g.* in Fig. 2.2, in which the 2-proton and 2-neutron separation energies for isotones are plotted. It is possible to observe jumps at some specific values, or "*magic-numbers*".

The potential which under the particles move around the nucleus is key for the model, one of the simplest is the harmonic oscillator, which works well for the reproduction of low-lying energies and several magic numbers, but as the energies and nucleon numbers increase, discrepancies start to appear, requiring a modification. In 1949, a *spin-orbit* term in the potential was suggested by Mayer, Haxel, Suess and Jensen [31,32], which reproduces the known magic numbers. Even though the model reproduces some energy levels, it is not capable of reproducing the energy of the Hoyle state in ^{12}C as Navrátil et al. showed in reference [4] in which they calculated the energy levels for ^{12}C using the no-core nuclear shell model with two different potentials, the CD Bonn [33] and the V8 Argonne [34] nucleon-nucleon potentials. The calculations for the CD Bonn model are shown in Fig. 2.3. Karataglidis was able to predict the first excited state at 4.4 MeV 2^+, but failed to predict the Hoyle state [35]. .

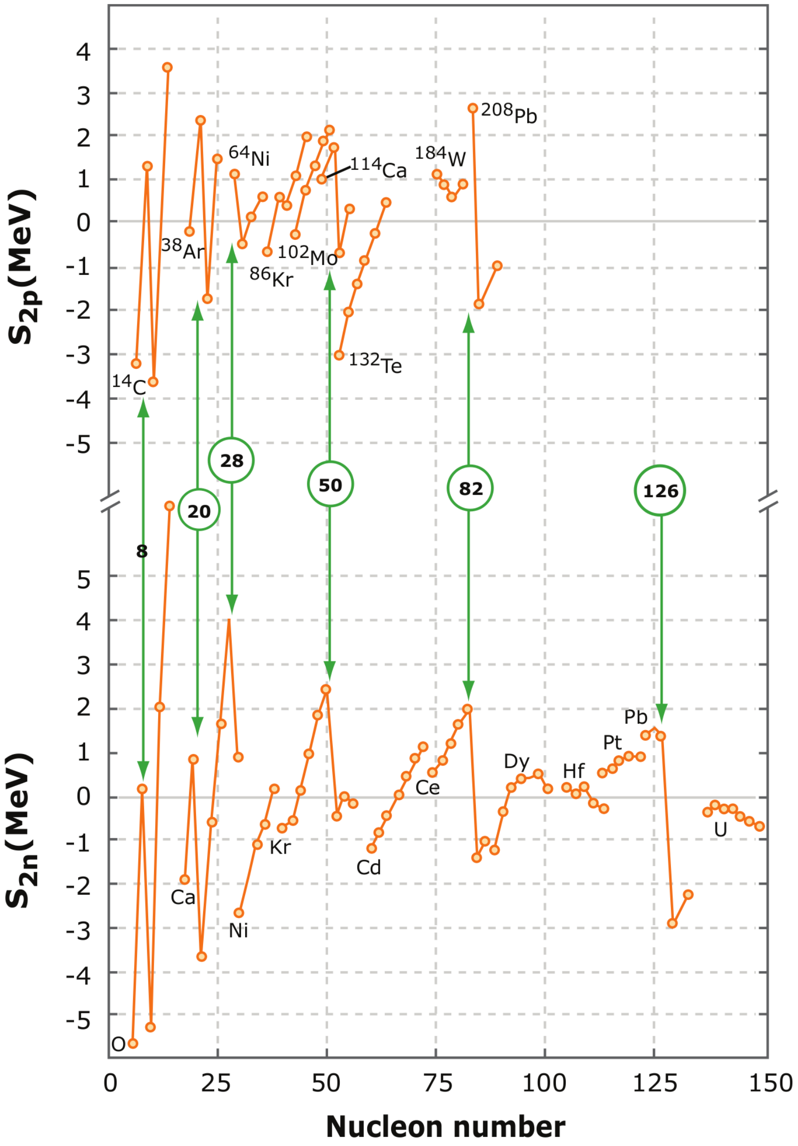

Figure 2.2: *Proton-proton (top) and neutron-neutron (bottom) separation energies plotted against Z (top) and N (bottom). It is possible to observe that the magic numbers (green-circled numbers) appear where sudden changes are present. Taken from [2] (adapted from Ref. [3]).*

2.1.3 Deformed Harmonic Oscillator (DHO)

The spherical harmonic oscillator has been used for a long time, particularly for investigating light atomic nuclei for wave function calculations, densities and shell structure and is consistent with more complete models. The harmonic oscillator has also been demonstrated to be useful in the study of nuclear clustering. Due to the high influence deformation has in the

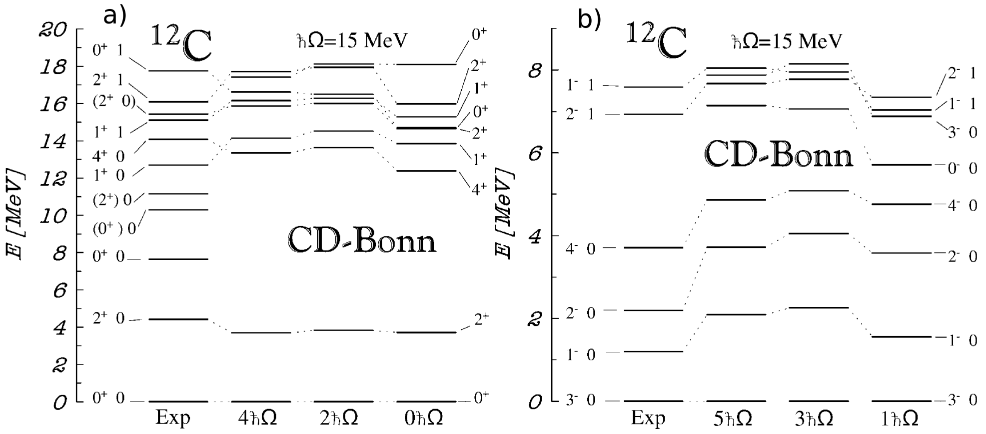

Figure 2.3: *Comparison of experimental positive (a) and negative (b)-parity excitation energies using the CD Bonn potential, taken and adapted from Ref. [4].*

determination of the structure of light nuclei, the spherical harmonic oscillator potential is insufficient [5]. Instead a better approximation is possible. The deformed harmonic oscillator potential (DHO), can describe how nucleons move in a field created by the interaction of a nucleon with the others in the nucleus [36] with a mean free path larger than the nuclear scale. Furthermore, the DHO can also take into account the deformation. Solving the deformed harmonic oscillator it is possible to obtain the energy levels given by

$$E = \hbar\omega_{\perp} n_{\perp} + \hbar w_z n_z + \frac{3}{2}\hbar\omega_0, \tag{2.3}$$

in which $\omega_{\perp}$ and ω_z are the oscillator frequencies, for those oscillations perpendicular and parallel to the deformation z-axis respectively and ω_0 is the parameter required for an undeformed nucleus. As the potential becomes deformed, the degeneracy presented at zero deformation is lost. The quadrupole deformation is given by

$$\varepsilon = \varepsilon_2 = \frac{(\omega_{\perp} - \omega_z)}{w_0}, \tag{2.4}$$

and if $\varepsilon > 0$ the shape of the nucleus will be a prolate (rugby ball) deformation, on the other hand, if $\varepsilon < 0$, the deformation will have an oblate (pumpkin) deformation and if $\varepsilon = 0$, the shape of the nucleus will be spherical, see Fig. 2.4. At zero deformation, the solutions of the harmonic oscillator establishes the allowed number of nucleons (neutrons and protons) which can occupy orbitals; such degeneracies are 2, 6, 12, 20, etc. When the potential is deformed the energy levels associated with oscillations parallel to the deformation axis are reduced in energy and for those with oscillations perpendicular, their energy is increased. As is shown in Fig. 2.4, for deformations of 2:1 and 3:1, multiple shell gaps are generated. The degeneracies are repeated, twice for the 2:1 and three times for the 3:1, indicating the existence of two and three clusters, respectively. These extra magic numbers were interpreted as cluster structures associated with each deformation, for example, ^{8}Be which has four protons and four neutrons, could be located at a deformation of 2:1 and therefore an $\alpha+\alpha$ structure, or the case of the ^{12}C nucleus, which could be formed from a linear arrangement of 3-α particles at a deformation of 3:1.

2.1.4 Alpha-Cluster Model

As discussed in section 2.1, Hafstad and Teller examined the number of bonds between geometrical arrangements of α-particles in α-conjugate nuclei and compared this to predictions of the Liquid Drop Model [29].

The Liquid-Drop Model [13] of the nucleus gave an adequate description for some nuclear properties such as the binding energies and the distribution of some resonant features, such as giant resonances. Furthermore, the shell-model is unable to reproduce the energy of the Hoyle state. In order to get a full description, or at least a better approximation, of the clustered nuclear states, new and more realistic models were needed. The Alpha Cluster Model (ACM) was first proposed by H. Margenau [37], in which α-particles were consider as strongly bound constituents with a proper identity within the nucleus, interacting in a similar way to that as if they were components in atomic molecules. The model was then developed

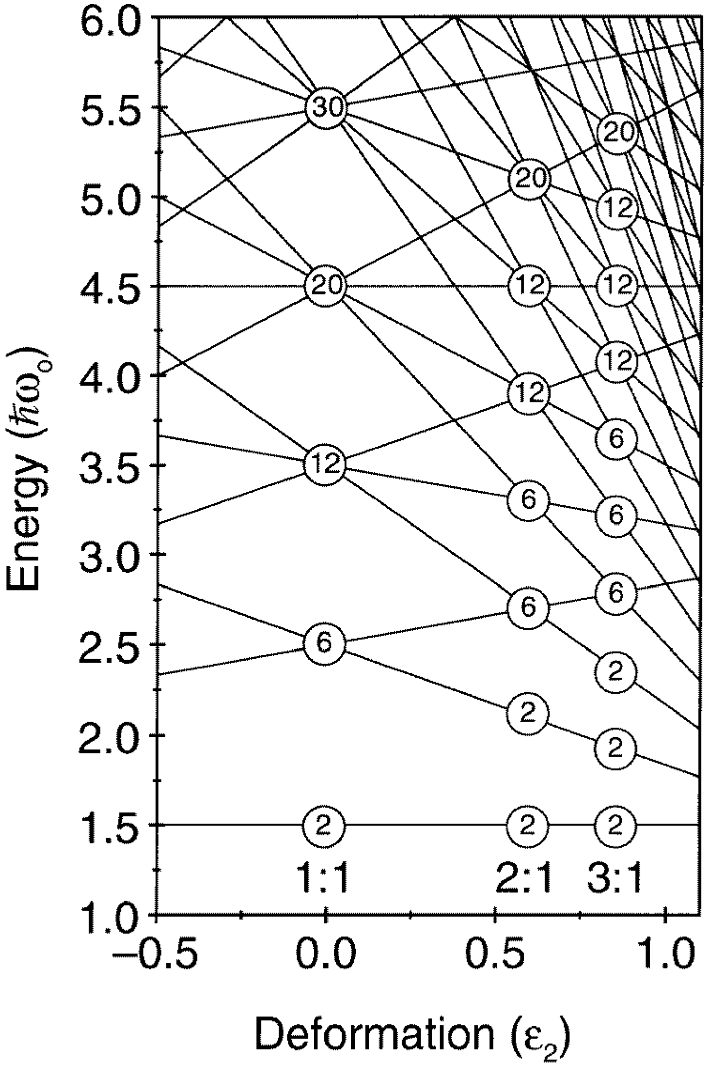

Figure 2.4: *Energy levels of the deformed-harmonic oscillator versus the quadrupole deformation* ε_2. *The circled numbers represent the degeneracies of the energy levels. Taken from Ref. [5].*

in more detail by Brink [6]. The basics of this model is that structures formed by pairs of protons and neutrons, *i.e.* α-particles with a total angular momentum is zero, as shown in see Fig. 2.5. At small distances between the α-particles the structure could disappear, while for longer distances they retain their bosonic structure. For the latter, it happens above the 3α-decay threshold in the case of ^{12}C. Because the Hoyle state appears above this threshold it has potentially a 3α-structure. The Brink model has been applied in order to describe different light clustered systems.

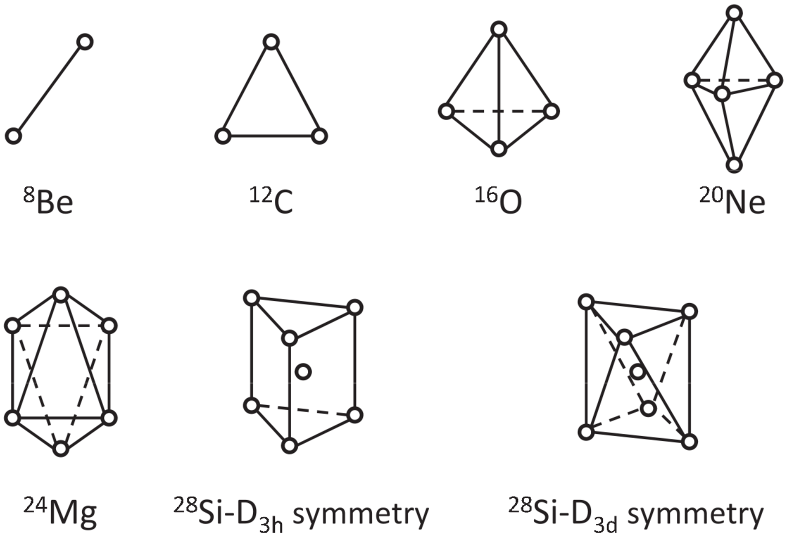

Figure 2.5: Brink's geometrical model of α-particles in light nuclei, *from Ref. [6].*

2.1.5 The Antisymmetrised Molecular Dynamics (AMD) Model

It is well known that nuclear structure involves shell-model-like states as well as cluster structures in light nuclei where both compete. Carbon-12 is a nucleus for which examples of these two types of structure are well known. On one side the shell-model describes and predicts resonances in light nuclei but on the other side it fails to reproduce some states which are strongly clustered such as the second excited state in ^{12}C. Antisymmetrised Molecular Dynamics (AMD) has been used to describe both the cluster and shell-model behaviour of nuclei. In this model, the single-nucleon wave functions are independent Gaussian wave packets and the assumption of a preformed cluster is *not* taken into account, one of many advantages the AMD model has over other models. The degrees of freedom contained in the model are as many as the number of nucleons. A nucleon-nucleon interaction is used to reproduce the energy of the system, which will describe both cluster and shell-model behaviours, governed by the Pauli Exclusion Principle.

The AMD predictions for ^{12}C are shown in Fig. 2.6, including the more shell-model-like states such as the first 2^+ resonance as well as the Hoyle cluster state [7,38] (the second 0^+ level).

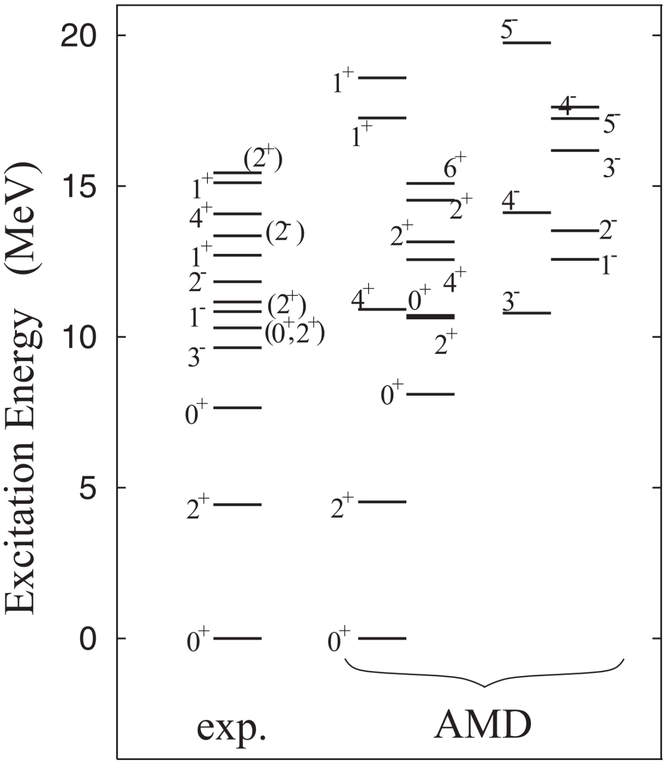

Figure 2.6: *Different energy levels in ^{12}C calculated with the AMD model (second and subsequent columns) compared with experimental data (first column), taken from Ref. [7].*

The density distributions obtained with the AMD model for ^{12}C are shown in Fig. 2.7 in which is possible to clearly observe the intrinsic structures of the first three $J^\pi=0^+$ states as well the first three $J^\pi=2^+$ and $J^\pi=4^+$ states in ^{12}C.

From the density distributions, the ground-state seems to be compact, with the cluster symmetry present but with no formation of distinct α-particle structures. On the other hand, the Hoyle state 0^+ possesses a larger volume, with the formation of α-particle components. Another variant of AMD is Fermionic Molecular Dynamics (FMD) and is briefly described below.

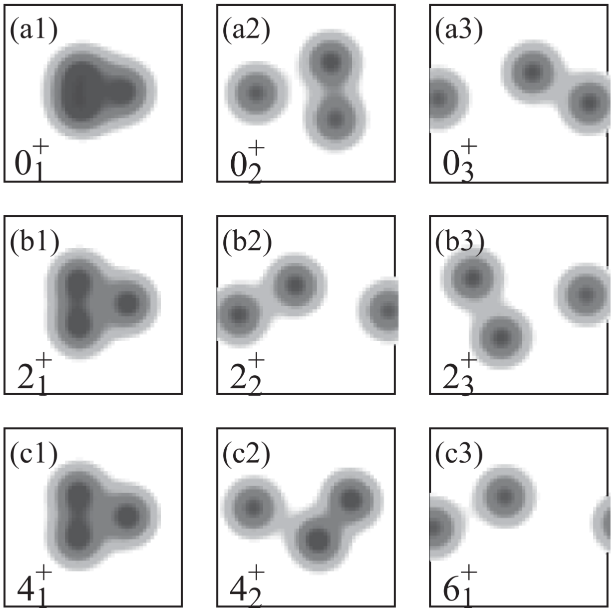

Figure 2.7: *Density distributions of the ground state band,* 0_1^+*,* 2_1^+ *and* 4_1^+*, Hoyle-band* 0_2^+*,* 2_2^+ *and* 4_2^+*, and* 0_3^+*,* 2_3^+ *and* 6_1^+ *band, in the first, second and third columns respectively. Adapted from Ref. [7].*

2.1.6 The Fermionic Molecular Dynamics (FMD) Model

The Fermionic Molecular Dynamics model is a similar to the AMD model, but containing an extra degree of freedom; the width parameter of the Gaussian wave-function which allows a more complete approximation of shell-model systems as well as those which are weakly bound [39]. Another advantage of this model is that it reproduces the charge form factor for elastic and inelastic reactions of electrons with the first and second 0^+ states. As for AMD, FMD shows a large volume for the density distribution for the Hoyle state, but instead of being reproduced by a simple single structure, it is formed by a superposition of 3 α-particles [8]; a characteristic that matches with that of an α-particle gas as shown in Fig. 2.8. The calculations using this model predict the Hoyle state lying at 9.5 MeV and the 2^+ resonance to be at 11.83 MeV, an energy separation of 2.33 MeV.

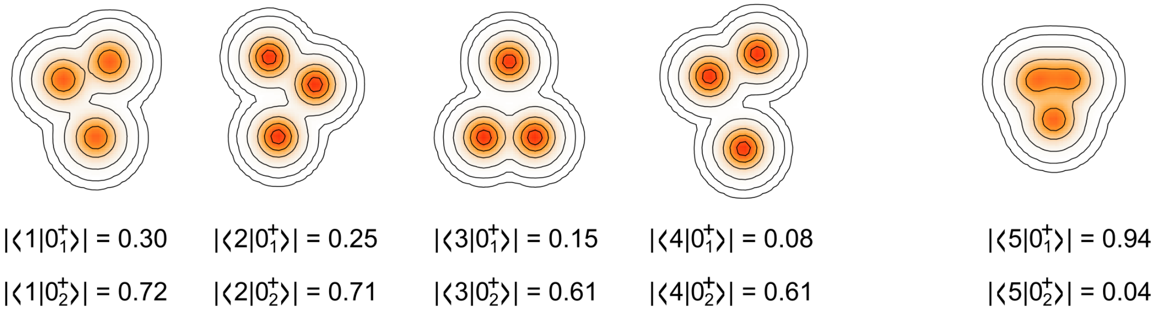

Figure 2.8: *The first four images from the left are the density distributions calculated by FMD for the Hoyle state 0_2^+ and the fifth is represents the ground state 0_1^+, from Ref. [8].*

2.1.7 The Algebraic Cluster Model (ACM)

A study of the dynamical symmetries associated with the structure of ^{12}C were first made by Hafstad and Teller in 1938 [29]. They were able to relate the triple α-structure with a classical spinning top with a triangular point symmetry, meaning that a triangle spinning along one of its axes that can also precess at the same time [18]. The rotational energies for a system such as this are described by

$$E_{J,K} = \frac{\hbar^2 J(J+1)}{2\Im_{Be}} - \frac{\hbar^2 K^2}{4\Im_{Be}}, \tag{2.5}$$

in which J is the quantum number for the total angular momentum, K is the component of the total angular momentum projection on the axis perpendicular to the plane formed by the three α-particles, $\Im_{Be}$ is the moment of inertia of the ^{8}Be *i.e* for two face-to-face α-particles, for which the distance between them has been taken as the same as in ^{12}C. If the triangular structure rotates around an axis lying in the plane of the three components, passing in the middle of one α-particle and in the middle of the other two, as shown in Fig. 2.9 a, will be the representation for when K^π=0 (with a projection equal to zero), giving rise to a series of resonances 0^+, 2^+, 4^+.... corresponding to a ^{8}Be nucleus rotating (or two α-particles). If the rotation occurs when the axis is perpendicular to the plane of the triangle, as shown in Fig. 2.9 b, will give rise to a state with J^π=3^- and the combination of the two different rotations will give the states $K^{\pi}=3^{-}$, 4^{-}, 5^{-}; rotations associated with an object with a $\mathcal{D}_{3h}$ point group symmetry. For a detailed description see Refs. [40–42] in which the applications of this theory in the hadron and molecular physics fields have been reviewed.

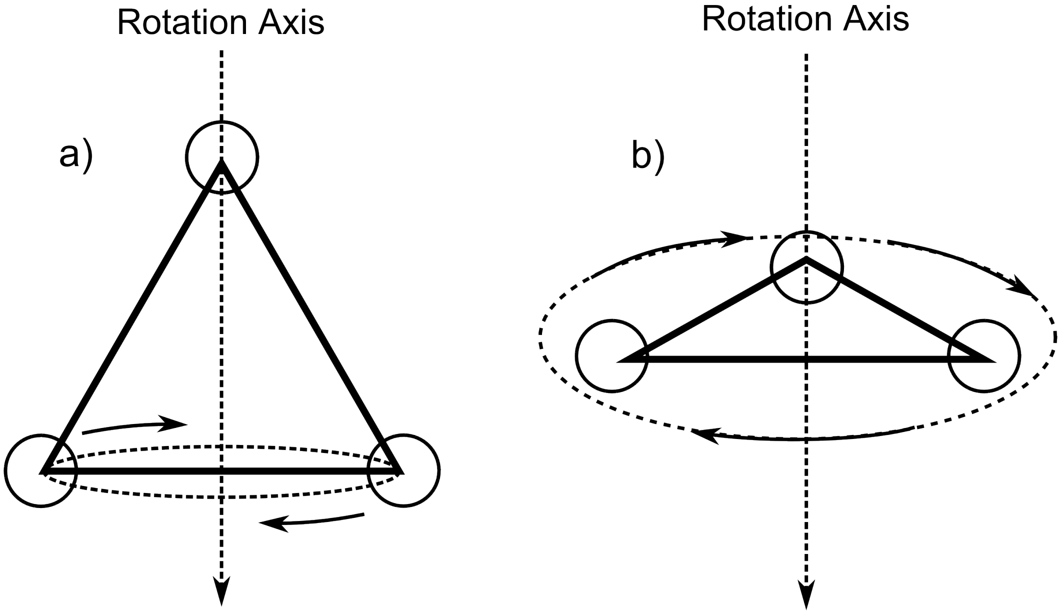

Figure 2.9: *Two different rotations considered by the ACM. a) The triangular structure rotating around an axis lying in the plane of the three components. b) The axis of rotation is perpendicular to the plane of the triangular structure.*

The Model

As noted above, a possible description of the ^{12}C nucleus has been suggested as an equilateral triangle, oblate top with dihedral group $\mathcal{D}_{3h}$ symmetry within the framework of the Algebraic Cluster Model. This method, like other Algebraic models and spectrum generating algebras, are a tool for the study of symmetries and selection rules as well as the calculation of physical observables. The nucleus is treated as a non-rigid compound cluster structure with a liquid-like (vibrational) behaviour [42]. This algebra is able to include different properties needed in order to give a complete description of clustering in nuclei; a list of these properties is given below:

- Cluster configurations are soft, making clusters behave more like liquid structures where the components are situated at specific locations.
- Vibrational and rotational motion energies are not clearly differentiated.
- The components occupy space which can be comparable to that of the total structure.
- Permutation symmetry is imposed since the components are identical.

The ACM treats the nucleus components as bosons, and describes how they move with the help of the spectrum generating algebra U($\nu + 1$), where $\nu = 3(n-1)$, the number of degrees of freedom of the n-body system (n is the number of α-particles) which are relative Jacobi coordinates:

$$\vec{\rho} = \frac{\vec{r}_1 - \vec{r}_2}{\sqrt{2}}, \tag{2.6}$$

and

$$\vec{\lambda} = \frac{\vec{r}_1 + \vec{r}_2 - 2\vec{r}_3}{\sqrt{6}}, \tag{2.7}$$

where $\vec{r}_i$ ($i = 1, 2, 3$) are the coordinates of the three clusters. The U(7) algebra is the appropriate one for such a system composed of three elements. In order to construct the U(7) algebra it is necessary to bring in two vector bosons b_ρ and b_λ and an extra auxiliary scalar boson s. This was previously put into practice in the description of the three-quark configurations in baryons as well as in the triatomic H_3^+ molecule, in which 49 bilinear products of creation and annihilation operators produce the Lie algebra U(7) [40], which are:

$$b^\dagger_{\rho,m}, b^\dagger_{\lambda,m}, s^\dagger \equiv c^\dagger_\alpha \quad (m = 0, \pm 1) \quad (\alpha = 1, ..., 7 \pm 1), \tag{2.8}$$

$$\mathcal{G} : G_{\alpha\beta} = c^\dagger_\alpha c_\beta \quad (\alpha, \beta = 1, ..., 7). \tag{2.9}$$

The Jacobi coordinates and the canonically conjugate momenta are represented by the creation and annihilation operators, while the spectrum generating algebra are represented by the auxiliary boson.

For a triangular configuration, the rotation-vibration wave functions can be written as:

$$|N,(v_1,v_2^{l_2}),K,L^P\rangle, \tag{2.10}$$

for which N represents the total number of bosons, v_1 and $v_2^{l_2}$ are a series of rotational bands, the first corresponds to the breathing vibration and the second to the doubly degenerate bending vibration respectively; l_2 represents the vibrational angular momentum of the doubly degenerate vibration, L is the angular momentum with K its projection on the symmetry axis and P the parity. The energy eigenvalues for an oblate top are given by:

$$\begin{aligned} E = E_0 + w_1\left(v_1+\frac{1}{2}\right)\left(1-\frac{v_1+1/2}{N}\right) + w_2(v_2+1)\left(1-\frac{v_2+1}{N+1/2}\right) \\ +k_1L(L+1)+k_2(K\mp 2l_2)^2+\left[\lambda_1\left(v_1+\frac{1}{2}\right)+\lambda_2(v_2+1)\right]L(L+1), \end{aligned} \tag{2.11}$$

in this formula are included both anharmonicities depending on N and the vibrational dependence of the moments of inertia, for which w_1 and w_2 are the vibrational energies and k_1, k_1, λ_1 and λ_2 are the coefficients determined by different moments of inertia.

For values of K=0, the angular momentum will get values of L=0, 2, 4, etc., and is represented by the rotation of a triangle plane along a line of symmetry. In the case for which K>0, L=K, K+1, K+2... So, the states for which K=0 will agree with the ground 0^+, 4.4 MeV 2^+ and 14.1 MeV 4^+ states. For the case in which K=3, the rotation corresponds to a triangle in which the three α-particles are placed at the vertices, rotating around the axis situated at the centre, which gives rise to the 9.6 MeV 3^- resonance and for a value of

K=6 a resonance with J^π=6^+. The predictions of this model are that there should exist a 4^- excitation almost degenerate with the 4^+ resonance and this would be a strong confirmation of the $\mathcal{D}_{3h}$ symmetry. The model also predicts that the Hoyle state will correspond to a vibrational excitation of the ground-state, in which the triangular symmetry will be fully developed as a three α-cluster structure, giving rise to the same sequence of excitations as for the ground-state [12, 42].

CHAPTER 3

EXPERIMENTAL METHODS

In the following sections, the experimental facility and some important features of charged particle spectroscopy, pertinent to the data analysis and results are described. There is also a description of the equipment that was custom designed and built especially for these measurements.

3.1 MC40 Cyclotron

The MC40 Cyclotron of the University of Birmingham was used to perform the present experiment. This machine was manufactured by Scanditronix, and is used primarily for the production of radio-isotopes (part of the machine is shown in Fig. 3.1). This cyclotron accelerates particles for different experimental purposes, from applications in medical physics to nuclear physics research. In general, an accelerator needs a source of charged particles and an accelerating force, namely an electric field. The cyclotron belongs to the class of accelerators in which the accelerating field is applied repetitively, *i.e.* it is pulsed.

In a cyclotron, the particles orbit under a magnetic field as they gain energy. In general, the path of the particles is through two D-shape cavities named *Dees*, made of a conductive material, which are connected to a *radio frequency* supply. The acceleration of the particles

Figure 3.1: *This photo shows parts of the MC40 cyclotron from above. This shapes the magnetic field which corrects for relativistic effects, from Ref. [9].*

occurs only if they are in phase with the radio frequency at the time they pass through the gap between the *Dees*, *i.e.* with the field in the right direction. The MC40 cyclotron is divided into four quadrants, which means that the main *Dees* are divided in two as shown in Fig. 3.2.

There are two different modes in which the cyclotron can be operated. The first one is when the radio frequency performs one cycle for each orbit of the beam and the potential of the *Dees* are in anti-phase. The second one, is when the radio frequency performs two cycles for each orbit, and the potentials are in phase. For non-relativistic particles, the period of a charged particle is independent of its energy while it is orbiting in a fixed magnetic field, B. The particles of mass, m, and charge, q, will orbit with radius, r, given by:

$$r = \frac{mv}{qB}, \tag{3.1}$$

where v is the speed [13]. Therefore, the cyclotron frequency, or orbital frequency is:

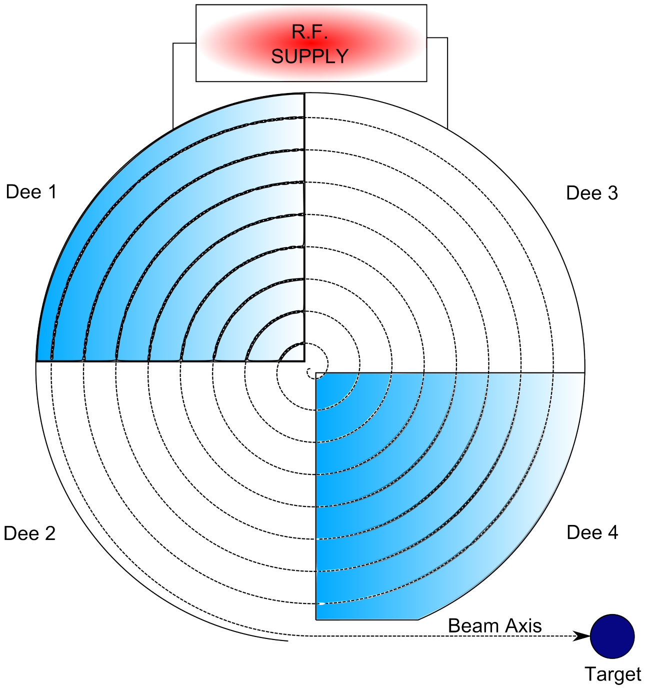

Figure 3.2: *Scheme of the MC40 cyclotron.*

$$f = \frac{v}{2\pi r} = \frac{qB}{2\pi m}. \tag{3.2}$$

For this frequency the accelerating voltage keeps in phase with the particles. At a radius, R, the particles are extracted from the *Dees* using a deflecting electrode (see Fig. 3.3). The energy at this point is given by:

$$E = \frac{1}{2}mv^2 = \frac{q^2B^2R^2}{2m}. \tag{3.3}$$

The frequency range over which this apparatus can be tuned is approximately 14.5 to 26 MHz. Ions of hydrogen and helium can be produced which perform about 500 orbits using a magnetic field of 1.8 T. The ion of interest for the current work, ^{4}He, can be accelerated to energies of 11-40 MeV and beams can be extracted to twelve different lines, one of which was used for the present measurements [9].

Figure 3.3: *The pipe at the right side of the photograph is used to extract the particles from the cyclotron once they reach the optimal energy, from Ref. [9].*

3.2 Charged-Particle Spectroscopy

3.2.1 Radiation Interaction with Matter

There are many different types of radiation in nature: charged and uncharged particles, X-rays and γ-rays, are some of them. Each radiation has its own way of interacting with matter and that is why their measurement and study requires an understanding of the processes that occur during an encounter with the detector medium. For the present study, a special type of detectors were used to acquire information about the emitted radiation, the size and material of such detectors were selected based on the nature of the radiation under study.

Since α-particles are the radiation detected in this work, and they lie in the charged-particles category, a description of their interaction with matter is provided below.

3.2.2 Alpha-Particles

Alpha-particles are charged particles and, therefore, mainly interact with the medium through the Coulomb force, ending up with the partial or total transfer of energy from the primary radiation.

However, α-particles also interact via Rutherford scattering or via other nuclear reactions. Despite this, the electronic interaction is the one used for the design of the detection systems. Each time an α-particle has an encounter with an electron from the medium, depending on how close it passes, the electron will be raised to a higher atomic orbit (excitation), or it could be completely removed (ionisation). In each case the α-particle loses part of its energy, decreasing its velocity.

On average charged particles lose $^{1}/_{500}$ of the particle energy per nucleon [43], which is transferred to an electron in a single collision or $^{4Em_0}/_{m}$, where m_0 is the electron mass, E and m are the kinetic energy and the mass of the α-particle respectively, meaning that many interactions are required in order to completely stop it. The result of an encounter with the medium will be an excited atom or the creation of electron-ion pairs. The latter is made up of a free electron and its corresponding positive ion (hole) [43]. This interaction will be described in detail in Section 3.2.3.

Another important characteristic to raise when discussing charged particles is the linear stopping power S, a property which describes the penetrability of the particles through a specific medium and is given by:

$$S = -\frac{dE}{dX} = \frac{4\pi e^4 z^2}{m_0 v^2} NB \tag{3.4}$$

This is also known as the Bethe-Bloch formula, where

$$B \equiv Z \left[\ln \frac{2m_0 v^2}{I} - \ln\left(1 - \frac{v^2}{c^2}\right) - \frac{v^2}{c^2} \right] \tag{3.5}$$

in which ${}^{-dE}\!/_{dX}$ is the rate of energy loss, v and ze are the velocity and charge of the primary particle, N and Z are the number density and atomic number of the medium atoms, m_0 is the electron rest mass, e is the electronic charge and I is the ionisation potential of the medium. For particles with $v \ll c$, only the first term in B is significant.

3.2.3 Double-Sided Silicon-Strip Detectors

Semiconductor detectors, as used here, are employed in a wide range of areas, from industry to research, due to the high energy resolution attainable for charged particle measurements. Generally, such detectors consist of a semiconductor crystal, such as silicon or germanium. Silicon detectors have been used in the current study. Electron-hole (e-h) pairs are created due to the passage of a charged particle losing energy in the crystal. This promotes electrons to the conduction band leaving holes in the valence band. The electrons in the conduction band are mobile and the electric field moves them through the crystal at a speed determined by its mobility which in turn depends on the temperature and the material. The vacancies or holes in the valence band move in opposite directions. Because of this movement, a current is created, proportional to the particle energy, and is directed to the electrodes. In order to create an e-h pair, an average energy of 3.6 eV is required [13]. In the case of silicon, the charged generated (signal) is small, $\sim 10^{-12}$ C. The silicon detectors used in this work are shown in Fig. 3.4, which are double-sided silicon-strip detectors.

On the front of the detector, there are 16 vertical parallel silicon strips and another 16 orthogonal strips on the back, effectively making 256 pixels and enabling the position of the particle to be measured in addition to the energy. Section 4 describes their arrangement and characteristics, relevant to the experimental set-up.

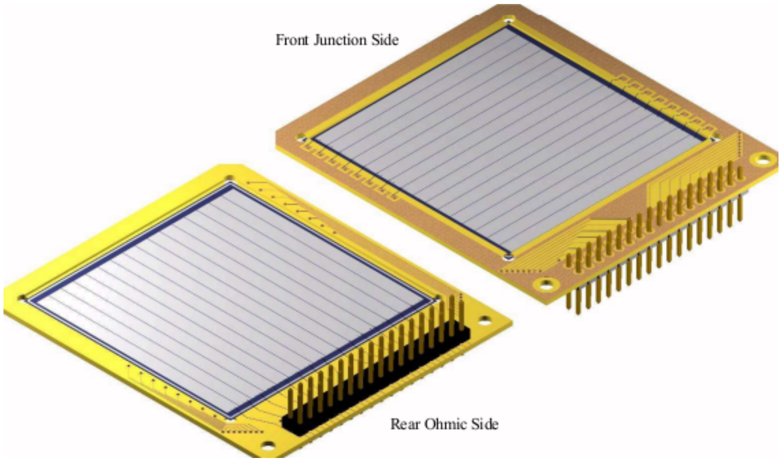

Figure 3.4: *Double-sided silicon-strip detector rear (left) and front (right) faces, from Ref. [10].*

3.3 Break-up Reactions

One type of nuclear reaction is the break-up reaction. Such a reaction was used for the study of the present work in which an incident beam collides with a target nucleus, interacting through inelastic scattering and losing some of its energy. In this collision the kinetic energy of the beam is transferred into excitation energy of the target. If the energy is higher than the energy of the α-decay threshold (3α-threshold $= 7.27$ MeV) for the break-up, then the excited nucleus decays into different products. The reaction utilized was $^{12}\mathrm{C}(^{4}\mathrm{He},^{12}\mathrm{C}^{*})^{4}\mathrm{He}$ for which the beam and target were ^{4}He and ^{12}C respectively. The excited ^{12}C nucleus subsequently decayed into different break-up products such as ^{8}Be (which also can be produced in a series of resonances) and α-particles. The break-up reactions have also the characteristic of having an angular distribution for the products from which the spins of the excited states may be determined. The kinematics of this reaction will be described below.

3.3.1 Reconstruction of the Reaction

Several conservation laws are relevant to nuclear reactions: the total energy of the system, linear momentum, angular momentum etc. In this work, a beam of α-particles was accelerated and collided with a ^{12}C target, transferring energy and leaving the target nucleus in an excited state which decays predominantly into a ^{8}Be nucleus and an α-particle. Subsequently, the ^{8}Be nucleus decays into two α-particles. A way to represent such break-up reactions is

$$^{12}C(\alpha,^{12}C^{*} \rightarrow \ ^{8}Be + \alpha)\alpha, \tag{3.6}$$

and subsequently

$$^{8}Be \rightarrow \ 2\alpha, \tag{3.7}$$

in which for left to right are the ^{12}C target, the α-particle beam, the break-up products (3 α-particles) and the scattered beam.

The complete reconstruction of the initial reaction requires the detection of at least three of the four final-state α-particles from the decay of ^{12}C or the scattered beam. When a particle hits a detector it deposits its kinetic energy, see Section 3.2.1. This information is consequently used to determine its energy, direction and, hence, the linear momentum components. The detectors are described in Section 3.2.3. Since the energy and the direction were measured, the linear momentum of each particle can be calculated by $P_{\alpha} = \sqrt{2m_{\alpha}E_{\alpha}}$, in which m_{α} and E_{α} are the mass and kinetic energy of the α-particle respectively. It is then possible to decompose the momentum for each particle into its three cartesian components, x, y and z, which allows the full reconstruction of the reaction. In Fig. 3.5 it is shown how the in-plane θ_x and out-plane θ_y angles are calculated when a particle hits any position on the detector. The other components are calculated as follows:

$$P_{\alpha(x)} = P_{\alpha}\sin(\theta_x)\cos(\theta_y) \tag{3.8}$$

$$P_{\alpha(y)} = P_{\alpha}\sin(\theta_y) \tag{3.9}$$

$$P_{\alpha(z)} = P_{\alpha}\cos(\theta_x)\cos(\theta_y), \tag{3.10}$$

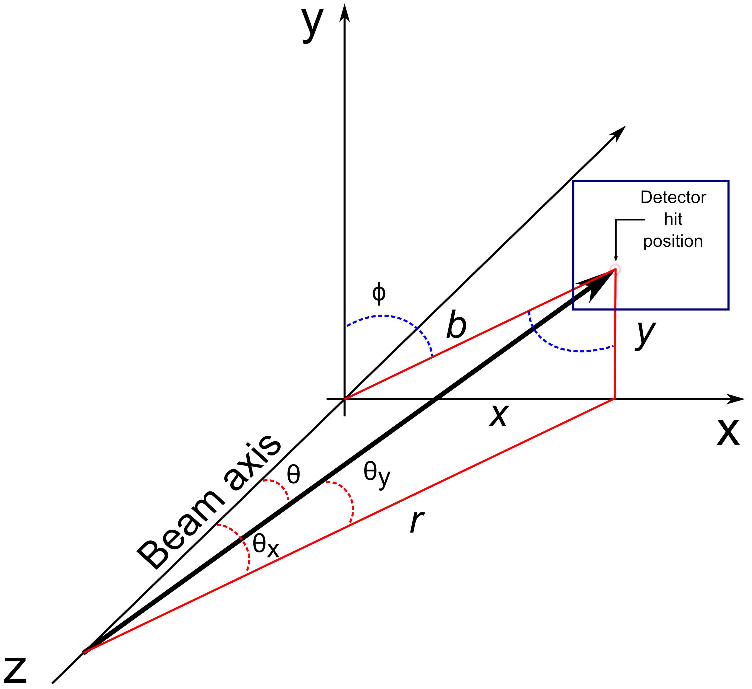

Figure 3.5: *Definition of the in-plane, θ_x, and out-plane, θ_y, angles. The beam line lies on the z-axis. Adapted from Ref. [11].*

and the reconstruction of the ^{12}C* momentum is obtained using, from the three detected α-particles, momentum conservation

$$\underline{P_{^{12}C}} = \underline{P_{\alpha 1}} + \underline{P_{\alpha 2}} + \underline{P_{\alpha 3}}, \tag{3.11}$$

and hence

$$P_{^{12}C^*} = \sqrt{\left[\sum_{i=1}^{3} P_{\alpha_i(x)}\right]^2 + \left[\sum_{i=1}^{3} P_{\alpha_i(y)}\right]^2 + \left[\sum_{i=1}^{3} P_{\alpha_i(z)}\right]^2}, \tag{3.12}$$

where $P_{^{12}C^*}$ is the ^{12}C* momentum and P_{α_i} are the momenta components for the i^{th} α-particle. Finally the ^{12}C* excitation energy is obtained by

$$E_{ex} = \sum_{i=1}^{3} E_{\alpha_i} - \frac{P^2_{^{12}C}}{2m_{(^{12}C)}} + E_{th(^{12}C)}, \tag{3.13}$$

in which E_{ex} is the ^{12}C* excitation energy, E_{α_i} is the kinetic energy for the i^{th} α-particle, $m_{(^{12}C)}$ is the ^{12}C mass and $E_{th(^{12}C)}$ is the ^{8}Be + α threshold (7.367 MeV). A representation of the reaction ^{12}C(^{4}He, ^{12}C*)^{4}He for which results are presented is shown in Fig. 3.6.

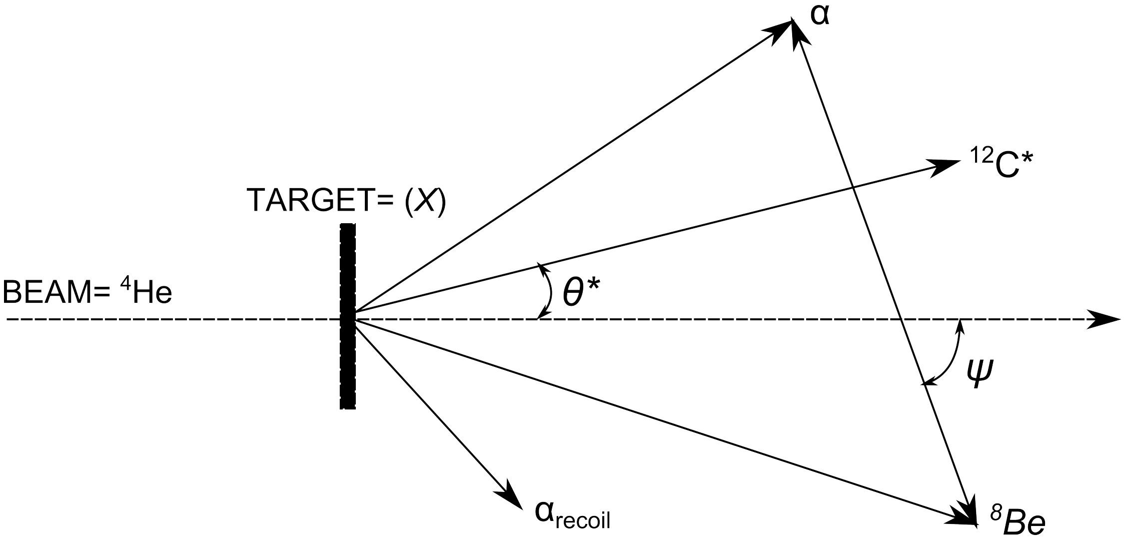

Figure 3.6: *The $^{12}C(^4He,\ ^{12}C^*)^4He$ break-up reaction. The beam is scattered, exciting the ^{12}C nucleus which then decays into an α-particle and a ^8Be nucleus. The latter subsequently decays into two α-particles.*

In order to reconstruct the recoil particle (scattered beam) the beam momentum is calculated

$$P_{beam} = \sqrt{2m_\alpha E_{beam}}, \tag{3.14}$$

where P_{beam} is the beam momentum exclusively in the z-direction, E_{beam} is the beam energy and the total momentum of the scattered beam nucleus is:

$$\underline{P_{rec}} = \underline{P_{beam}} - \underline{P_{\alpha 1}} - \underline{P_{\alpha 2}} - \underline{P_{\alpha 3}}. \tag{3.15}$$

Taking the scalar product gives

$$P_{rec}^2 = \left[\sum_{i=1}^{3} P_{\alpha_i(x)}\right]^2 + \left[\sum_{i=1}^{3} P_{\alpha_i(y)}\right]^2 + \left[\sum_{i=1}^{3} P_{\alpha_i(z)} - P_{beam}\right]^2, \tag{3.16}$$

thus:

$$E_{rec} = \frac{P_{rec}^2}{2m_\alpha}, \tag{3.17}$$

where E_{rec} is the energy of the recoil particle. Finally the total energy of the reaction is given by:

$$E_{tot} = \sum_{i=1}^{3} E_{\alpha_i} + E_{rec}, \tag{3.18}$$

which is used for further analysis in Section 5.1.2.

3.4 Angular Correlations

The angular correlation technique is a robust tool used in order to achieve the characteristics of the nature of resonances, particularly in this work for those in ^{12}C. Together, sequential break-up reactions (see Section 3.3.1) and the angular correlation analysis were used. The latter, a method in which the pattern of the products are analysed in order to measure the spin of the recoil excited states from the reaction. This type of analysis has to be done carefully in order to get definitive results. The angular coverage of the detection system is one of the most important restrictions since the number of detected events depends on its configuration. As mentioned above, the break-up reaction measured in this work was ^{12}C(^{4}He,^{12}C*)^{4}He. The three final products of the reaction ^{8}Be$+\alpha+\alpha$ are correlated and it is possible to parametrise them by means of spherical polar angles as shown in Fig. 3.7. Here θ^* is the polar centre-of-mass scattering angle of the resonant ^{12}C* particle, and Ψ is the polar emission angle of the first α-particle coming from the decay of the ^{12}C* nucleus in the recoil particle centre-of-mass frame. Both angles are measured with respect to the beam axis. The systematic dependence of the correlations on the resonant particle (which for the present work is ^{12}C) allows the determination of the transferred angular momentum [44].

In order to apply this method it is required that both the initial and final particles have zero spin. In such reactions only natural parity states $(-1)^J$ can be populated. This also limits the range of reaction amplitudes and angular momenta which may contribute.

3.4.1 Calculating θ^* and Ψ

Typically, correlation data are plotted as θ^*-Ψ histograms. In order to calculate θ^* and Ψ the following procedure was performed. The magnitude of θ^* (see Fig. 3.7a), which is the centre-of-mass angle of the recoiling ^{12}C nucleus, can be obtained by means of:

$$\theta^* = tan^{-1}\left(\frac{P_{Cx}}{P_{Cz(cm)}}\right), \tag{3.19}$$

where P_{Cx} and $P_{Cz}(cm)$ are the ^{12}C momentum components along the x-axis and z-axis respectively, the latter in the projectile target centre-of mass frame. Here, the reaction is assumed to occur in the x-z plane – the horizontal plane. This is a sufficiently good approximation for analysis of the current data, due to the placement of the detectors in this plane. Improvements to this have been explored through rotations of the plane in which θ^* and Ψ are calculated, though these are not needed to observe the correlations sought in the present work. See Ref. [45]. The momentum components for the ^{12}C nucleus are calculated as follow

$$P_{Cx} = -P_{\alpha_1(x)} - P_{\alpha_2(x)} - P_{\alpha_3(x)} \tag{3.20}$$

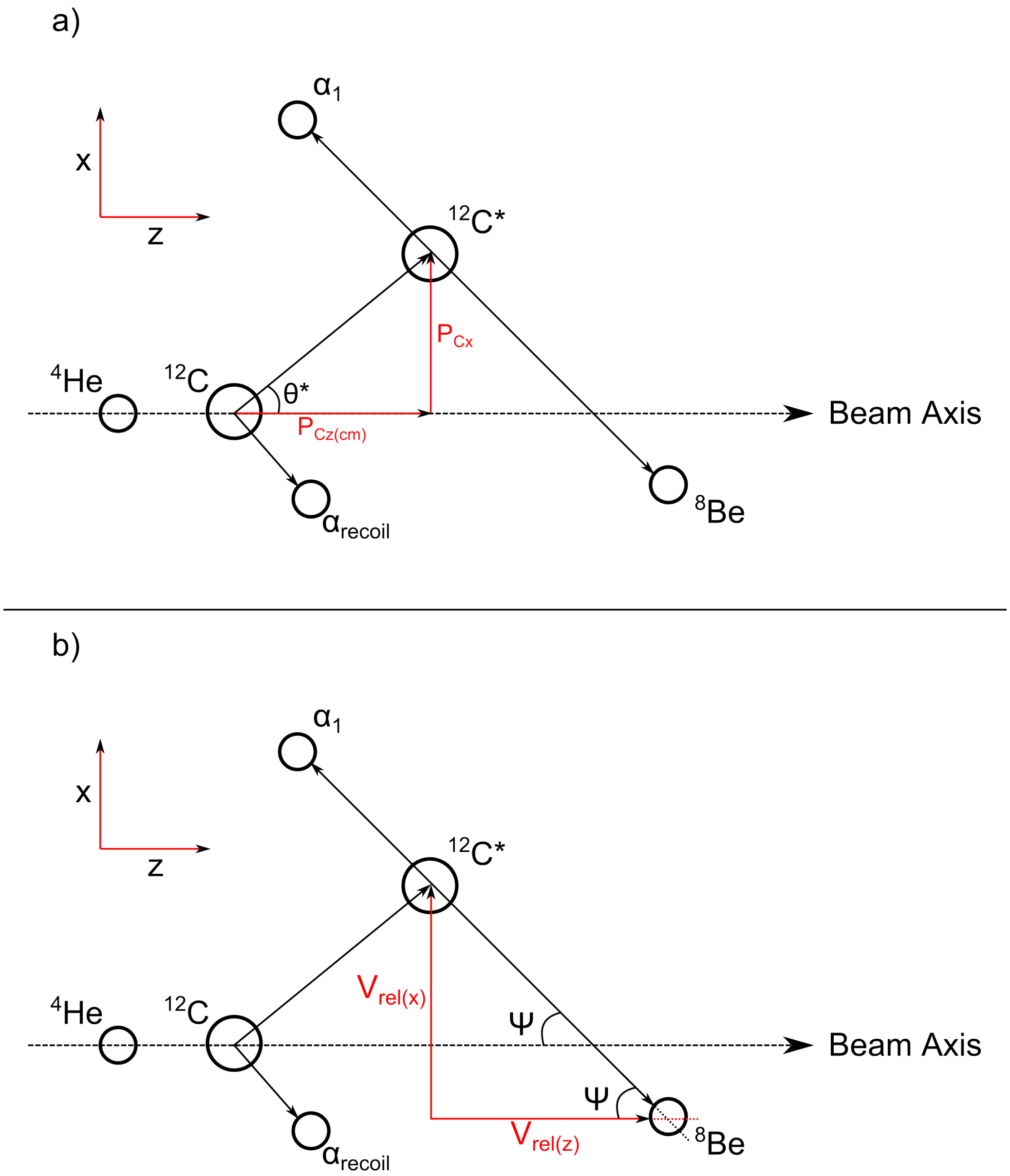

Figure 3.7: *The* $^{12}C(^{4}He,^{12}C^{*})^{4}He$ *break-up reaction in which the* $^{12}C^{*}$ *nucleus decays into an* α*-particle and a* ^{8}Be *nucleus, in which the latter subsequently decays into two* α*-particles. The angle* θ^{*} *is the emission angle of the* ^{12}C *nucleus and* Ψ *corresponds to the emission angle of the first* α*-particle in the* ^{12}C*, both in the centre-of-mass frame. The angles are used to calculate the momenta and velocity components along the* x *and* z *axes.*

and

$$P_{\alpha_{rec}(z)} = P_{beam} - P_{\alpha_1(z)} - P_{\alpha_2(z)} - P_{\alpha_3(z)}, \tag{3.21}$$

And so,

$$P_{Cz(cm)} = \frac{m_{(^4He)} P_{beam}}{m_{(^4He)} + m_{(^{12}C)}} - P_{\alpha_{rec}(z)}, \tag{3.22}$$

is the momentum in the z direction in the centre-of-mass frame. For the case of Ψ, as shown in Fig. 3.7b), is given by:

$$\Psi = tan^{-1}\left(\frac{V_{rel(x)}}{V_{rel(z)}}\right), \tag{3.23}$$

using Eqns. 3.8 and 3.10 it is possible to calculate the ^{8}Be components along the x and z-axis by means of:

$$P_{^8Be(x)} = P_{\alpha_1(x)} + P_{\alpha_2(x)} \tag{3.24}$$

and

$$P_{^8Be(z)} = P_{z\alpha 1} + P_{z\alpha 2} \tag{3.25}$$

thus:

$$V_{rel(x)} = \frac{P_{^8Be(x)}}{m_{(^8Be)}} - \frac{P_{x\alpha 3}}{m_{(^4He)}} \tag{3.26}$$

and

$$V_{rel(z)} = \frac{P_{^8Be(z)}}{m_{(^8Be)}} - \frac{P_{z\alpha 3}}{m_{(^4He)}}, \tag{3.27}$$

in which $V_{rel(x)}$ and $V_{rel(z)}$ are the relative velocity components in the x and z directions respectively, between the nuclei of ^{8}Be and the first emitted α-particle coming from the ^{12}C* nucleus.

Having calculated θ^* and Ψ angles it is worth mentioning how they are related to the spin, J, and the grazing angular momentum, l_{gr} [46], by:

$$\Delta\Psi = \Delta\theta^{*}\left(\frac{l_{gr} - J}{J}\right), \tag{3.28}$$

from Ref. [44]. The grazing angular momentum is dependent on the nature of the beam and the target and is calculated as:

$$\underline{l_{gr}} = \underline{r} \times \underline{p}, \tag{3.29}$$

for which when touching

$$r = r_0(A_{target}^{\frac{1}{3}} + A_{beam}^{\frac{1}{3}}), \tag{3.30}$$

and

$$p = \sqrt{2\mu E_{beam_{(CM)}}} = \frac{A_{target}}{A_{target} + A_{beam}}\sqrt{2A_{beam}E_{beam}}, \tag{3.31}$$

where r is the impact parameter (the closest distance between the beam and the target nuclei), p is the momentum in the reaction, r_0 can take values between 1.1 to 1.5 fm, in which the value used for this analysis was 1.2 fm, A_{target} and A_{beam} are the target and beam masses respectively, μ is the reduced mass and E_{beam} the laboratory beam energy.

For an angle $\theta^{*}= 0$, the ^{12}C distribution pattern will follow

$$W(\theta^{*}\Psi) \propto \mid P_J[\cos(\Psi)] \mid^2 . \tag{3.32}$$

Here, P_J is the Legendre polynomial of order J, which is key to determining the spin of a state. This is dependent on all initial and final-state particles having spin J=0. The orbital angular momentum vectors are perpendicular to the beam axis and hence the resonant ^{12}C is populated in the m=0, magnetic substate. On the other hand, when $\theta^{*} \neq 0$, a small variation in Ψ, $\Delta\Psi$ is associated with a small variation in θ^{*}, $\Delta\theta^{*}$, via Eqn. 3.28, and so the pattern will be dominated by:

$$W(\theta^{*}\Psi) \propto | \; P_{J}[\cos(\Psi + \Delta\Psi)] \; |^{2} \; . \tag{3.33}$$

In the latter case, within the θ^{*}-Ψ plane, the formation of sloped features will appear with a specific gradient ${}^{\Delta\theta^{*}}/_{\Delta\Psi}$, given by Eqn 3.28, the periodicity of which yields the spin of the resonance under analysis [25, 44].

CHAPTER 4

SIMULATIONS AND EXPERIMENTAL SETUP

In the following sections a description of the Monte-Carlo simulations performed before and after the experiment are presented. Additionally, the set-up of the experiment, including the detector-array geometry, electronics, data acquisition system and analysis software are described. Finally the detector calibration and the reaction and kinematics are mentioned.

4.1 Monte-Carlo Simulations – Resolution8

Monte-Carlo simulations were performed both before and after the experiment using a fortran code which was written by members of the Charissa collaboration and modified according to the characteristics of the reaction investigated in the present work [47]. The simulations carried out before the experiment had the purpose of calculating the optimal detector-array efficiency, *i.e.* the distances and angles at which each detector should be placed in order to maximise the experimental coverage. In the Monte-Carlo simulations the break-up, scattering, resonant particles and break-up products are simulated *i.e.* the entire reaction. The simulation code reads, from an input file, all the details regarding the reaction and also the parameters describing the detection array.

These details consist of the beam energy, the masses and the charges of the target, resonant particle, recoil particle and products, the reaction Q-value and all the dimensions and characteristics of each detector as the number of strips in which are divided, energy loss of the beam and products through the target as well as energy and angular straggling. Some of these parameters included in the input file are shown in Table 4.1. Additionally, the simulations were re-run after the experiment with the actual detector position. This was to obtain the acceptance in order to normalise the results of the angular correlation analysis. This angular correlation analysis was explained in more detail in Section 3.4.

Reaction and Q-value	^{12}C(^{4}He,^{12}C*)^{4}He, Q=0 MeV
First Break-up and Q-value	$^{12}\mathrm{C} \rightarrow {}^{8}\mathrm{Be}_{(g.s.)} + \alpha$, Q=$-7.367$ MeV
Second Break-up and Q-value	$^{8}\mathrm{Be}_{(g.s.)} \rightarrow \alpha + \alpha$, Q=0.092 MeV
Simulated excitation energy	E_x=13.3 MeV
Beam energy	E_{beam}=40 MeV
Target thickness	100 $^{\mu g}/_{cm^2}$
Target density	2.25 $^{g}/_{cm^3}$
Beam energy spread from accelerator	E_x=0.0004 MeV
In-plane beam divergence	0.1°
Out-of-plane beam divergence	0.1°

Table 4.1: *Parameters used for the Monte-Carlo simulation in the Resolution8 code for the* $^{12}C(^{4}He,^{12}C^{*})^{4}He$ *reaction.*

4.2 Detector Array Configuration and Efficiency

The detector array was composed of four double-sided silicon-strip detectors (DSSSDs), which covered a polar angular range of $\theta = 20^\circ$ to 75° and an azimuthal angular range $\Delta\phi = 26^\circ$, as shown in Fig. 4.1. Each (DSSSD) consists of 16 horizontal strips on the front and 16 vertical strips on the back yielding effectively 256 pixels, making the determination of both the direction and energy of the detected particles possible. The active area for each of the (DSSSDs) was 5×5 cm^2 with a thickness of 500 μm [10]. The detector energy thresholds were measured to be approximately 700 keV, and the typical energy resolution was 100 keV Full Width at Half Maximum (FWHM). The centres of each detector together with the beam axis formed the x-z plane. Detectors 1−4 were placed 13, 11, 11 and 13 cm from the target position at centre in-plane angles of 62.5°, 32.5°, −32.5° and −62.5° respectively, as shown in Fig. 4.1. The positive angles lie on the left side with respect to the beam axis in the direction of the beam. As can be recognised the positions of the detectors are slightly different to those calculated by the simulations (described in a previous section).

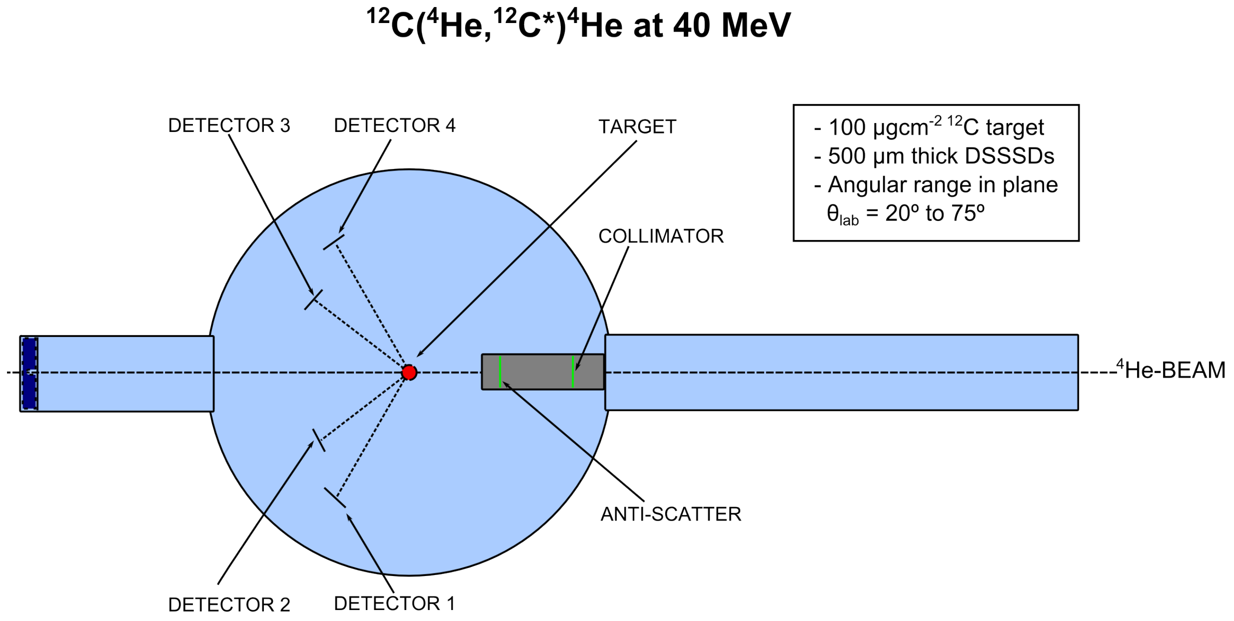

Figure 4.1: *The detector array comprising four DSSSD detectors, the collimator, the anti-scatter and the target.*

The simulations mentioned above were performed with several different detector positions in order to determine the optimum detector array position, but with the rest of the parameters fixed. In Table 4.2 are shown the values of the detector array efficiency, it is possible to observe that as the position of the detectors gets closer to the beam axis, the efficiency increases. The first and the last position are not realistic since the detectors can not overlap each other, they are mentioned with the purpose of having values for the whole 360°coverage.

Due to the overlapping of the detectors at angles close to the beam-line as well as the position of the anti-scatter and collimator, it was not possible to place them at the most

Detector Position	Angle Coverage	Efficiency	Error
1	42.5°-12.5°	13.84	0.33
2	52.5°-22.5°	11.56	0.27
3	62.5°-32.5°	9.76	0.23
4	92.5°-62.5°	3.14	0.07
5	122.5°-92.5°	1.18	0.30
6	152.5°-122.5°	3.66	0.08
7	182.5°-152.5°	5.95	0.13

Table 4.2: *Efficiency values obtained from the Monte-Carlo simulations for the 13.3 MeV resonance in ^{12}C detected at different angles (the angles correspond to the in-plane centres of the detectors).*

efficient position, instead, the 62.5°and 32.5°angles were selected with an efficiency of almost 10% as shown in Fig. 4.2.

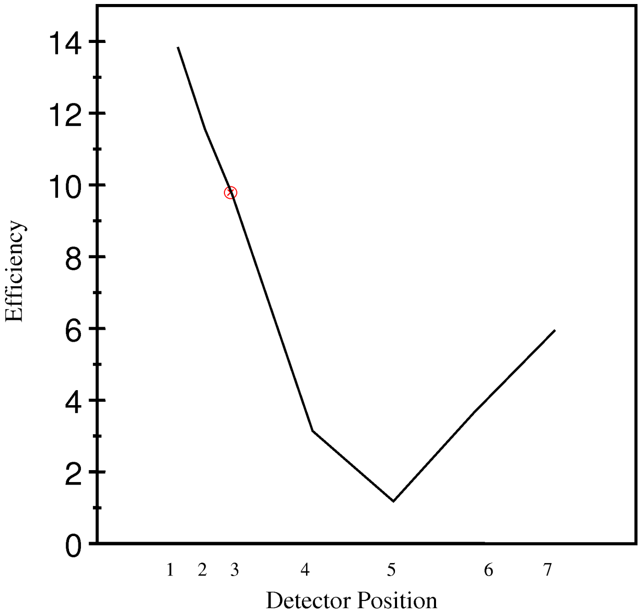

Figure 4.2: *Efficiencies for different detector configurations given in Table 4.2. The red dot represents the value chosen for the set-up of the experiment with an almost 10% efficiency. The centroids of the detectors were placed at 62.5°and 32.2°with respect to the beam axis, as shown in Fig. 4.1.*

4.3 Chamber and Electronics Setup

The target and the detector array were sited within a vacuum chamber, at the centre of which is located the target position; see Fig. 4.1. Before the experiment and simulations were performed, the interior mechanics of the scattering chamber was re-designed. As the angle of the detectors is critical for event reconstruction, a graduated steel disc with scored angle divisions was custom made for this experiment. In the photograph Fig. 4.3 it is possible to observe that the disc has concentric circles and radial lines, the former separated by 1 cm each and the latter by 5°. The rings start at 10 cm from the target position, which is the minimum distance at which a detector base could be placed.

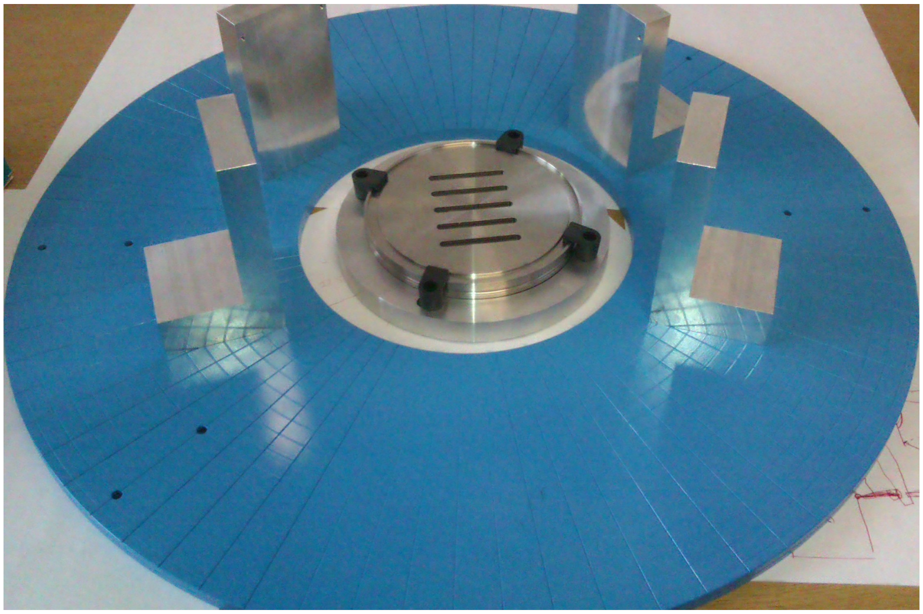

Figure 4.3: *This photo shows the disc on which the detectors were fixed using the aluminium bases.*

The disc was made of steel to permit the flexible placement of the detectors, without the necessity of fixing screws. To facilitate this, two rare-earth neodymium magnets were recessed and glued in to the bases of the aluminium mounting blocks, which are also shown in Fig. 4.3. Hence, the detectors and mounts could be slid to the desired position. The bases were made of aluminium, in a simple L shape, to the top of which detectors could be fixed with screws. Vertically, the centre of the detector is at the same level as the beam.

Since the chamber is under vacuum, a feed-through flange was required to pass the electrical signals out and the detector bias in. A new flange design was required and this was made with two components, an adapter ring (made of aluminium) and a small DN100 stainless steel flange including 8 large lemo connectors each of which is sufficient for 16 signals (*i.e.* one detector face). The flange is shown in Fig. 4.4, which is mounted on one side of the chamber. It is possible to differentiate the two parts of the flange assembly. The eight vacuum tight lemo connectors carrying the signals and detector bias can be seen clearly in the central plate. This twin-size flange solution was chosen to be compatible with a large range of laboratory scattering chambers that the group exploits.

Figure 4.4: *Photo showing the flange assembly mounted on the vacuum chamber.*

4.3.1 Data Acquisition System (DAQ)

The Data Acquisition System (DAQ) consisted of 128 channels of electronics, 32 for each (DSSSD). When a particle is detected, *i.e.* when it is incident on a strip, an electric signal is created. The signals are sent to Mesytec MPR-32 pre-amplifier units for charge integration. The outputs of the pre-amplifier are packed in groups of 16 channels, and connected to CAEN 568B NIM modules where they are shaped and amplified. A diagram of the system is shown in Fig. 4.5. The amplified signals are sent to Silena 9418 Analogue-to-Digital Converters (ADCs). Additionally, the amplified signals from the front face of each detector are sent to CAEN V895 VME discriminators. The resulting logic pulses were used to generate the trigger and gate the ADCs. The data are read-out and buffered in 16 kB blocks by a Motorola VME processor which subsequently sends the data via network to the acquisition software MIDAS [48], that writes the blocks to disk. In addition, these events are made available via memory to the on-line sorting and visualisation software, SUNSORT [49]. The master trigger condition was set at multiplicity ≥ 3, meaning ≥ 3 hits on the combined front detector faces of the 4 detectors.

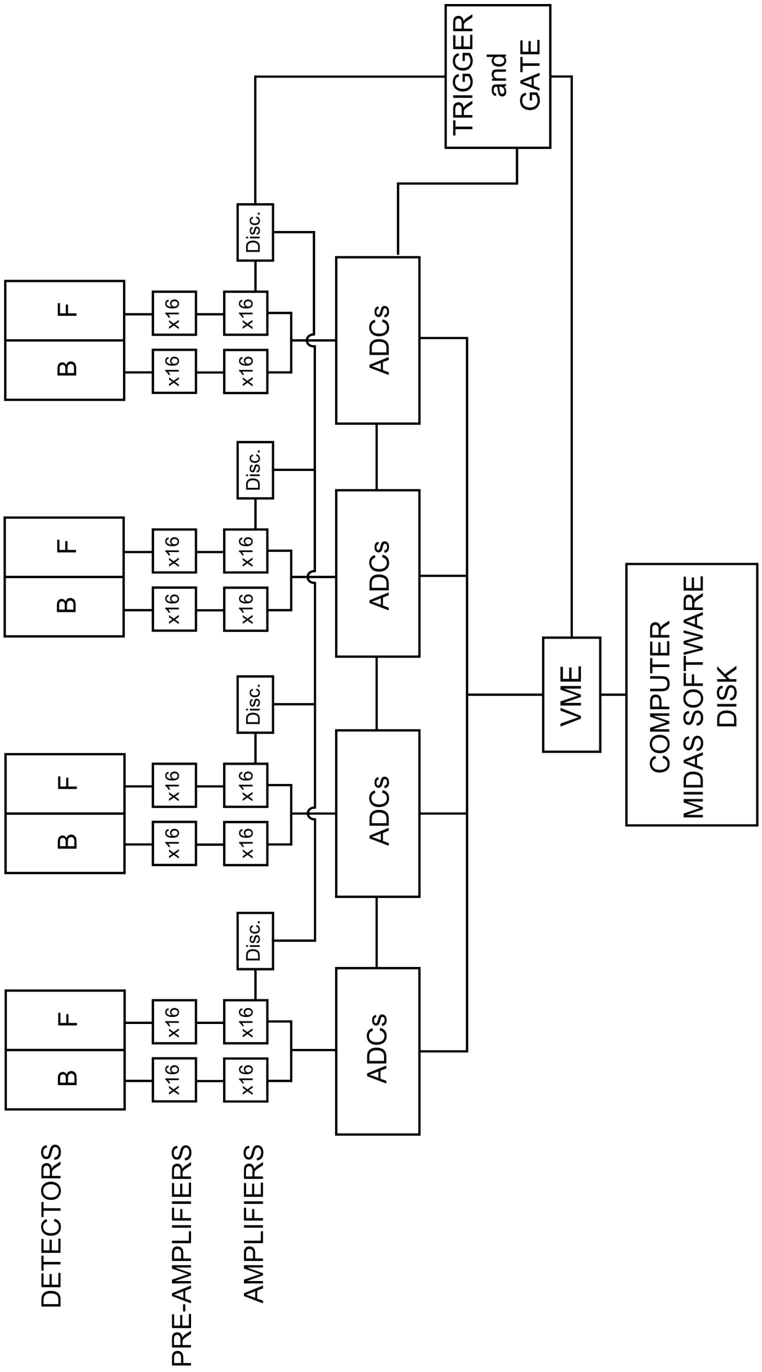

Figure 4.5: *A schematic of the electronics set-up.*

4.4 Sorting and Analysing Software

4.4.1 SUNSORT

The events were sorted on an event-by-event basis using SUNSORT, the software used to analyse the simulations and both, on-line and off-line experimental data. This software allowed access to data from different streams such as disk, tape or memory. It comprises a user-written fortran code with specific instructions to calculate and analyse features of the data through subroutines that the user can include, which permit a free manipulation of the data. Energy and direction of the particles as well as the full kinematic reconstruction of the reaction are some of the tasks the code can perform. Another task performed by this software is the visualisation of 1- and 2-dimensional histograms for both, simulated and real data, increasing the flexibility and ease by which gates can be placed to select the events of interest. The calibration of the detectors is also performed using the software. More detail can be found in Refs. [50, 51].

4.5 Energy Calibration

4.5.1 Alpha Calibration

The detectors were calibrated with a triple α-source with energies of 5.149 MeV, 5.479 MeV and 5.795 MeV produced by the decay of ^{239}Pu, ^{241}Am and ^{244}Cm respectively (FWHM$\approx$0.15 MeV). The calibration is necessary in order to align all the detector/ADC channels to a precise common energy scale. When a particle event is recorded the signals are associated with particular ADC channels which in turn corresponds to known detector-strip numbers. The calibration coefficients are applied to each ADC channel to yield energy. An α calibrated spectrum for the total 128 strips is shown in Fig. 4.6.

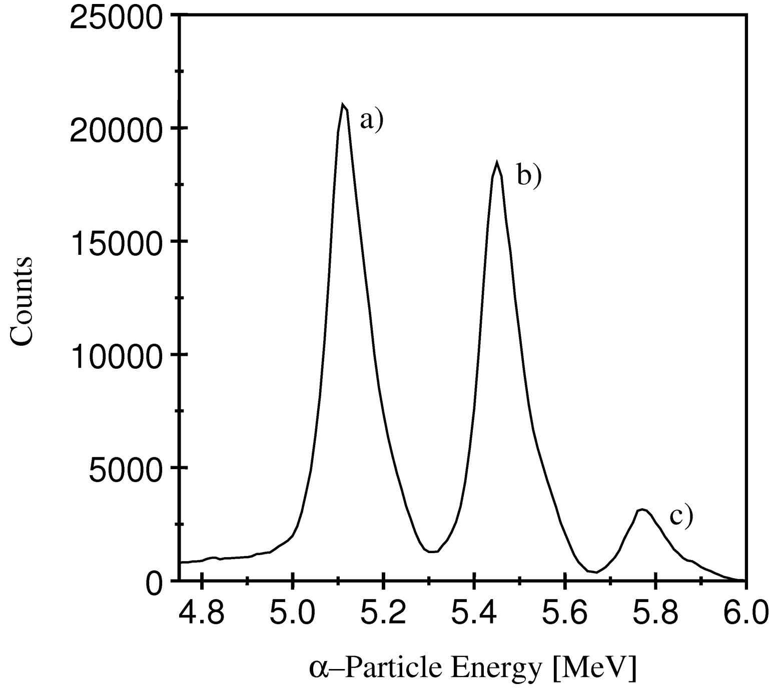

Figure 4.6: *Calibrated triple α-particle spectrum. It is possible to identify the three peaks, a, b and c corresponding to α-particles coming from the decay of* ^{239}Pu*,* ^{241}Am *and* ^{244}Cm *respectively.*

4.6 Reaction and Kinematics

In these measurements a ^{4}He beam with an energy of 40 MeV was used to bombard a 100 μgcm^{-2} ^{12}C target in which the reaction of interest for this experiment was ^{12}C(^{4}He,3α)^{4}He, in which 3 of the 4 α-particle products were detected using an array of four 500 μm thick double-sided silicon-strip detectors (DSSSDs) as shown above in Fig. 4.1. The detectors were mounted on aluminum bases as Fig. 4.7 shows, held to the steel base plate by rare-earth (neodymium) magnets. It is also possible to observe the beam collimator and anti-scatter which defines the beam spot size and some shielding structures used in order to avoid particles scattered from the collimator reaching the detectors. The entrance and the exit of the collimator are made of lead with a diameter of 2 mm and 4 mm respectively.

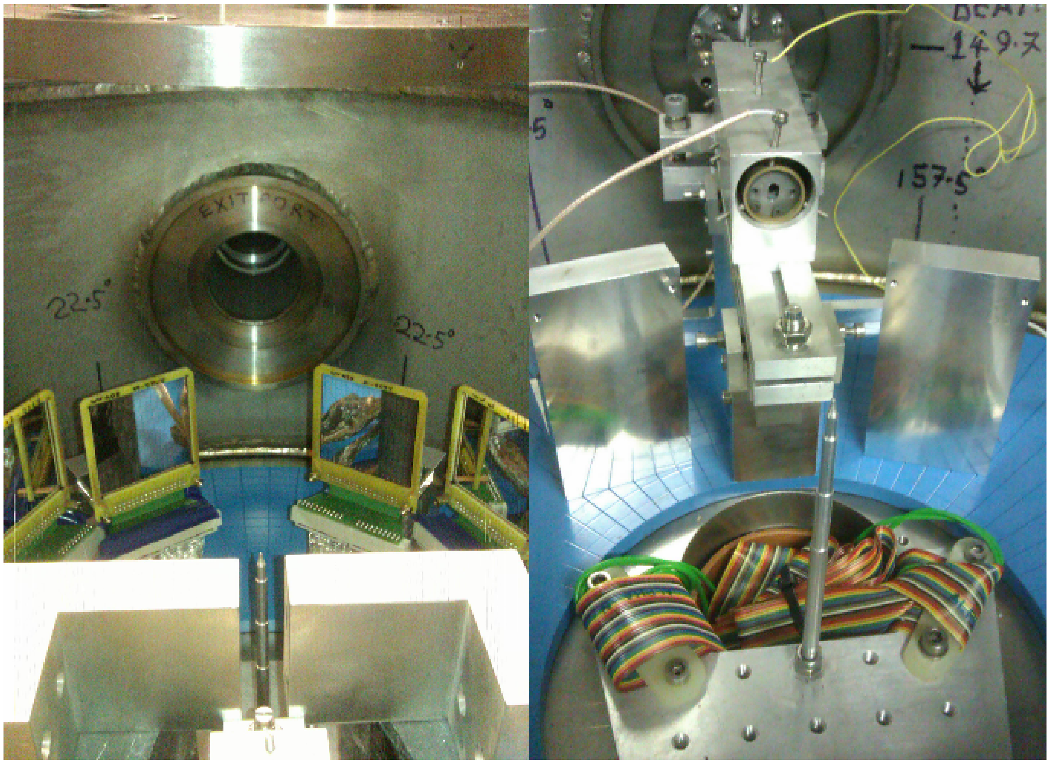

Figure 4.7: *Detector array (left) and collimator system (right) inside the chamber.*

CHAPTER 5

ANALYSIS AND INTERPRETATION

In the following sections, results from the experiment are presented. Firstly, the analysis procedure used to determine the beam energy, subsequently selection of the data, filtering and gating as well as the spectrum generating process to identify the populated resonances in ^{12}C. Following this, the angular correlation technique applied to extract their spin is given. Finally, a comparison between the Monte-Carlo simulations and the experimental data is presented along with the results for the spin of the newly observed resonance at 22.4 MeV.

5.1 Data Analysis Procedure

5.1.1 Determination of the Beam Energy

During the experiment, the beam energy was not precisely known. Theoretical kinematic lines for the recoiling beam particles were compared to the observed experimental lines in order to determine the beam energy. The theoretical lines are shown in Fig. 5.1 corresponding to those recoil α-particles (scattered beam) related to the decay of the different excited states in ^{12}C populated during the reaction. From top to bottom, a) is related to the decay of ^{16}O which was also populated during the reaction, b) ground state, c) 4.438 MeV (2^+), d) Hoyle state at 7.653 MeV (0^+), e) 9.641 MeV 3^-, f) 10.844 MeV 1^-, g) 14.083 MeV 4^+, h) a possible state that has not previously been observed and its description and characterisation are the main aim of the present work and i) which is related to the ^{1}H nucleus, produced during the decay of ^{16}O. This chapter describes only the analysis performed for those resonances related with the ^{12}C nucleus.

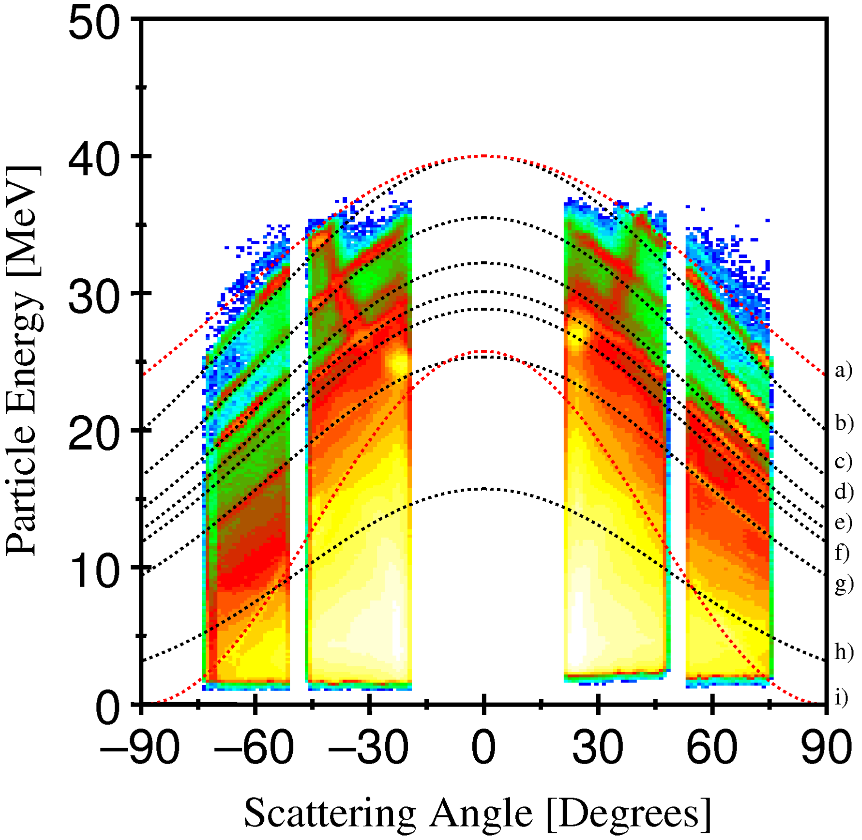

Figure 5.1: *Calculated kinematic lines and experimental data. Red dotted lines a) and i) correspond to α-particles coming from the decay of ^{16}O and ^{1}H respectively. Black dotted lines b), c), d), e), f), g) and h) are the recoil α-particle lines corresponding to the 0.0, 4.43, 7.65, 9.64, 10.84, 14.08 and 22.4 MeV ^{12}C states respectively.*

In Fig. 5.1 it is possible to observe a mismatch between the high energy theoretical kinematic lines and the experimental ones. The reason for this inconsistency could be caused by the energy of the α-particles used to calibrate the detector system, for which, as mentioned in Section 4.5.1, the energies of the α-particles were around 5 MeV. When extrapolating the values of the low energy α-particles the match is almost perfect, but because of the low energy of the source, the more energetic the particles are, the worse the calibration becomes. To correct this problem it would be better to have either an energetic α-source similar to the energy of the beam, which is clearly not possible. The gain-matching process therefore looks as though it was done correctly since it works well for all the individual detector strips which end up with an almost identical energy response. The energies of the known ^{12}C states can be used to correct for any extrapolative effect in the calibration gradient. See Fig. 5.8 and associated text. The cyclotron operators did not have an accurate value of the beam energy, but it was approximately 38.5 MeV. From the comparison of the theoretical and experimental kinematic lines it is possible to observe that the elastic scattered beam (line b) corresponding to the ground-state on Fig. 5.1) has an energy of 40 MeV (± 0.5 MeV); this energy value was found by varying the kinematic curves until a good agreement was found. It was this value for the beam energy that was subsequently used in the kinematic construction that follows.

5.1.2 Total Energy Spectrum

The spectrum of the sum of the three α-particle energies and the recoil α-particle is calculated using Eqn. 3.18 and is shown in Fig. 5.2, in which the Q-value completes the beam energy of E_{beam}=40 MeV. Events within the peak are selected for the reconstruction of the ^{8}Be and used for the analysis below. This peak corresponds to the reaction Q-value for all four final-state α-particles which are in their ground state.

Gating on ^{8}Be

With the information provided from the detectors, *i.e.* the energy and angle for each detected α-particle and the reaction kinematics, it is possible to identify events and also to reconstruct the momentum for each particle. Using the principle of momentum conservation (Eqns. 3.16 and 3.17) the momentum and energy of the fourth, undetected particle, was cal-

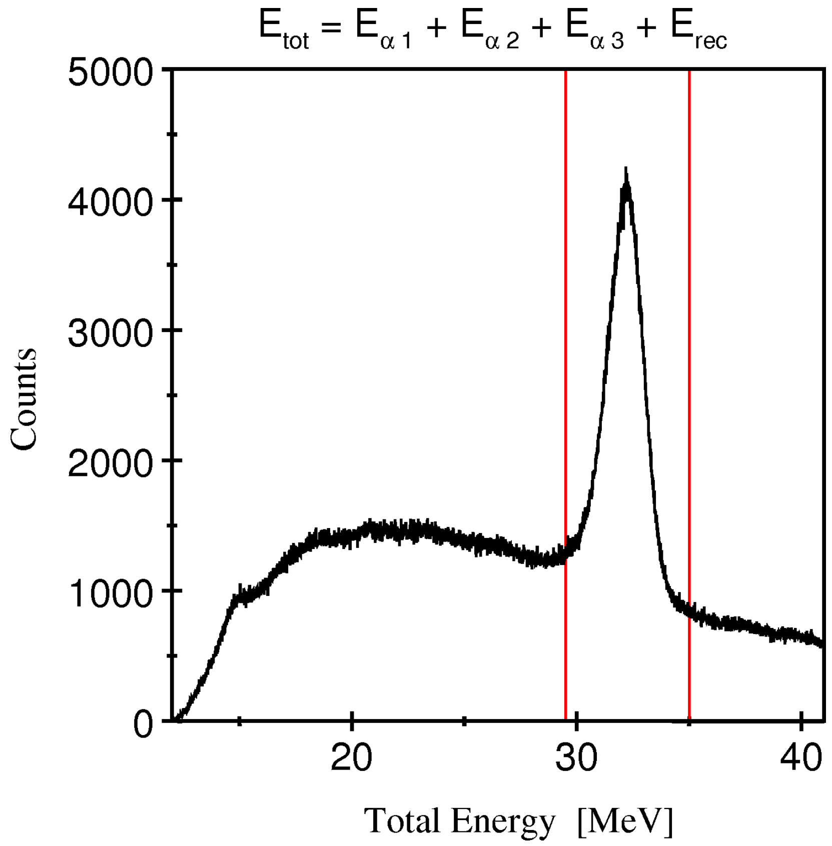

Figure 5.2: *Total energy spectrum. The data within the peak between the red lines were selected assuming they were proceeding form the* $^{12}C(^{4}He,\ 3\alpha)^{4}He$ *reaction.*

culated. Following the calibration, the events within the desired energy range were recorded. Both events registered in the front (vertical strips) and back (horizontal strips) of the detectors were selected and the average between the two values of energy (front and back signal) was calculated for each hit, as well as the angles at which the particles were emitted. It was important to make an energy correction for the energy loss the particle suffers in its path through the target. These calculations were included in the user-defined code mentioned above.

The first step in the reconstruction was to calculate the Q-value of the reaction from the difference between the final and initial energies. By plotting this value it was possible to select those events of interest as shown in Fig. 5.2. This peak clearly identifies the reaction of interest, in which the Q-value for the reaction ^{12}C(^{4}He, ^{4}He + ^{4}He + ^{4}He)^{4}He is -7.275 MeV. The selection of the data was done by gating on those events close to the centroid of the peak (≈32.1 MeV).

Following this event selection, additional event filtering was implemented. Two of the three detected α-particles can come from the decay of the ^{8}Be ground-state and it is possible to select only those events. The reconstructed ^{8}Be spectrum is shown in Fig. 5.3, generated by choosing two α-particles selected from the gating made on the peak of Fig. 5.2 for which all combinations of the three detected α-particles were considered. This selection is implemented in the analysis code in which a comparison between the α-particle energy deposited into the front and rear strip of the detector has to be done in order to corroborate that both detection signals come from the same α-particles of interest. Alpha-particles are detected simultaneously and those coming from the decay of ^{8}Be are likely to hit the same detector, so, by identifying these events it is possible to calculate the sum of their relative energy. If the relative energy is equal to the centroid of Fig. 5.3 (break-up threshold of ^{8}Be), the event is selected because it is assumed that it proceeds from such α-decay. At the same time a third α-particle hits the detection system and its energy, along with the other two identified α-particles is compared in order to know its origin and corroborate if was a product of the ^{12}C* nucleus. The calculation of the relative energy of the ^{8}Be was performed using:

$$\underline{P_{^8Be}} = \underline{P_{\alpha 1}} + \underline{P_{\alpha 2}}, \tag{5.1}$$

$$P_{^8Be} \cdot P_{^8Be} = P^2_{^8Be} = (p_{\alpha 1(x)} + p_{\alpha_2(x)})^2 + (p_{\alpha_1(y)} + p_{\alpha_2(y)})^2 + (p_{\alpha_1(z)} + p_{\alpha_2(z)})^2 \tag{5.2}$$

and

$$E_{^8Be} = \frac{P^2_{(^8Be)}}{2m_{(^8Be)}} \tag{5.3}$$

The events selected through this method were filtered for further analysis. There are four different scenarios in which the 4α final state can be produced: the 3 detected α-particles came from the decay of states in ^{12}C; the ^{8}Be and the unobserved α-particle were related with the decay of the ^{12}C; the 2 detected particles and the unobserved particle came from the ^{12}C decay with only one of the detected particles originating from ^{8}Be decay; or it was also possible that ^{8}Be+^{8}Be reactions were observed where one of the ^{8}Be nuclei was produced in an excited state.

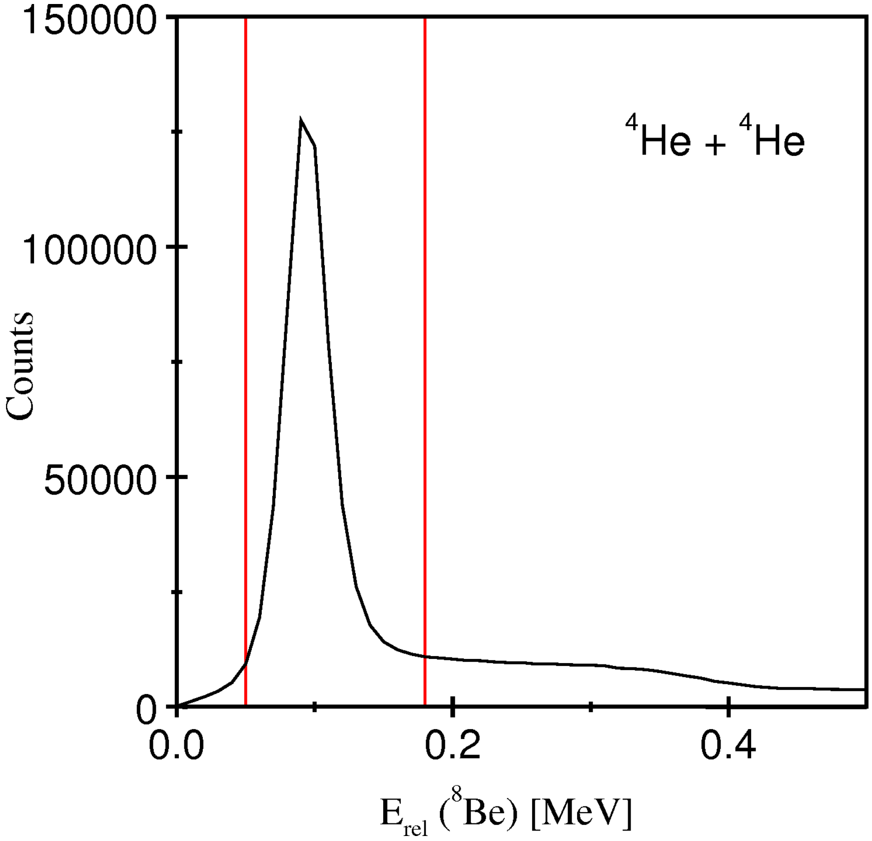

Figure 5.3: *Peak associated with the decay from the ^{8}Be ground state at 92 keV. Data between the two red vertical lines were selected for further analysis.*

Reconstruction of ^{12}C Excitation Energies

The next step after selecting those events arising from the decay of ^{8}Be in its ground state was the reconstruction of the ^{12}C excitation energies. Two scenarios were considered, first, it was assumed that the three detected α-particles were coming from the decay of the ^{12}C* and second, that two of the three particles were the product of the decay of the ^{8}Be in its ground state and the third undetected α-particle was reconstructed by momentum conservation. A representation for the two different possible combinations of detected particles which were used for further analysis is shown in Fig. 5.4.

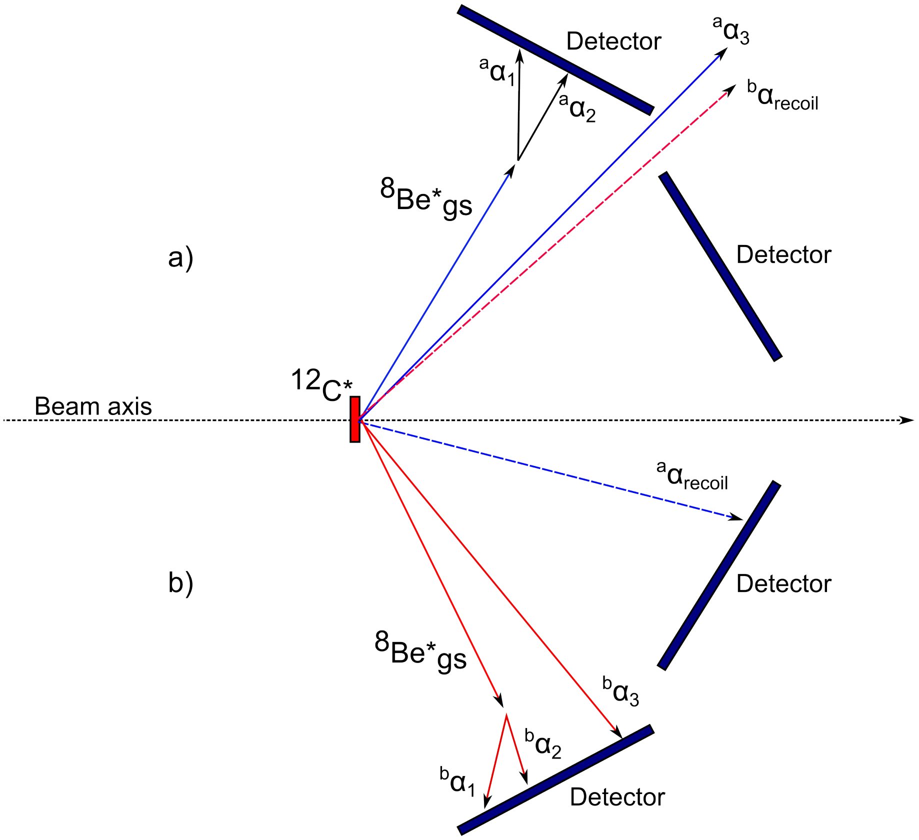

Figure 5.4: *Representation of the two different event detections. a) Detection of two α-particles coming from the decay of the ^{8}Be nucleus (α_1^a and α_2^a) and the scattered beam (α_{recoil}^a), blue lines. b) Detection of three α-particles coming from the decay of the ^{12}C excited nucleus (α_1^b, α_2^b, α_3^b), red lines.*

By plotting these two different assumptions one versus the other, it was possible to generate the Dalitz-like plot shown in Fig. 5.5. This plot contains specific and valuable information about the populated states. It is possible to observe features running parallel to the horizontal and the vertical axes, as well as diagonal ridges (gradient equal to -1). Along both axes, the ^{12}C resonances at 7.654 MeV 0^+ (Hoyle state), 9.641 MeV 3^-, 10.844 MeV 1^-, 14.083 MeV 4^+ and another resonance at 22.4 MeV can be clearly observed. The latter being the principal subject of the present work and will be discussed and characterised further. The diagonal ridges are those events which correspond from right to left to intermediate states in ^{8}Be: the ground state, 2^+ and 4^+ states. A gap is visible in the Dalitz-like plot on the top left area which is related with the angular coverage of the detector array; there is a big gap between the two detectors closest to the beam-line and a smaller gap between the detectors at bigger angles. The existence of these gaps implies that those areas are not sensitive to detecting the products of the reaction.

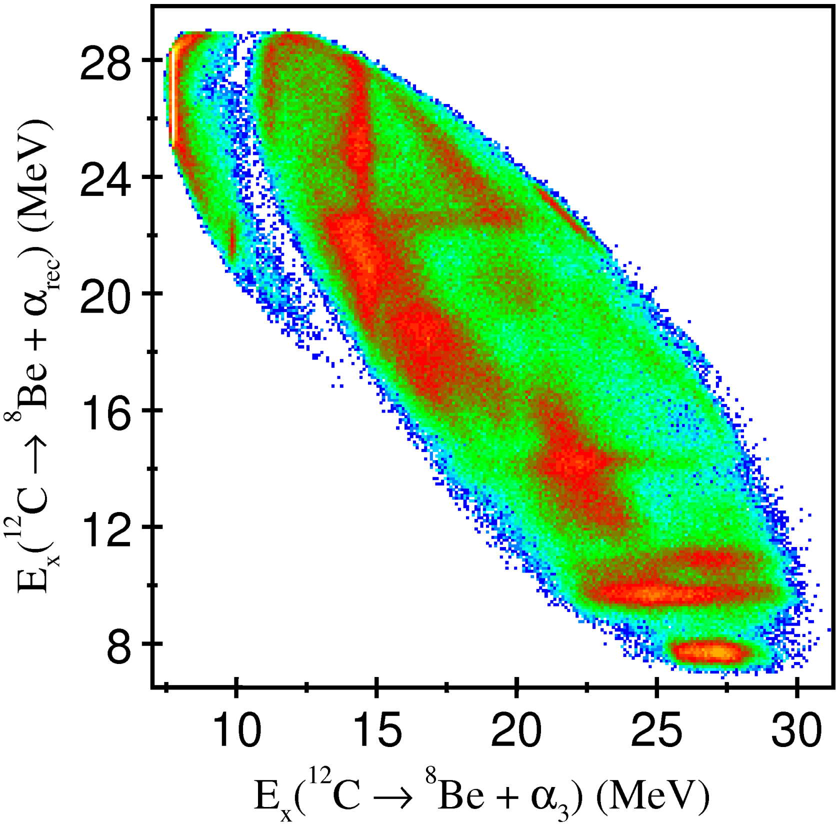

Figure 5.5: *Dalitz-like plot for the* $^{12}C(^4He,\ ^4He + {}^4He + {}^4He)^4He$ *reaction performed at a beam energy of 40 MeV. On the horizontal axis, the* ^{12}C *excitation energy is reconstructed from the three detected* α*-particles. On the vertical axis the* ^{12}C *excitation energy is reconstructed from two detected* α*-particles and the undetected particle.*

In order to have a clear view of ^{12}C from the Dalitz-like plot of Fig. 5.5, projections onto the horizontal and vertical axes are shown in Figs. 5.6 and 5.7 respectively. As mentioned above, different excited states in ^{12}C are present in the two spectra. Fig. 5.6 clearly has a peak at an energy of 22.4 MeV, which is observed here for the first time.

The spectrum in Fig. 5.6 shows the resonances populated during the ^{12}C(^{4}He, ^{4}He + ^{4}He + ^{4}He)^{4}He reaction. It is possible to observe, from left to right, the Hoyle state at 7.654 MeV, 9.641 MeV 3^-, 10.844 MeV 1^- and 14.083 4^+ MeV excited states in ^{12}C. Similarly, from the spectrum shown in Fig. 5.7 it is possible to observe those states populated, from left to right, the Hoyle state at 7.654 MeV, 9.641 MeV 3^-, 10.844 MeV 1^- and 14.083 4^+ MeV excited states in ^{12}C. Note that in reconstructing ^{12}C from three α-particles, the detector energy resolution appears three times, making the resolution of Fig. 5.6 worse than that of Fig. 5.7. The detector acceptance is also different in each case.

In order to get a more accurate value for the energy of the newly observed resonance the centroid of the peaks were calculated and a linear regression was applied to the well-known resonances. The fitted values are shown in Fig. 5.8, in which the energy value of the newly observed state lies at 22.4(0.2) MeV.

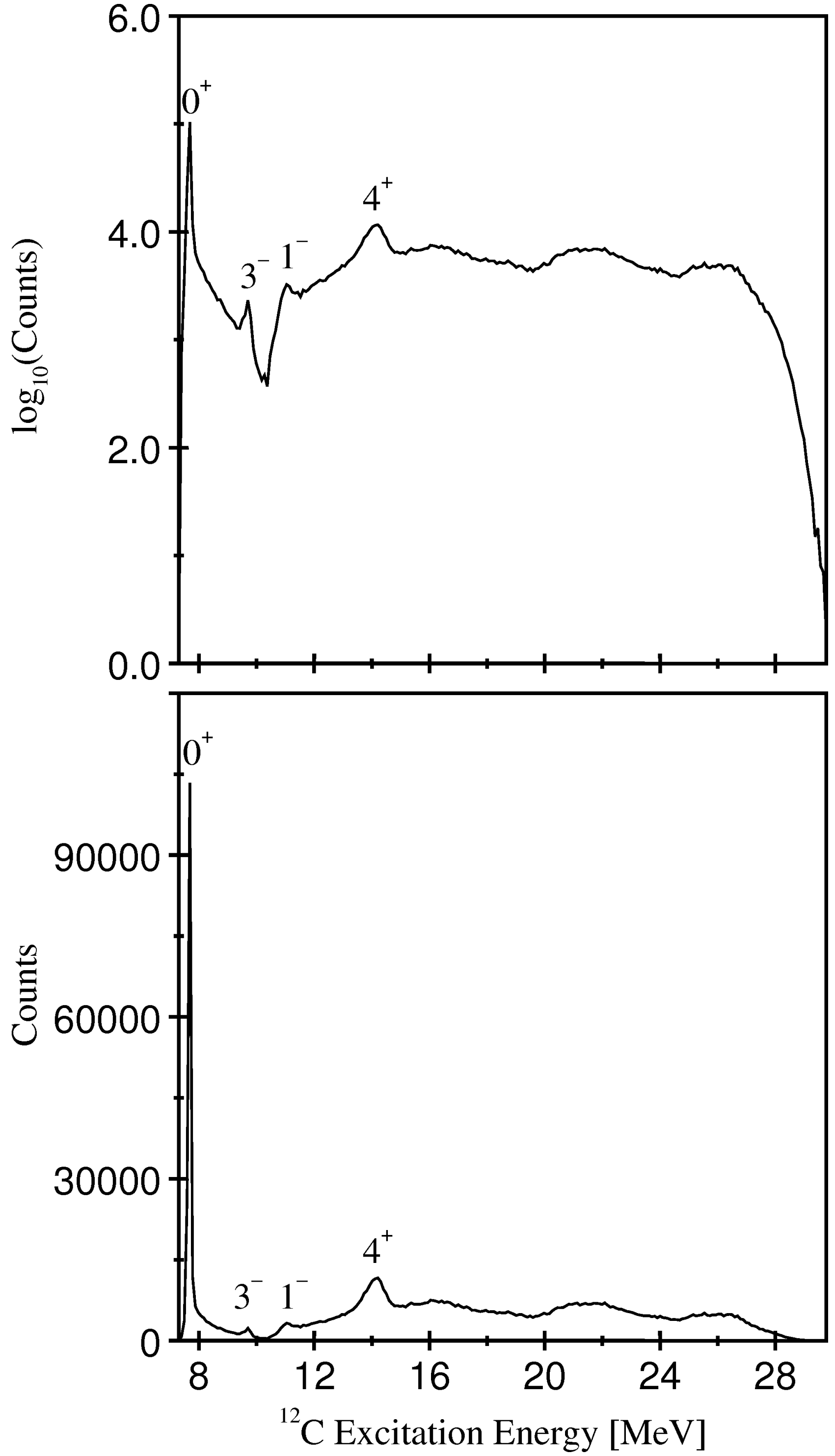

Figure 5.6: *Projection of the Dalitz plot of Fig. 5.5 onto the horizontal axis resulting in a spectrum of* ^{12}C *resonances, reconstructed assuming that the three detected* α*-particles came from the decay of* ^{12}C*. Both top and bottom panels show the same data, but the vertical scale of the top panel is logarithmic.*

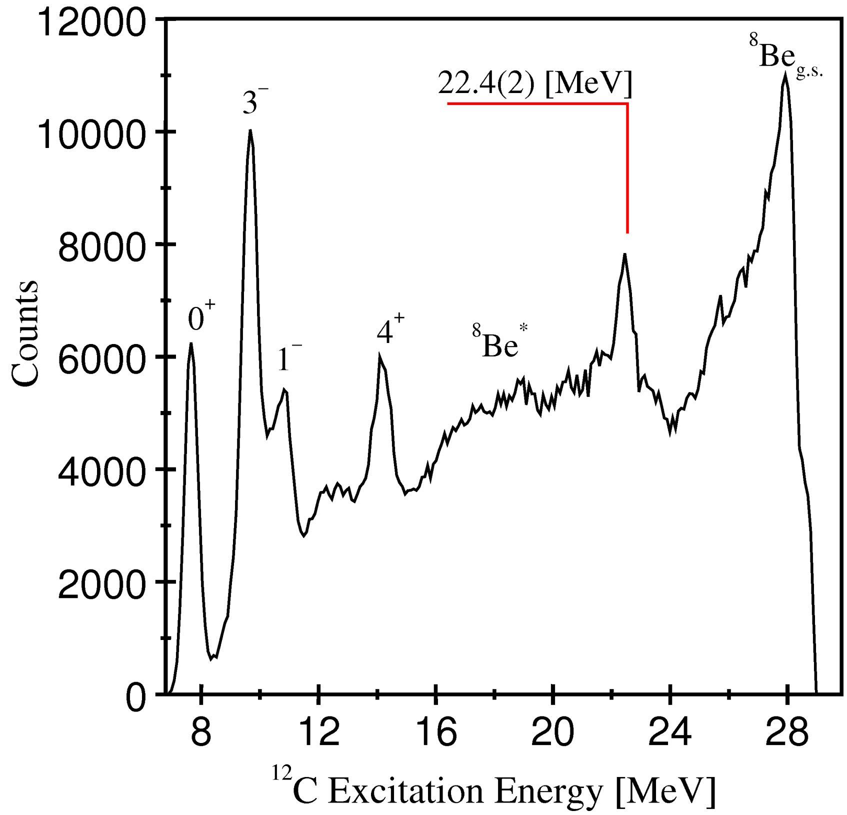

Figure 5.7: *Projection of the Dalitz plot of Fig. 5.5 onto the vertical axis resulting in a spectrum of ^{12}C resonances, reconstructed from two detected α-particles (coming from the decay of ^8Be in its ground-state) and the undetected particle. The bump between 16-19 MeV is related to events coming from the decay of ^8Be resonances.*

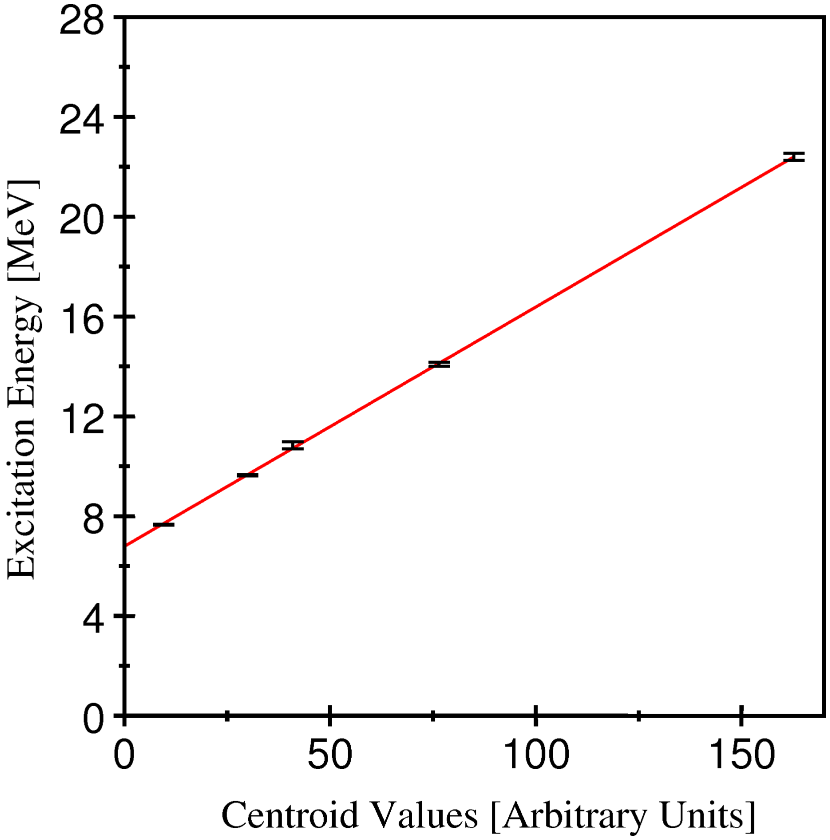

Figure 5.8: *Linear regression applied to the known excitation energies. The fit has been done only to the lowest four resonances and therefore is extrapolated in order to show the energy of the newly observed state.*

5.2 Angular Correlation Analysis

5.2.1 Well Known Resonances in Carbon-12

As mentioned in Section 3.4, angular correlations are a powerful tool in order to obtain a description of the new state by studying the distribution pattern of the α-particles in the decay [25]. This procedure was first applied to the well-known resonances, 9.641 MeV 3^-, 10.844 MeV 1^- and 14.083 MeV 4^+, with the purpose of verifying the analysis technique. Since the initial and final products are spin zero, any grazing angular momentum, l_{gr}, and the gradient of the ridges for a particular excited state populated with the ^{12}C(^{4}He, ^{4}He + ^{4}He + ^{4}He)^{4}He reaction can be calculated. As some of the resonances populated in the reaction are well known in terms of their spin (7.654 MeV, 9.641 MeV, 10.844 MeV and 14.083 MeV), a process can be undertaken to confirm the robustness of the angular correlation method. With this in mind, the gradient ${}^{\Delta\theta^*}/{}_{\Delta\Psi}$ required for angular correlations analysis has to be calculated for different values of spin J= 1, 3, 4, 5 and 6 and this procedure is explained in the following section.

Grazing Angular Momentum Calculation

In order to calculate the grazing angular momentum for a specific resonance it is first necessary to calculate the total angular momentum, l_{gr}, for a specific spin J value. This procedure is performed using a code written in fortran in which Eqns. 3.29 to 3.31 are used [52]. The calculations are also performed for different r_0 values and so, the results yield different values for l_{gr}. These results are shown in Table 5.1.

As can be seen from Table 5.1, the l_{gr} and the ridge angle values are different for each r_0. This ambiguity can be resolved from the analysis of the two dimensional angular correlation plots, generated by plotting θ^* *vs.* Ψ for each resonance. For this, it is important to use only events related to a specific excitation energy. It is here where the Dalitz-like plot of Fig. 5.5

$\mathbf{r_0}$ **(fm)**	l_{gr} ($\hbar$)	$\frac{\Delta\theta^*}{\Delta\psi}$, $\boldsymbol{J}$**=1**	$\frac{\Delta\theta^*}{\Delta\psi}$, $\boldsymbol{J}$**=3**	$\frac{\Delta\theta^*}{\Delta\psi}$, $\boldsymbol{J}$**=4**	$\frac{\Delta\theta^*}{\Delta\psi}$, $\boldsymbol{J}$**=5**	$\frac{\Delta\theta^*}{\Delta\psi}$, $\boldsymbol{J}$**=6**
1.1	9.0	7.1°	28.8°	46.2°	72.3°	116.1°
1.2	9.8	6.5°	25.3°	39.7°	60.0°	91.1°
1.3	10.6	5.9°	22.6°	34.7°	51.2°	74.8°
1.4	11.4	5.5°	20.4°	30.9°	44.7°	63.6°
1.5	12.2	5.1°	18.6°	27.8°	39.6°	55.2°

Table 5.1: *Calculation of the grazing angular momentum, l_{gr}, and the ridge angles for different values of r_0 and J. In red colour are the theoretical values which best matched the ridge angles observed in the 2-d correlation plots for the well-known resonances. See text and Table 5.2 for details.*

plays its main role and it is used for placing windows around a specific 2-d excitation energy region, as shown in Fig. 5.9. Once the events have been selected, the calculation of θ^* and Ψ can be performed using Eqns. 3.19 and 3.23 and finally the gradient ${}^{\Delta\theta^*}/_{\Delta\Psi}$ can be obtained. For the case of the Hoyle state, which has a spin of zero, the gradient of the ridges should be zero as is shown in Fig. 5.10.

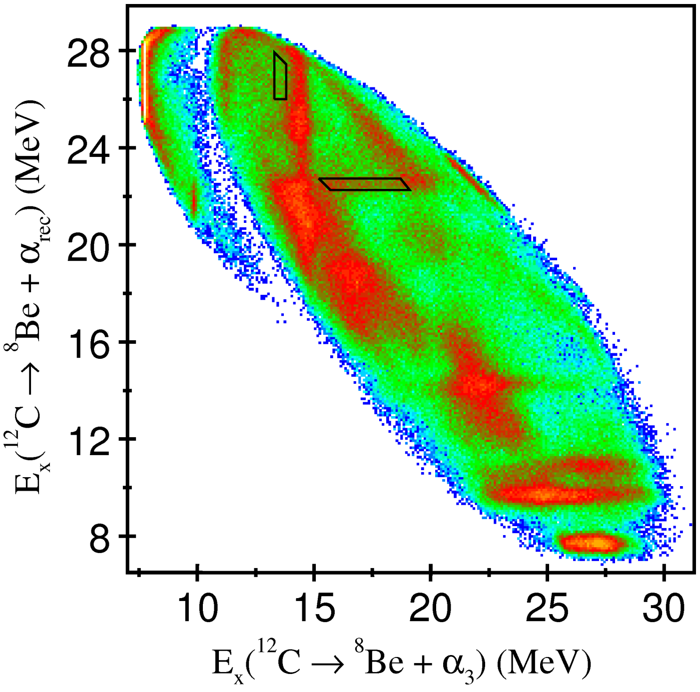

Figure 5.9: *Vertical and horizontal boxes (black colour) for the area selection for the angular correlation analysis for the 13.3 and 22.4 MeV respectively.*

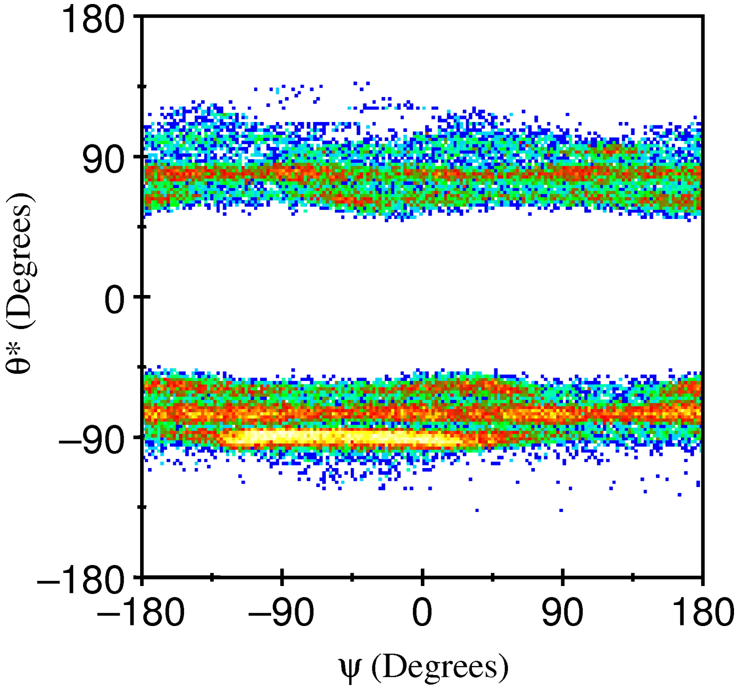

Figure 5.10: *Angular correlations for the Hoyle state.* θ^* *vs.* Ψ *angles.*

This resulting 2-d angular correlation plot is generated by placing a window in the Dalitz-like plot around the Hoyle state. As well as for the Hoyle state, the data selection for the 3^-, 1^- and 4^+ states was performed and the corresponding windows are shown in Fig. 5.11 for which the resulting angular correlation plots are shown in Figs. 5.12, 5.13 and 5.14 respectively. There, the dashed red boxes represent the windows used to select the specific area of interest. From these plots it is possible to observe the presence of ridges with a specific gradient for each state, as expected.

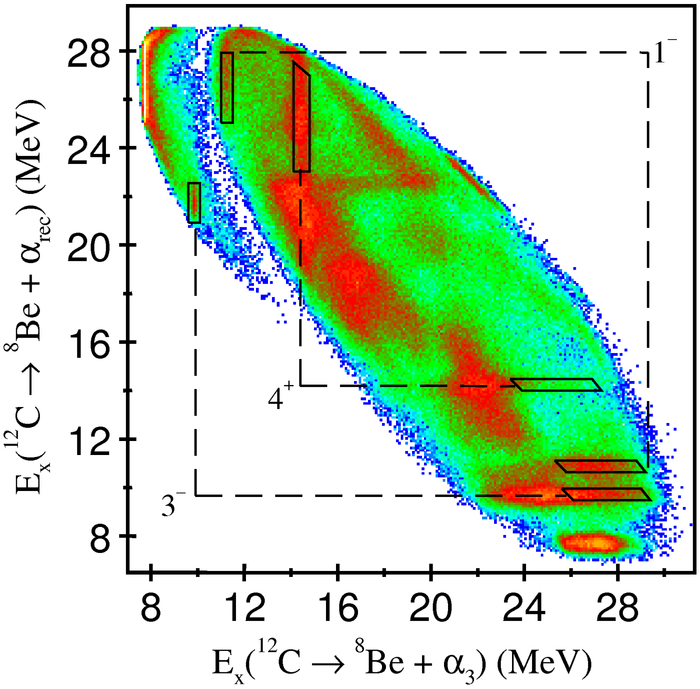

Figure 5.11: *Gates used to select specific areas. With this selection process it is possible to avoid those events which can influence as background as those close to the diagonal (gradient −1) corresponding to different excitations of* ^{8}*Be.*

Searching for the Projection Gradient

As mentioned earlier, from Eqn. 3.33 there is a relation between the Legendre polynomials, grazing angular momentum, the gradient of the ridges and the spin values of the states. For the present analysis, the projection of the angular correlation plots onto the horizontal Ψ-axis at an angle $^{\Delta\theta^*}/_{\Delta\Psi}$ is required, as mentioned above, given by Eqn. 3.28. The projection is then compared with the periodicity of the Legendre polynomials of different order, for which the best match will establish the spin of the state. In the first instance, the projections for a range of angles (see Table 5.1) were made and compared to the Legendre polynomial corresponding to the known spin. In Table 5.2 the value of the angles at which the periodicity of the projections match with the polynomials are shown. Comparing these values with those given in Table 5.1, it is possible to observe that the values in red represent the closest fit to the polynomial periodicity, yielding a grazing angular momentum $l_{gr} = 9.8\hbar$, (r_0=1.2 fm).

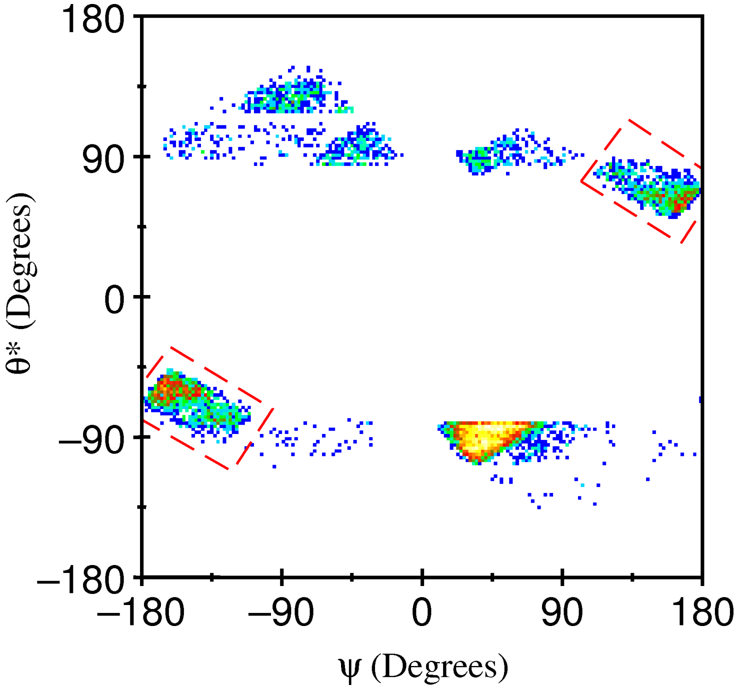

Figure 5.12: *Angular correlations for the 9.641 MeV resonance in* ^{12}C. θ^* *vs.* Ψ *angles. Red dashed boxes were use to select the area of interest.*

	$\frac{\Delta\theta^*}{\Delta\psi}$ $(^\circ)$	l_{gr} $(\hbar)$		$\frac{\Delta\theta^*}{\Delta\psi}$ $(^\circ)$	$\mathbf{l}_{gr}$ $(\hbar)$
***J*=1**	6.6	9.6	***J*=3**	22.4	10.6
	7.8	8.3		25.0	9.8
	14.7	4.9			
***J*=4**	28.4	12.0	***J*=5**	45.3	11.32
	37.7	10.0		60.0	9.7
	45.8	9.0			

Table 5.2: *Grazing angular momentum values calculated from the angles selected because of a close match with the Legendre polynomial periodicity.*

The projection of the angular correlations for the values bracketing the value chosen from Table 5.2 are shown in Figs. 5.15, 5.16 and 5.17.

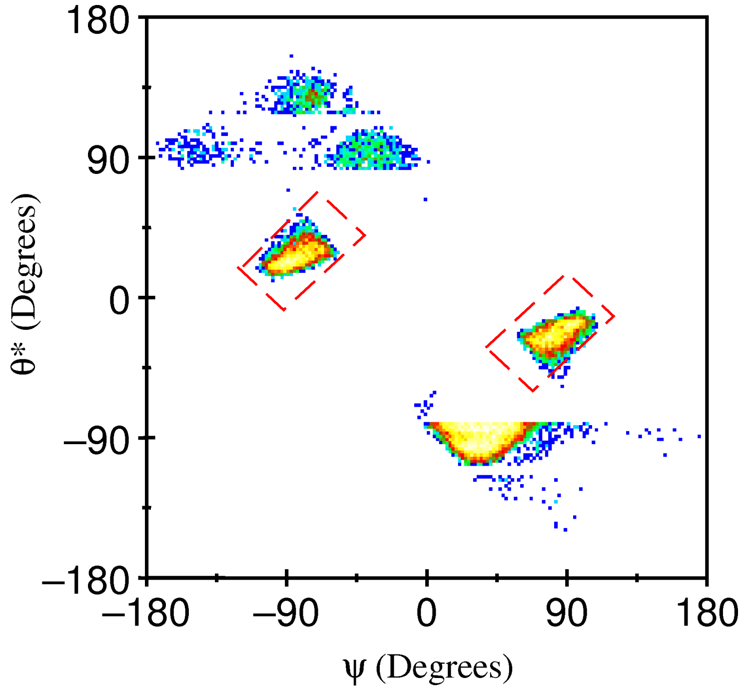

Figure 5.13: *Angular correlations for the 10.844 MeV resonance in ^{12}C. θ^* vs. Ψ angles. Red dashed boxes were use to select the area of interest.*

Extracting the spins J of the Well Known Resonances

As a final check on the consistency of the $l_{gr} = 9.8\hbar$ value, Table 5.3 combines the experimentally detected ridge gradients with thus chosen, $l_{gr} = 9.8\hbar$, and lists the corresponding spins, J, for each of the four states [53].

	$\frac{\Delta\theta^*}{\Delta\psi}$ (°)	J		$\frac{\Delta\theta^*}{\Delta\psi}$ (°)	J
E=10.84 MeV, J=1	6.6	1.0	**E=9.64 MeV, J=3**	22.4	2.74
	7.8	1.2		25.0	2.97
	14.7	2.00			
E=14.08 MeV, J=4	28.4	3.2	**J=5**	45.3	4.32
	37.7	3.9		60.0	5.11
	45.8	4.3			

Table 5.3: *Spin values, J, calculated from the projection angles made by "hand".*

The last step is to compare the projection onto the Ψ axis of the angular correlations for the 9.641 MeV 3^-, 10.844 and 14.083 MeV 4^+ states with the Legendre polynomials

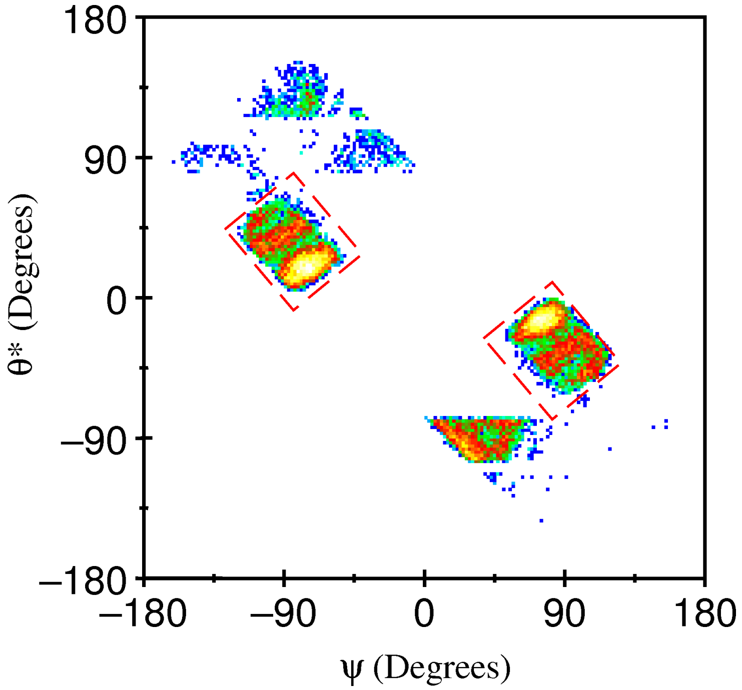

Figure 5.14: *Angular correlations for the 14.083 MeV resonance in ^{12}C. θ^{*} vs. Ψ angles. Red dashed boxes were use to select the area of interest.*

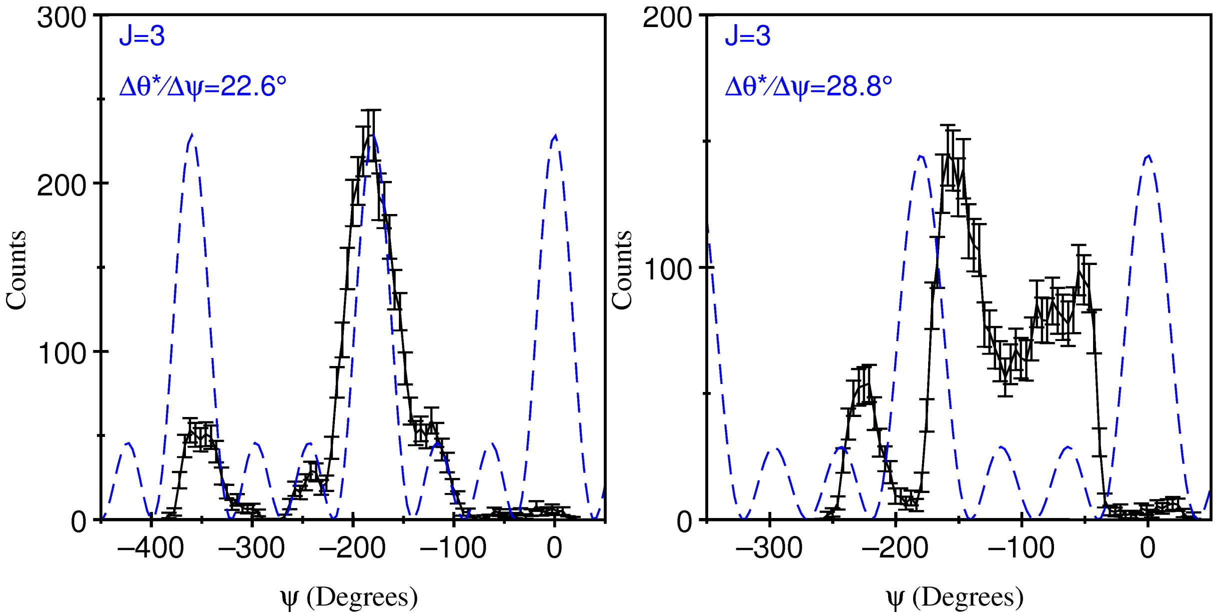

Figure 5.15: *Projection of the angular correlation data for the 9.641 MeV resonance onto the Ψ axis at angle of 22.6°(left) and 28.8°(right) compared with a Legendre polynomial of order J=3 for comparison (blue dashed line).*

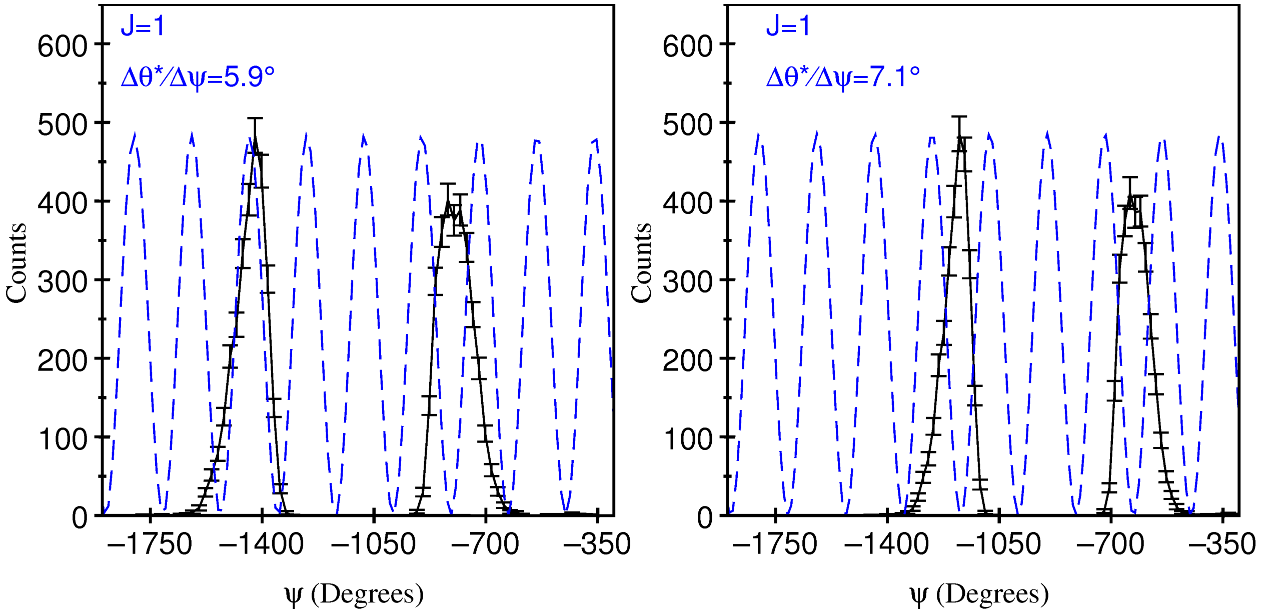

Figure 5.16: *Projection of the angular correlation data for the 10.844 MeV resonance onto the Ψ axis at angle of 5.9° (left) and 7.1° (right) compared with a Legendre polynomial of order J=1 for comparison (blue dashed line).*

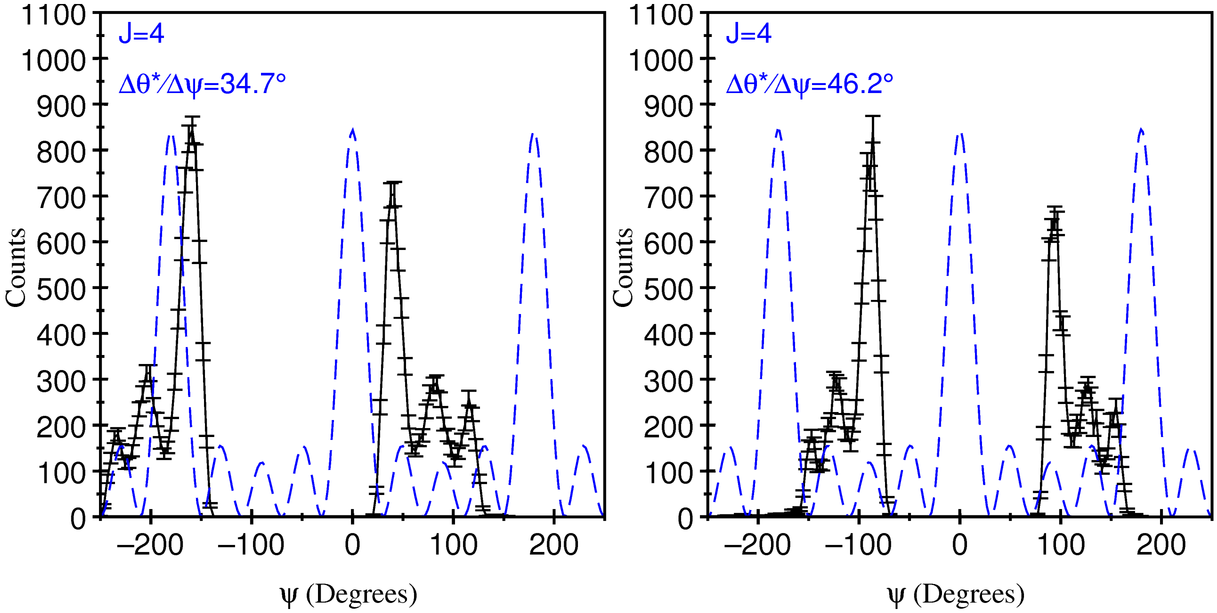

Figure 5.17: *Projection of the angular correlation data for the 14.083 MeV resonance onto the Ψ axis at angle of 34.7° (left) and 46.2° (right) compared with a Legendre polynomial of order J=4 for comparison (blue dashed line).*

$| \ P_3[\cos(\Psi)] \ |^2$, $| \ P_1[\cos(\Psi)] \ |^2$ and $| \ P_4[\cos(\Psi)] \ |^2$ respectively as shown in Figs. 5.18, 5.19 and 5.20. In conclusion, the correct projection angle values $^{\Delta\theta^*}/_{\Delta\Psi}$ corresponding to $r_0 = 1.2$ and a grazing angular momentum, $l_{gr} = 9.8\hbar$ should be 25.3°, 6.5°and 39.7°for the 3^-, 1^- and 4^+ states respectively. Figs. 5.18, 5.19 and 5.20 clearly show how the oscillations of the 9.641, 10.844 and 14.083 MeV resonances and the Legendre polynomials are in phase, with very good agreement confirming the established spins of the states (*J=3, 1, 4*), proving the effectiveness of the angular correlations. Since the purpose of these plots is only to show the periodicity of the oscillations, the data of these figures have not been normalised to account for the variation in acceptance or detection efficiency.

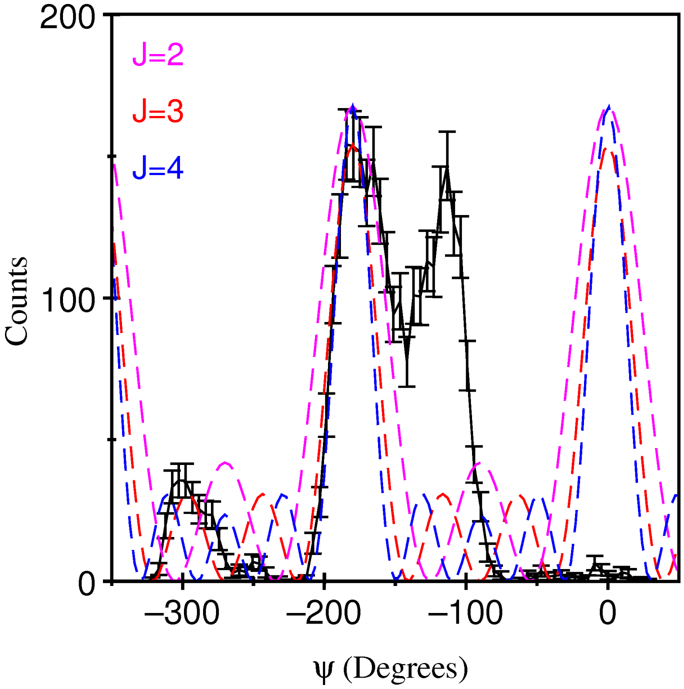

Figure 5.18: *Projection of the angular correlation data for the 9.641 MeV resonance onto the Ψ axis at angle of 25°(black line). The Legendre polynomials of order J=2, J=3 and J=4 are plotted for comparison (magenta, red and blue dashed lines respectively).*

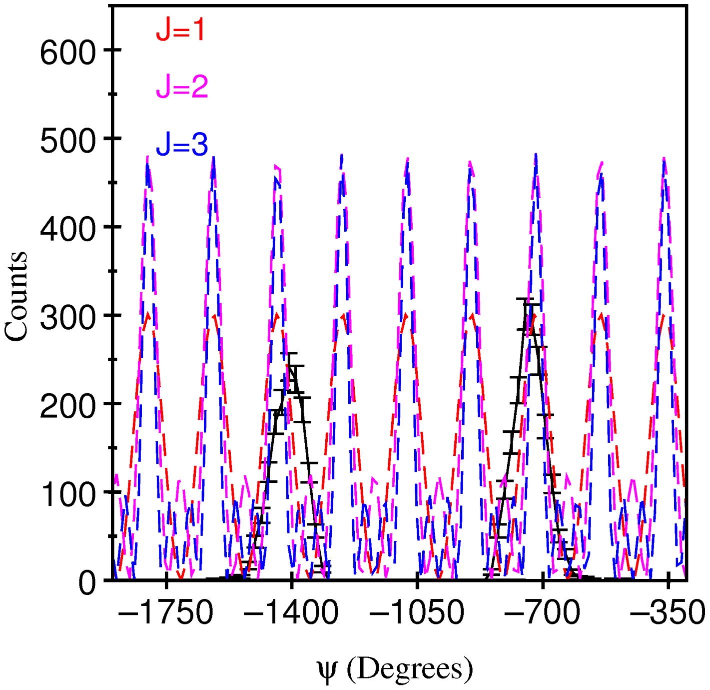

Figure 5.19: *Projection of the angular correlation data for the 10.844 MeV resonance onto the* Ψ *axis at angle of 6.6°(black line). The Legendre polynomials of order J=1, J=2 and J=3 are plotted for comparison (red, magenta and blue dashed lines respectively).*

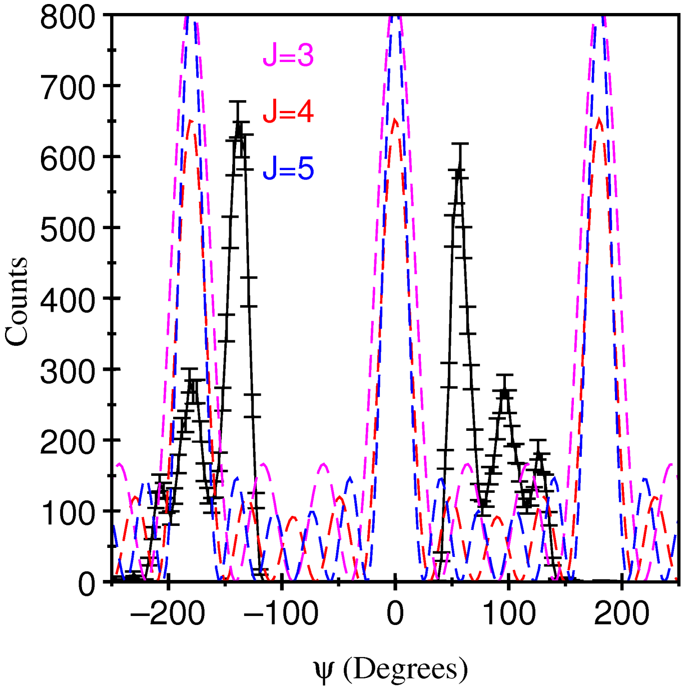

Figure 5.20: *Projection of the angular correlation data for the 14.083 MeV resonance onto the Ψ axis at angle of 37.7°(black line). The Legendre polynomials of order J=3, J=4 and J=5 are plotted for comparison (magenta, red and blue dashed lines respectively).*

5.3 Simulations – Data Normalisation

As mentioned in Section 4.1 this procedure was performed with the aim of correcting the experimental data for detector acceptance and also to confirm that the experimental data and their analysis is consistent with the simulations. The aim was to be confident with both, the procedure and results. Figs. 5.21, 5.22, 5.23, 5.25 and 5.27 show the comparison between the angular correlation plane governed by θ^* and Ψ for both the experimental data and the simulated data for the well known resonances in ^{12}C as well as for the 13.3 and 22.4 MeV excited states. The figures show a good agreement with the experimental data, though the statistics for the real data are lower than for the simulations, the latter having a wider area due to the uniform distribution selected for the simulations.

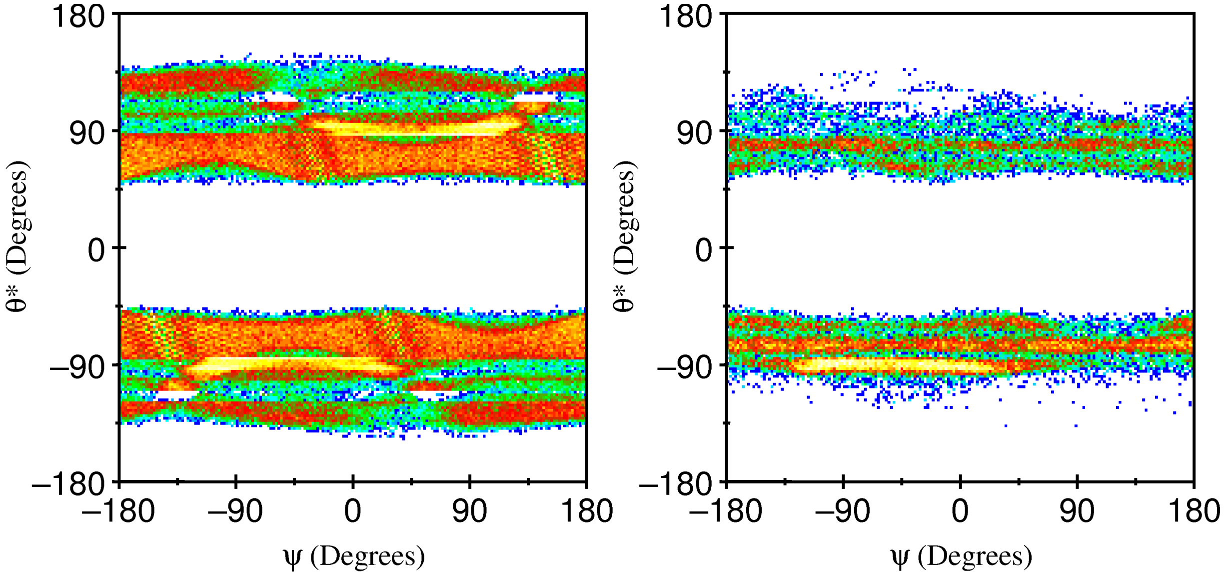

Figure 5.21: *Comparison between the angular correlations for the simulated data (left) and the experimental data (right) for the ^{12}C 7.654 MeV excited state. θ^* vs. Ψ angles.*

The simulations were performed using the *Resolution8* program described in Section 4.4.1. Using the Dalitz-like plot and the simulated data, the same windows as shown in Fig. 5.9 were

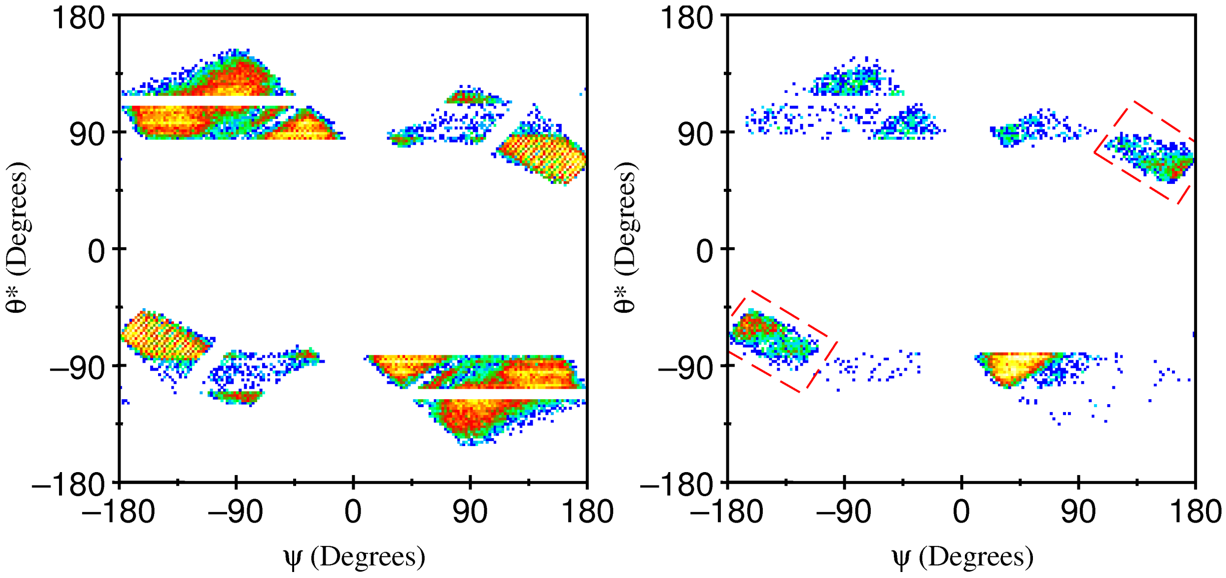

Figure 5.22: *Comparison between the angular correlations for the simulated data (left) and the experimental data (right) for the* ^{12}C *9.641 MeV excited state.* θ^* *vs.* Ψ *angles.*

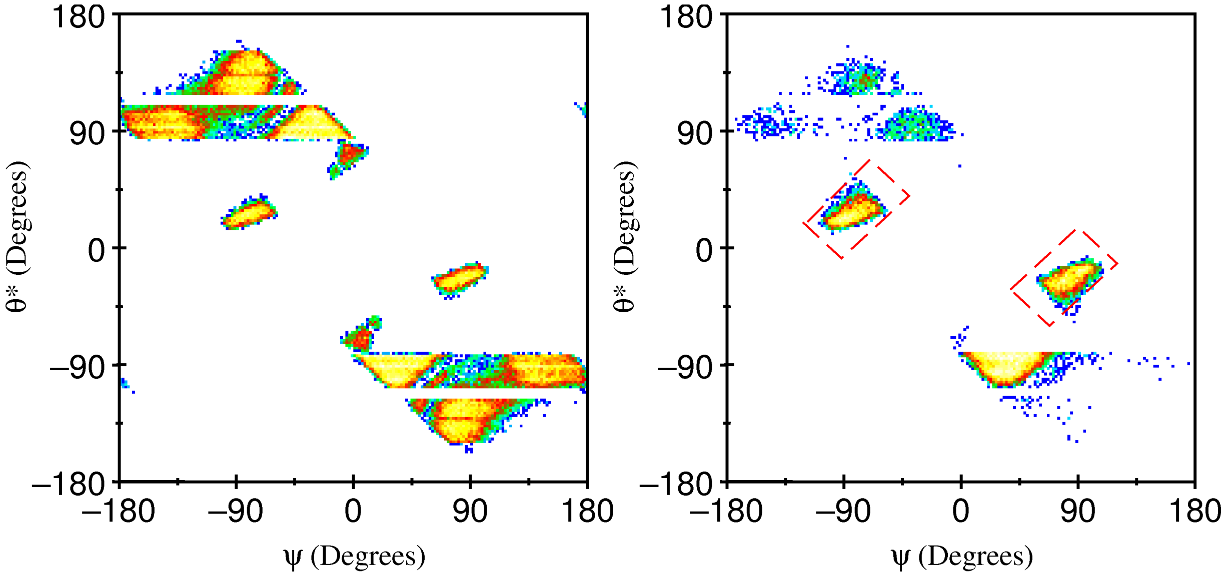

Figure 5.23: *Comparison between the angular correlations for the simulated data (left) and the experimental data (right) for the* ^{12}C *10.844 MeV excited state.* θ^* *vs.* Ψ *angles.*

used to select the areas of interest for both the simulations and the real data. The comparison shows a consistency between the areas from the simulated data and the experimental data, giving confidence in the angular correlation procedure applied for both, the well known

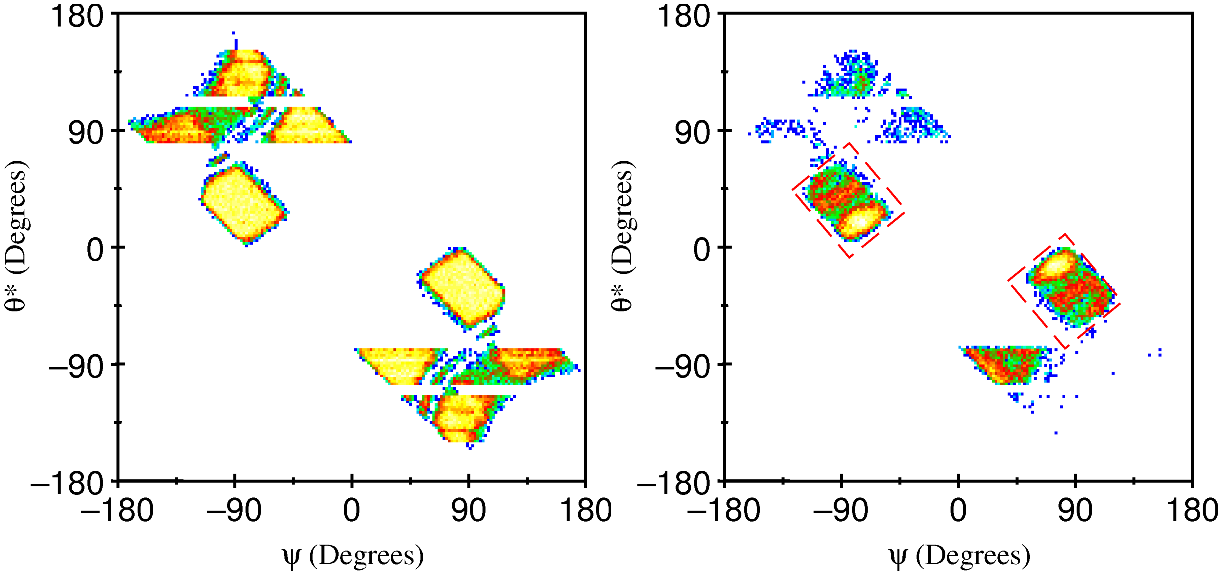

Figure 5.24: *Comparison between the angular correlations for the simulated data (left) and the experimental data (right) for the previously observed* ^{12}*C 14.083 MeV excited state.* θ^* *vs.* Ψ *angles.*

resonances and the previously observed 13.3 MeV excitation as well as for the newly observed level at 22.4 MeV.

5.3.1 The 13.3 MeV Resonance in Carbon-12

As outlined in Section 1.2.2, evidence for the 13.3 MeV resonance in ^{12}C has been obtained from several measurements [26, 54], along with tentative evidence for its spin. In order to extract its characteristic spin using the angular correlation method, events at this resonance energy were analysed. As for the well established resonances, the data corresponding to the 13.3 MeV resonance were selected from the Dalitz plot of Fig. 5.5, and the associated angular correlations are shown in Fig. 5.25. These are projected onto the Ψ axis in order to compare the data with the Legendre polynomial, for which order 4 was used, as shown in Fig. 5.26.

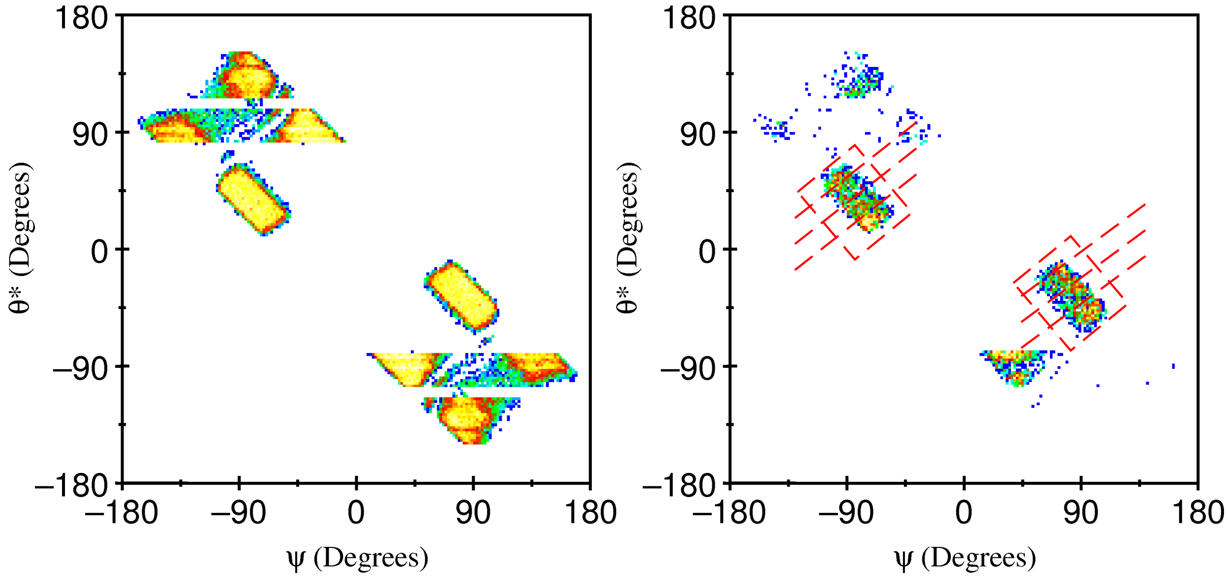

Figure 5.25: *Comparison between the angular correlations for the simulated data (left) and the experimental data (right) for the* ^{12}C *13.3 MeV excited state.* θ^* *vs.* Ψ *angles.*

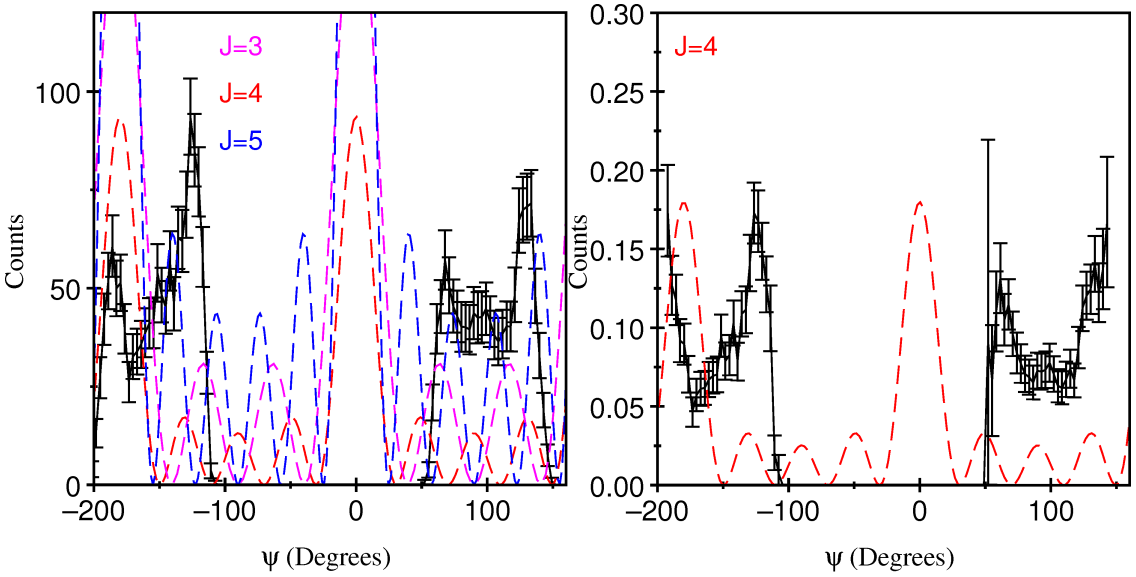

Figure 5.26: *On the left, the projection at angle of 39.7° of the angular correlation data for the 13.3 MeV (black line) resonance onto the* Ψ *axis before normalisation. The Legendre polynomials of order J=3, J=4 and J=5 are plotted for comparison (magenta, red and blue dashed lines respectively). On the right, the projection after normalisation and comparison with the Legendre polynomial of order J=4.*

5.3.2 The Newly Observed 22.4 MeV Resonances in Carbon-12

The same procedure was applied to the newly observed state at 22.4 MeV. The angular correlations for this state are shown in Fig. 5.27. The comparison of the angular correlation projection data with the Legendre polynomials of order 3 (red colour) and 5 (blue colour) is shown in Fig. 5.28. On Fig. 5.29 the comparison is with Legendre polynomials of order order J=4, 5 and 6 (red, blue and magenta respectively). From the measured α-spectrum and their angular correlations it is possible to conclude that the spin of the newly observed excited state at 22.4 MeV is most likely of a resonance with $J = 5$.

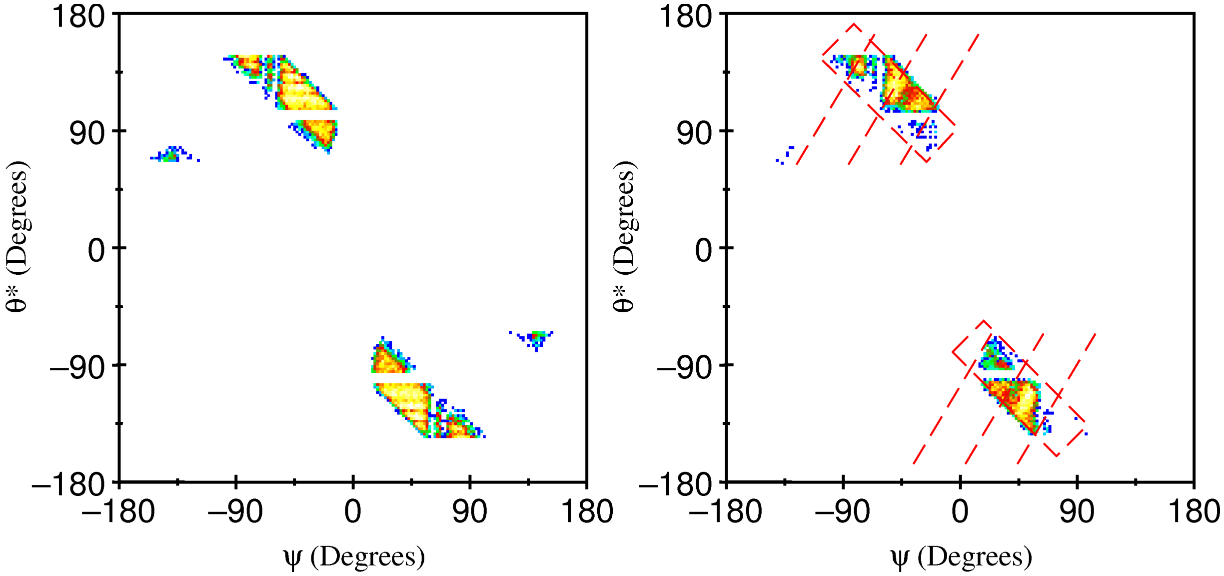

Figure 5.27: *Comparison between the angular correlations for the simulated data (left) and the experimental data (right) for the newly observed* ^{12}C *22.4 MeV excited state.* θ^* *vs.* Ψ *angles.*

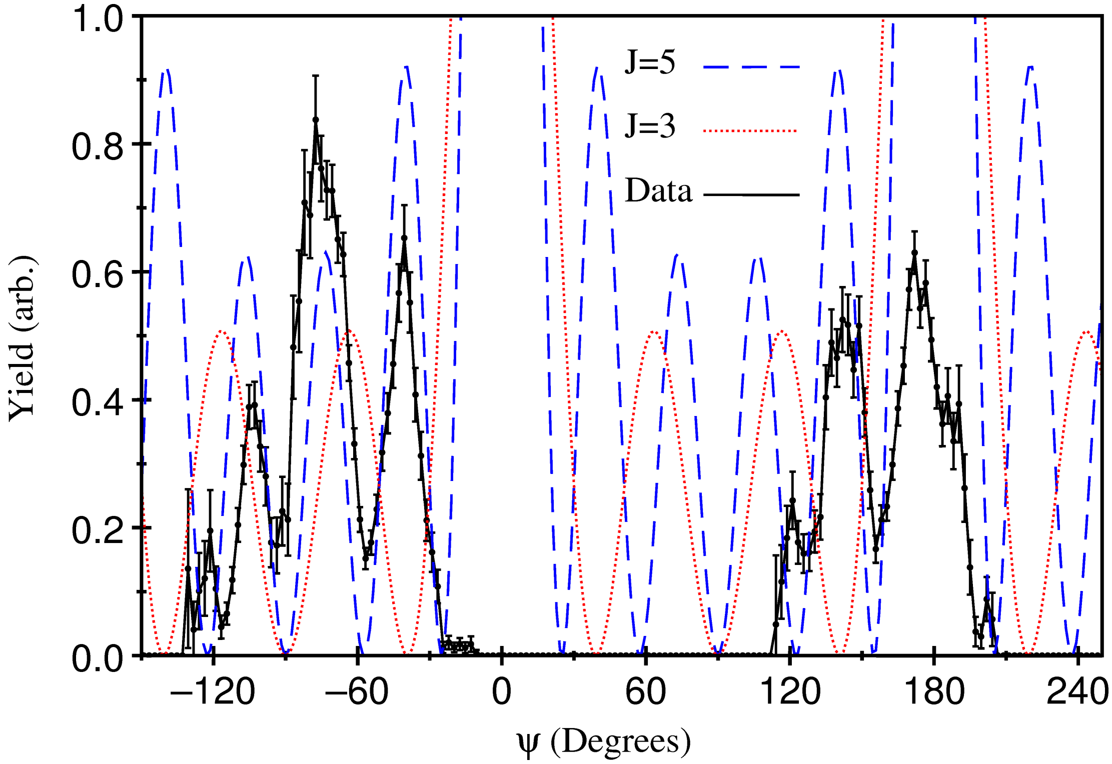

Figure 5.28: *Projection of the angular correlation data for the 22.4 MeV resonance onto the* Ψ *axis at angle of 60.0° (black line). The Legendre polynomials of order J=3 and 5 are plotted for comparison (red and blue respectively). from Ref. [12].*

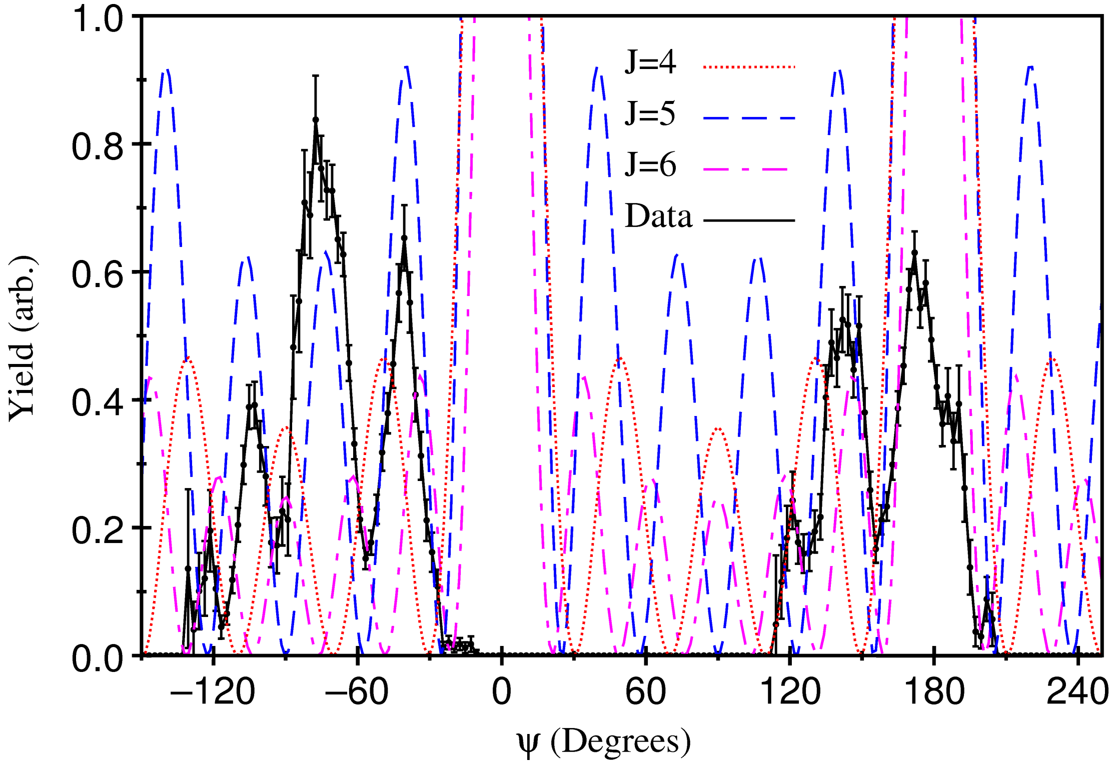

Figure 5.29: *Projection of the angular correlation data for the 22.4 MeV resonance onto the* Ψ *axis at angle of 60.0°(black line). The Legendre polynomials of order J=4, 5 and 6 are plotted for comparison (red, blue and magenta respectively).*

5.4 Theoretical Interpretation

In the alpha cluster model (ACM) approach for a ^{12}C nucleus, three α-particles are located at the vertices of an equilateral triangle [42, 55]. According with this model, using Eqn. 2.11 it is possible to generate an spectrum which is shown in Fig. 5.30, where it is possible to observe three different bands, with specific angular momenta and parity values. The first and the second are the ground-state rotational band and the Hoyle-band, comprised by resonances with angular momenta and parity values J^{π}=0^{+}, 2^{+} and 4^{+} for the case in which the projection of J onto the symmetry axis is K=0; J^{π}=3^{-}, 4^{-} and 5^{-} (the last one previously unobserved) for K=3. The parity doublet gives a strong signature of a J^{π}=$4^{\pm}$ doublet, also present in the two bands. The third band, the bending vibration, has a sequence predicted to be J^{π}=1^{-}, 2^{-}, 3^{-}, 4^{-} for K=1, J^{π}=2^{+}, 3^{+}, 4^{+} for K=2 and J^{π}=4^{+} for K=4. See [55] and Section 2.1.7 for a detailed explanation.

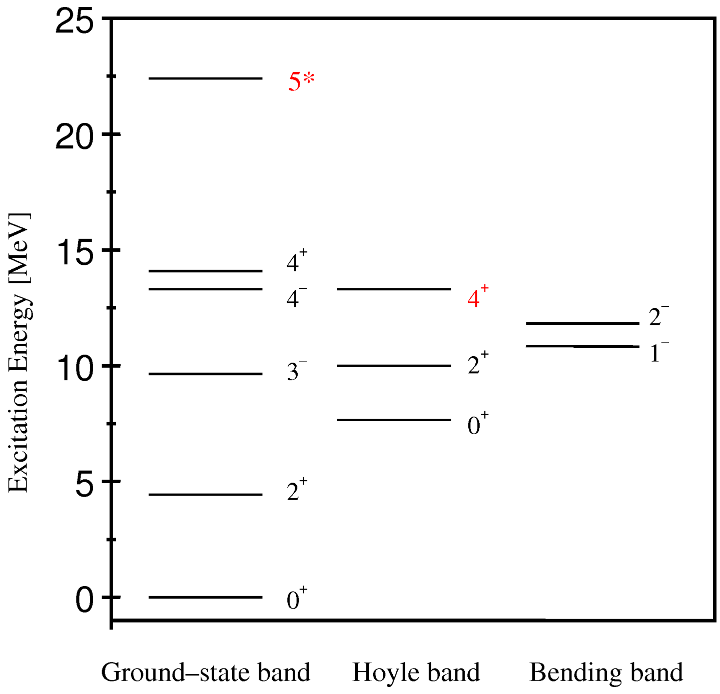

Figure 5.30: *Comparison between the spectrum generated for three clusters at the vertices of an equilateral triangle with $\mathcal{D}_{3h}$ symmetry using Eqn. 2.11.*

In agreement with the present model, the experimental sequences are the fingerprint of a configuration in which three particles are situated at the vertices of an equilateral triangle, with a $\mathcal{D}_{3h}$ symmetry, which belongs to the Dihedral group symmetry $\mathcal{D}_{nh}$; the symmetry group of a regular polygon with n sides (when $n>2$) and with $2n$ elements, *i.e.* n rotations and n reflections [56]. The first resonance of the Hoyle-band (Hoyle-state) is understood as the band head of a stretching vibration or breathing mode of the triangular configuration which shares the same geometrical array and structure as the ground state rotational band. The Hoyle state moment of inertia is predicted to have twice the magnitude of the ground state band [12]. And the third band, the bending band, with a band head at 10.84 MeV 1^-. In Fig. 5.31 it is possible to observe the ground and Hoyle rotational bands as well as the bending vibration band in ^{12}C. The ground state band consists of the 0^+, 2^+, 3^-, $4^\pm$, and the newly observed 5^- resonances, following a $J(J+1)$ trajectory. The Hoyle-band comprises the recently identified 2^+ and 4^+ resonances; the sequence corresponds to a larger moment of inertia (shallower gradient) than the ground state. The bending vibration-band has assigned resonances with a moment of inertia with almost the same magnitude as the Hoyle-band [12].

In summary, through the ACM it is possible to describe the rotational and vibrational structure of many-body systems such as molecular, nuclear and hadronic physics, not just as rigid structures, but also as liquid-like structures. The model has also been used to describe the low-lying states in ^{16}O as four α-particles located at the vertices of a tetrahedral rotating and vibrating as an object with $\mathcal{T}_d$ symmetry [57]. In particular, for the present work, the results this model has produced in terms of the study of the ^{12}C nucleus are very important; the prediction of a resonance in ^{12}C at 22.4 MeV which was not previously observed and which was populated during the performance of the experiment as reported in the present work.

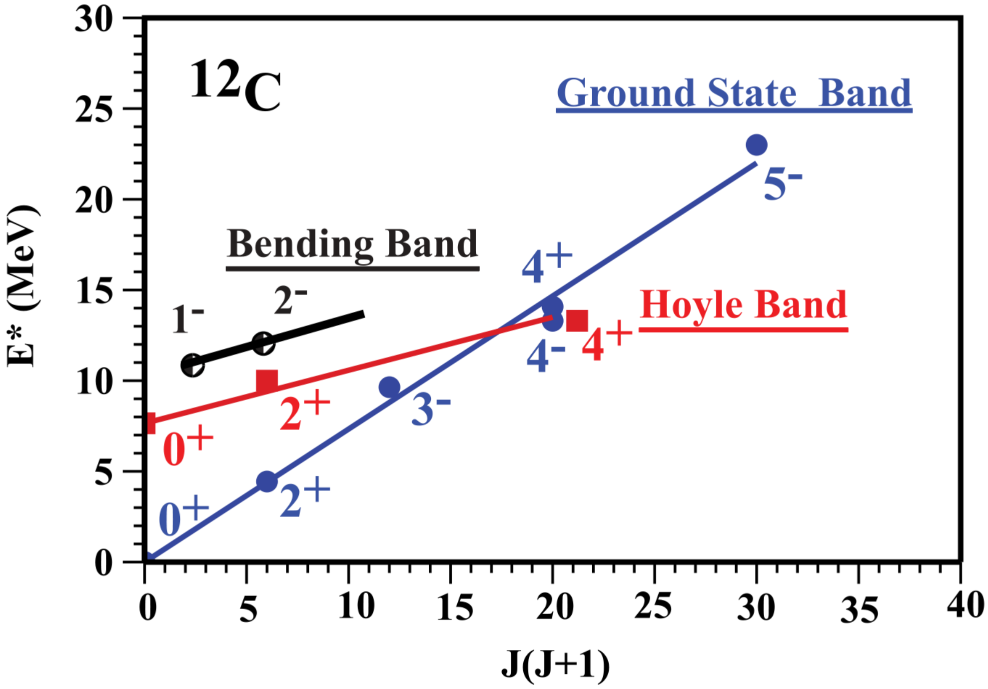

Figure 5.31: *Ground state rotational band structure (blue colour), Hoyle-band structure (red colour) and Bending band (black colour), from Ref. [12].*

CHAPTER 6

CONCLUSIONS AND FUTURE WORK

6.1 Conclusions

The measurement of the ^{12}C(^{4}He,^{4}He+^{4}He+^{4}He)^{4}He reaction has been performed using four DSSSDs in a detector array with which three of the four final products of the reaction were detected and subsequently used to reconstruct the populated resonances in ^{12}C. Such excited states were well known *e.g.* as the Hoyle-state. The characterisation of the 13.3 MeV resonance was made, with the most probable spin and parity value being $J^{\pi} = 4^{+}$. Moreover, a resonance at 22.4 MeV was also populated, observed for the first time and an angular correlation analysis was performed in order to confirm its spin and parity, which was found to be $J^{\pi} = 5^{-}$. Furthermore, this newly observed resonance is evidence for triangular $\mathcal{D}_{3h}$ symmetry in the arrangement of the three α-particles in the ground state of ^{12}C. This is the first time such a symmetry has been established in nuclear physics [12], having previously been observed in molecular physics [41].

According to the algebraic cluster model, the 0^{+} Hoyle state in ^{12}C is interpreted as the band head of a symmetric stretching vibration or breathing mode of a triangular configuration, with a similar geometrical arrangement and rotational structure to the ground state rotational band in which three α-particles are situated at the corners of a triangle, but with a predicted moment of inertia larger than the ground state band.

The interpretation of this model, for the ground-state rotational band of ^{12}C suggests that it comprises both positive and negative parity states for K=0, J^{π}=0$^+$, 2$^+$, 4$^+$ and for K=3, J^{π}=3$^-$, 4$^-$ and 5$^-$, respectively. The K=0 and K=3 bands, usually considered as different bands, coalesce to form a unique ground state rotational structure and by merging them together leads to the predicted J^{π}=4$^{\pm}$ degenerate parity doublet which is also a strong signature of the $\mathcal{D}_{3h}$ symmetry. The 1$^-$ state at 10.84 MeV is assigned as the bandhead of the vibrational bending mode whose lowest-lying rotational excitations consist of degenerate parity doublets of 2$^{\pm}$ 3$^{\pm}$ states, for which so far only the 2$^-$ has been identified.

Whereas the observed moment of inertia of the Hoyle-band excludes the proposed linear chain structure of the Hoyle state, there are other two geometrical alternatives of either equilateral triangular arrangement or a bent arm structure are considered for the arrangement of the three alpha particles in the Hoyle state, the latter can be resolved by the future measurements proposed below.

The Birmingham group carried out a second experiment at the University of Birmingham MC40 cyclotron in which the ^{12}C(^{3}He,^{3}He)3α reaction at 40 MeV was used to populate the high excitation energy region in ^{12}C. Evidence was found of the existence of a series of states at 16.3(0.2), 17.2(0.2), 18.4(0.2), 19.7(0.2), 22.2(0.3) and 25.1(0.3) MeV, for which the 22.2(0.3) MeV excitation supports the observation of the 22.4 MeV resonance presented in this work [58], which has been important within both the algebraic cluster model description, giving strong support to its predictions. Apart from those predictions, the algebraic cluster model predicts several additional states, which require accurate data as measured for the second 2$^+$ Hoyle-state.

6.2 Future Work

Over the past years there has been a solid contribution both from the experimental and theoretical field to understand the physics of light nuclei in which the presence of α-cluster structures has been demonstrated. A clear example is the ^{12}C nucleus, for which special attention has been focused on one of its resonances, namely the Hoyle-state. The results of the present thesis included the measurement of a newly observed resonance and its characterisation, linked with the ground-state rotational band of ^{12}C. Despite this, it is evident that there is still a lot work to be done in order to fully and unambiguously characterise the structure of the Hoyle-state moving towards a full description of the ^{12}C nucleus. For the case of the rotational band associated with the Hoyle-state, the measurement of the existence of a 2^+ resonance has been established, though its connection to the Hoyle-state is vague including its electromagnetic properties and α-decay partial widths [28, 59].

Even though there is significant evidence pointing to the existence of a broad 4^+ resonance at 13.3 MeV, additional work is required in order to corroborate its existence and character unequivocally. In the near future new measurements involving high statistics, precision measurements of the relatively weak electromagnetic transitions are needed [60] as well as experiments involving the selectivity of γ-ray beams as well as electron beams would aloud the population of the states of interest and resolve the broad interfering states mentioned above. Another example is a detailed measurement of the α-decay correlations following proton and α-inelastic scattering measurements using the high energy resolution spectrometers, as was demonstrated previously for ^{12}C excited states in the 16-24 MeV range in a proton scattering experiment with a 156 MeV proton beam [61]. The purpose of such measurements is to address, in more detail, the properties of high spin resonances mentioned in references [12, 58], which are suggested to be higher-spin (5, 6) members of the more deformed structures linked with the Hoyle-state, ground-state or other ^{12}C structures. The latter, with the aim to understand the structure of ^{12}C at higher energies, in particular to pin down the T=1 and T=2 states, but also the search for higher spin members of the ground-state and the 3- bands. As well, a key step for the clearly identification of the Hoyle-band configuration will be the identification of the negative parity states 3^- and 4^- through electron scattering experiments. Carbon-12 is an interesting system and though our knowledge has improved significantly in recent years, there remains much work to be done. These experiments promises to shed new light on the clustering phenomena in light nuclei, in particular in ^{12}C nucleus, which its structure has been unknown for 60 years.

APPENDIX A

PUBLICATION: EVIDENCE FOR TRIANGULAR D3H SYMMETRY IN CARBON-12.

PRL **113,** 012502 (2014)   PHYSICAL REVIEW LETTERS   week ending
4 JULY 2014

Evidence for Triangular $\mathcal{D}_{3h}$ Symmetry in ^{12}C

D. J. Marín-Lámbarri,[1] R. Bijker,[2] M. Freer,[1] M. Gai,[3,4] Tz. Kokalova,[1] D. J. Parker,[1] and C. Wheldon[1]
[1]*School of Physics and Astronomy, University of Birmingham, Birmingham B15 2TT, United Kingdom*
[2]*Instituto de Ciencias Nucleares, Universidad Nacional Autónoma de México, A.P. 70-543, 04510 México, D.F., Mexico*
[3]*LNS at Avery Point, University of Connecticut, Groton, Connecticut 06340-6097, USA*
[4]*Wright Lab, Department of Physics, Yale University, New Haven, Connecticut 06520-8124, USA*

(Received 11 March 2014; published 30 June 2014)

We report a measurement of a new high spin $J^\pi = 5^-$ state at 22.4(2) MeV in ^{12}C which fits very well to the predicted (ground state) rotational band of an oblate equilateral triangular spinning top with a $\mathcal{D}_{3h}$ symmetry characterized by the sequence 0^+, 2^+, 3^-, $4^\pm$, 5^- with almost degenerate 4^+ and 4^- (parity doublet) states. Such a $\mathcal{D}_{3h}$ symmetry was observed in triatomic molecules, and it is observed here for the first time in nuclear physics. We discuss a classification of other rotation-vibration bands in ^{12}C such as the (0^+) Hoyle band and the (1^-) bending mode band and suggest measurements in search of the predicted ("missing") states that may shed new light on clustering in ^{12}C and light nuclei. In particular, the observation (or nonobservation) of the predicted ("missing") states in the Hoyle band will allow us to conclude the geometrical arrangement of the three alpha particles composing the Hoyle state at 7.654 MeV in ^{12}C.

DOI: 10.1103/PhysRevLett.113.012502   PACS numbers: 25.20.-x, 21.10.-k, 21.10.Hw, 21.60.Fw

Geometrical equilateral triangular configurations [1,2] have been identified in the triatomic H_3^+ molecule [3] where the predicted spectrum of a triangular oblate spinning top with a $\mathcal{D}_{3h}$ symmetry was observed [1–3]. It was suggested [1,2] that the three alpha particle system of ^{12}C should lead to similar "triatomic like" structure in nuclei. The application to ^{12}C of the $\mathcal{D}_{3h}$ symmetry, a mathematical tool that was developed to describe molecular structure, emphasizes the role of symmetry across very different energy scales, and it leads to a model of ^{12}C that correctly predicts several new observations that we report for the first time in this Letter. Such a polyatomiclike description of light nuclei should lead to a better understanding of the clustering phenomena in light nuclei.

In this Letter, we demonstrate that this $U(7)$ model [1,2] as applied to ^{12}C predicts all known low spin (cluster) states below 15 MeV, as well as the measured $B(E\lambda)$ and form factors measured in electron scattering [4]. But perhaps more importantly, the model predicts new ("missing") states, the observation (or nonobservation) of which will allow us to resolve a major problem of current concern on the geometrical arrangement of the three alpha particles in the Hoyle state at 7.654 MeV. We demonstrate that the observed rotation-vibration spectrum of ^{12}C in of itself already indicates the geometrical structure of ^{12}C.

We report the observation of a new $J^\pi = 5^-$ state that fits very well the rotational $J(J+1)$ trajectory of the ground state band of ^{12}C as predicted by the $U(7)$ model. In addition, the 4^- state recently observed by some of us at 13.35 MeV in ^{12}C [5,6] confirms the $J^\pi = 4^\pm$ parity doublet predicted by this $U(7)$ model for the ground state band of ^{12}C. The ground state rotational band including the states of $J^\pi = 0^+, 2^+, 3^-, 4^\pm$, and 5^- is a strong signature of a $\mathcal{D}_{3h}$ symmetry, and it is observed here for the first time in a nucleus.

The triatomic $U(7)$ mixed-parity structure observed in ^{12}C resembles the diatomic $U(4)$ mixed parity structure [7] observed in ^{18}O [8] and the tetrahedral symmetry (T_d) mixed parity structure recently observed in ^{16}O [9].

The structure of ^{12}C has recently attracted much theoretical attention due to the availability of *ab initio* no-core shell model calculations [10], the no-core symplectic model [11], and effective field theory calculations on the lattice [12]. These calculations attempt to provide a microscopic description of cluster states that are well described in the traditional clustering model [13] and antisymmetrized molecular dynamics [14], as well as in the more modern fermionic molecular dynamics model [15] and more exotic cluster models [16]. However, thus far, *ab initio* shell model calculations have failed to predict [10] the Hoyle state at 7.654 MeV in ^{12}C that is known to be one of the best examples of alpha clustering in nuclei.

The effective field theory lattice calculations [12] and the fermionic molecular dynamics model [15] predict an equilateral arrangement of the three alpha particles in the ground state of ^{12}C and hence, they provide the microscopic foundation of the conjectured $\mathcal{D}_{3h}$ symmetry of the ground state of ^{12}C. But these models are currently unable to predict the high spin 5^- state reported here or the $4^\pm$ parity doublet that we observe in ^{12}C.

The identification of the rotational excitations of the Hoyle state with 2^+ [17] and 4^+ [18] raises an intriguing question of current concern regarding the geometrical structure of the Hoyle state, whether it is a bent-arm configuration [12] or rather an equilateral triangular configuration just as the ground state. In this Letter, we point out that future measurements of predicted ("missing") rotation-vibration states in ^{12}C will allow us to understand the geometrical arrangement of the three alpha particles in the Hoyle state—a problem which is as old as the discovery of the Hoyle state itself.

The present measurements were performed at the Birmingham MC40 cyclotron facility. A beam of ^{4}He nuclei at an energy of 40 MeV was incident on a 100 μg/cm^2 carbon target. The reaction of interest was ^{12}C(^{4}He, 3α)^{4}He, in which the ^{12}C nuclei were excited above the α-decay threshold through the inelastic scattering process. An array of four, 500 μm thick, silicon strip detectors was used in order to detect three of the four final state α particles. Each detector had a surface of 5×5 cm^2 subdivided into 16 horizontal and 16 vertical strips, front and back, respectively. The detectors were placed at distances 13.0, 11.0, 11.0, 13.0 cm from the target at angles 62.0°, 32.0°, −32.0°, −62.0°, respectively (the signs indicate opposing sides of the beam axis). The array covered an angular range of $\theta_{\text{lab}} = 20°$ to 75°. The detection system was calibrated with a triple α-particle source. These detectors allowed the energy and emission angle of each particle to be determined and hence, the momentum, assuming each to be an α particle.

The 4th undetected α-particle's properties were reconstructed using conservation of energy and momentum. Events in which any two of the three detected α particles resulted from the decay of ^{8}Be$_{gs}$ were selected. In order to reconstruct the origins of the final state particles, a Dalitz plot was created as shown in Fig. 1. Here the excitation energy in ^{12}C was calculated by reconstructing $E_x(^{12}\text{C})$ from the ^{8}Be and either the detected (horizontal axis) or undetected (vertical axis) α particle. The horizontal and vertical loci correspond to ^{12}C excited states and the weak diagonal loci of states in ^{8}Be.

The projection of the Dalitz plot onto the vertical axis is shown in Fig. 2. States at 7.654 (0^+), 9.641 (3^-), 10.844 (1^-), 14.083 MeV (4^+) are observed. In Figs. 1 and 2, it is also possible to observe a peak which would correspond to a state at 22.4(2) MeV which has not been previously reported.

In order to achieve a characterization into the nature of the proposed new state in ^{12}C, we have used the angular correlations technique, a method in which the distribution pattern of the products are analyzed [19]. This method yields a model independent spin determination when the initial and final state particles are all spin zero, and is described in more detail in [18,19]. Using the Dalitz plot in Fig. 1, it is possible to set a window around the specific data of interest (shown by the tilted rectangular box) and then generate the angular correlation plot for the selected events (similar to those in Ref. [18]) for the proposed 22.4 MeV state.

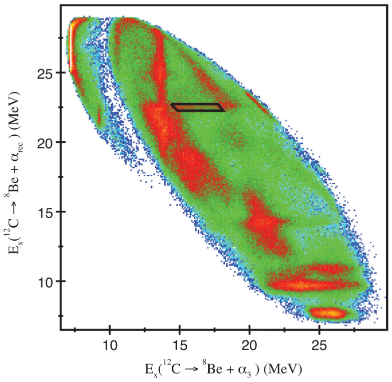

FIG. 1 (color online). Dalitz plot for the ^{12}C(^{4}He, ^{12}C*)^{4}He reaction. Excitation energies of ^{12}C are plotted on the horizontal axis in which three α particles were detected. On the vertical axis, the ^{12}C excitation energies are calculated by the reconstruction of the undetected α particle and the ^{8}Be nuclei. The tilted rectangular box shows the region selected for the angular distribution analysis.

In the ^{12}C(^{4}He, ^{12}C*)^{4}He reaction, there are two center-of-mass frames, the first corresponding to the inelastic excitation, the second to the decay of ^{12}C into ^{8}Be + α. The emission angle of the ^{12}C decay process with respect to the beam axis is described by the angle ψ which is explicitly in the center of mass of the $\alpha + {}^8$Be system, hence, arising from a state in ^{12}C and not in ^{16}O. For a ^{12}C state of spin J,

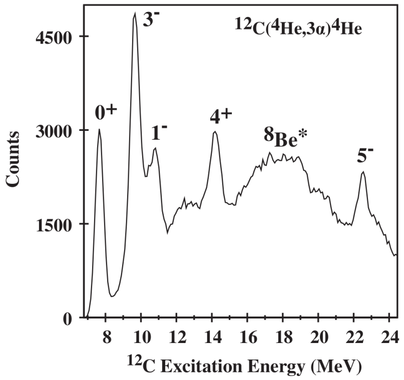

FIG. 2. Projection of the Dalitz plot in Fig. 1 onto the vertical axis. In addition to the known states, a peak is observed at 22.4 (2) MeV. The broad background (between 12 and 20 MeV) is due to "leaking" of excited states of ^{8}Be into the projected region.

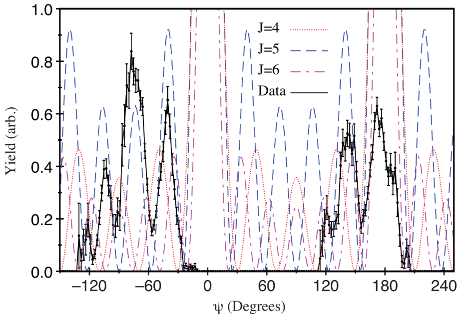

FIG. 3 (color online). The projection onto the ψ axis of the angular correlations for the 22.4 MeV state. The data points are corrected for the acceptance of the detectors and connected with a (continuous black) line to guide the eye. They are compared with the Legendre polynomials $|P_5[\cos(\psi)]|^2$ (dashed blue line) as well as for $\ell = 4$ (dotted red line) and $\ell = 6$ (dotted-dashed red line). Note that due to the unknown m-substate population of the $J^\pi = 5^-$ state, the height of the oscillations cannot be predicted, but the oscillatory phase determines the angular correlation to arise from a $J^\pi = 5^-$ state.

it would be expected that the angular correlation should oscillate with a period given by $|P_J[\cos(\psi)]|^2$. As described in Refs. [18,19], it is possible to infer from the oscillation pattern of the data, the spin of the excited state. The dependence of the yield on the angle ψ is shown in Fig. 3, in which the data are compared with several Legendre polynomials. The measured alpha spectrum and angular correlation clearly point to the existence of a state at 22.4 (2) MeV with $J^\pi = 5^-$.

In Fig. 4, we show the rotational band structure in ^{12}C. The ground state rotational band consisting of the levels 0^+, 2^+, 3^-, $4^\pm$, and the newly measured 5^- state, follow a $J(J+1)$ trajectory. Also, the recently identified rotational excitations with 2^+ [17] and 4^+ [18] of the Hoyle state form a $J(J+1)$ sequence, albeit with a larger moment of inertia. Finally, as we discuss below, the negative parity states 1^- and 2^- shown in Fig. 4 are assigned as members of the bending vibration with almost the same moment of inertia as the Hoyle band.

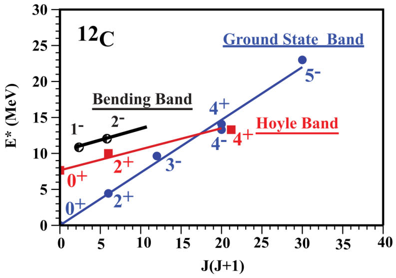

FIG. 4 (color online). Rotational band structure of the ground-state band, the Hoyle band, and the bending vibration in ^{12}C.

We present an analysis of the cluster states in ^{12}C in terms of oblate symmetric top which is a special case of the algebraic cluster model [1,2]. In this approach, the three alpha particles are located at the corners of an equilateral triangle. Their relative motion is described by two perpendicular Jacobi vectors, $\vec{\rho}$ and $\vec{\lambda}$, one vector connecting two points on the triangle and the second one along the half angle perpendicular to it. The corresponding algebraic model describing such a system is based on the $U(6+1) = U(7)$ spectrum-generating algebra [1,2].

Of particular interest is the oblate symmetric top limit which corresponds to the geometric configuration of three α particles located at the vertices of an equilateral triangle. The rotation-vibration wave functions of a triangular configuration can be written as [1,2]

$$|N, (v_1, v_2^{\ell_2}), K, L^P\rangle. \tag{1}$$

Here, N is the total number of bosons. The energy spectrum consists of a series of rotational bands labeled by $(v_1, v_2^{\ell_2})$. Here, v_1 corresponds to the breathing vibration with A symmetry and v_2 to the doubly degenerate bending vibration with E symmetry; ℓ_2 denotes the vibrational angular momentum of the doubly degenerate vibration, L the angular momentum, K its projection on the symmetry axis, and P the parity. Since we do not consider the excitation of the α particles, the wave functions describing the relative motion have to be symmetric, i.e., $|K \mp 2\ell_2| = 3m$ a multiple of 3 [1,2]. This imposes some conditions on the allowed values of the angular momenta and parity. For vibrational bands with $(v_1, 0^0)$, the allowed values of the angular momenta and parity are $L^P = 0^+, 2^+, 4^+, \ldots,$ with $K = 0$ and $L^P = 3^-, 4^-, 5^-, \ldots,$ with $K = 3$. The threefold symmetry excludes states with $K = 1$ and $K = 2$ and leads to the lowest predicted $L^P = 4^\pm$ parity doublet in the $(v_1, 0^0)$ vibrational band. The predicted $L^P = 4^\pm$ parity doublet both in the ground band and the Hoyle band is a strong signature of this model. For the bending vibration with $(0, 1^1)$, the rotational sequence is given by $L^P = 1^-, 2^-, 3^-, 4^-, \ldots,$ with $K = 1$, $L^P = 2^+, 3^+, 4^+, \ldots,$ with $K = 2$ and $L^P = 4^+, \ldots,$ with $K = 4$. The degeneracy of the states with the same value of the angular momentum L but different value of K is split by the κ_2 term in Eq. (2) [2]. Since in the application to the cluster states of ^{12}C, the vibrational and rotational energies are of the same order, we expect sizeable rotation-vibration couplings.

In the $U(7)$ algebraic cluster model, the energy eigenvalues of the oblate top, up to terms quadratic in the rotation-vibration interaction, are given by:

$$\begin{aligned} E = {} & E_0 + \omega_1\left(v_1 + \frac{1}{2}\right)\left(1 - \frac{v_1 + 1/2}{N}\right) \\ & + \omega_2(v_2 + 1)\left(1 - \frac{v_2 + 1}{N + 1/2}\right) \\ & + \kappa_1 L(L+1) + \kappa_2(K \mp 2\ell_2)^2 \\ & + \left[\lambda_1\left(v_1 + \frac{1}{2}\right) + \lambda_2(v_2 + 1)\right]L(L+1). \qquad (2) \end{aligned}$$

This formula includes both the anharmonicities which depend on N and the vibrational dependence of the moments of inertia. In Fig. 5, we show a comparison of the cluster states of ^{12}C with the spectrum of the oblate top according to the approximate energy formula of Eq. (2). The coefficients κ_1, λ_1, and λ_2 are determined by the moments of inertia of the ground state band, the Hoyle band, and the bending vibration. The value of κ_2 term is determined from the relative energies of the positive and negative parity states in the ground state band. The vibrational energies ω_1 and ω_2 are obtained from the excitation energies of the 0^+ Hoyle state and the 1^- state, respectively. Whereas in molecules, the anharmonicities are small and hence N is large, in ^{12}C the situation is completely different. The rotation-vibration couplings and anharmonicities are large and, therefore, N is small. Here, it is taken to be $N = 10$ [1,2]. The large anharmonicities lead to an increase of the rms radius of the vibrational excitations relative to that of the ground state.

In this analysis, the ground state rotational band of ^{12}C is composed of both positive parity states with $J^\pi = 0^+, 2^+, 4^+$ with $K = 0$ and negative parity states with $J^\pi = 3^-, 4^-, 5^-$ with $K = 3$. Since these states belong to a single rotational structure, the electromagnetic transition probabilities from the ground state to the 2^+ and 3^- (and 4^+) states are related. The measured strong electromagnetic transitions $B(E2; 2^+ \to 0^+) = 4.9 \pm 0.3$ W.U. and $B(E3; 3^- \to 0^+) = 12.9 \pm 1.7$ W.U. indicate collectivity. The agreement with the predicted $B(E\lambda)$ values for the 2^+ and 3^- states of the ground state rotational band [2,4] and the agreement of the predicted form factors measured in $^{12}\mathrm{C}(e, e')$ scattering for $2^+, 3^-$, and the 4^+ state [2,4] indicates that the $K = 0$ and $K = 3$ bands which are usually considered as separate bands, coalesce to form a single ground state rotational structure. As we discussed above, the merging of the $K = 0$ and $K = 3$ bands leads to the predicted $J^\pi = 4^\pm$ degenerate parity doublet which is a strong signature of the $\mathcal{D}_{3h}$ symmetry.

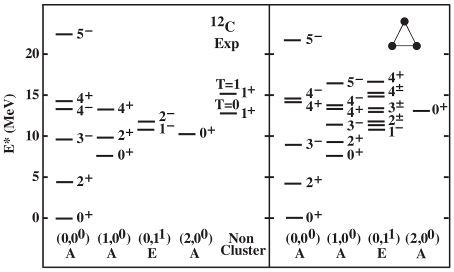

FIG. 5. Comparison between the low-lying experimental spectrum of ^{12}C and the energies of the oblate symmetric top calculated using Eq. (2) with parameters that are discussed in the text. The levels are organized in columns corresponding to the ground state band and the vibrational bands with A and E symmetry of an oblate top with triangular symmetry. The last column on the left-hand side, shows the lowest observed noncluster (1^+) levels.

The 0^+ Hoyle state in ^{12}C at 7.654 MeV is interpreted as the band head of the A symmetric stretching vibration or breathing mode of the triangular configuration with the same geometrical arrangement and rotational structure as for the ground state rotational band, as shown in Fig. 5. The nonharmonicity of the potential discussed above leads to larger rms radii for higher vibrational states; hence, the Hoyle rotational band is predicted to have a moment of inertia larger than the ground state band (by a factor of 2). Recent measurements revealed the existence of the 2^+ [17] and 4^+ [18] members of the Hoyle rotational band which raises the question of the identification of the predicted negative parity states shown in Fig. 5. The 4^- state which is predicted to be nearly degenerate with the 4^+ state, can be measured, for example, in 180° electron scattering off ^{12}C [20]. We note that a (broad) 3^- state was suggested to lie between 11 and 14 MeV [5] which is close to the predicted energy shown in Fig. 5. In order to distinguish between different geometric configurations of the Hoyle band, e.g., equilateral triangular or bent arm, the identification of the negative parity states 3^- and 4^- is crucial which is a strong motivation for a dedicated experimental search [20].

The 1^- state at 10.84 MeV is assigned as the bandhead of the vibrational bending mode whose lowest-lying rotational excitations consist of nearly degenerate parity doublets of $2^\pm$ and $3^\pm$ states. So far, only the 2^- has been identified.

In addition to the cluster states, there are other (noncluster) states in ^{12}C. In particular, with 3α configurations, no 1^+ can be formed. The two 1^+ $(T = 0)$ and 1^+ $(T = 1)$ states at 12.71 MeV and 15.11 MeV, respectively, shown in Fig. 5, are therefore clearly noncluster states and indicate the energy above which the identification of cluster or noncluster low spin states becomes difficult. The cluster states are characterized by large alpha widths ($\Gamma_{\alpha 0}$, the decay to the ground state of ^{8}Be or $\Gamma_{\alpha 1}$, the decay to the first excited 2^+ state of ^{8}Be) with reduced widths that exhaust a large fraction of the Wigner limit.

Of particular interest [21] is the Hoyle state with a geometrical arrangement of the alpha particles that may be deduced from the rotational band built on top of the Hoyle state [17,18,21]. While the observed moment of inertia of the Hoyle band excludes the proposed linear chain structure of the Hoyle state [17], two geometrical alternatives of either equilateral triangular arrangements or obtuse triangular arrangement are considered for the arrangement of the three alpha particles in the Hoyle state of ^{12}C and can be resolved by the future measurements we propose here.

In conclusion, we presented evidence for triangular $\mathcal{D}_{3h}$ symmetry in the arrangement of the three alpha particle in the ground state of ^{12}C. Such a symmetry is now established in molecular physics and nuclear physics. Another interesting application would be to odd-mass nuclei. Finally, the algebraic cluster model predicts several additional states. The predicted broad and overlapping states require accurate data as measured for the second 2^+ Hoyle state [17]. The selectivity of gamma-ray beams [17] as well as electron beams [20] would aid in populating the states of interest and resolve the broad interfering states. These new capabilities should initiate an extensive experimental program for the search of the predicted ("missing") states and promises to shed new light on the clustering phenomena in light nuclei.

The authors wish to acknowledge extensive discussions with Professor Francesco Iachello and thank him for stimulating this Letter. This work is supported in part by the U.S. Department of Energy, Grant No. DE-FG02-94ER40870, and in part by research projects from DGAPA-UNAM and CONACyT, Mexico.

---

[1] R. Bijker and F. Iachello, Phys. Rev. C **61**, 067305 (2000).

[2] R. Bijker and F. Iachello, Ann. Phys. (Amsterdam) **298**, 334 (2002).

[3] R. Bijker, A. E. L. Dieperink, and A. Leviatan, Phys. Rev. A **52**, 2786 (1995).

[4] A. Tumino, R. Bijker, and F. Iachello, in *Clustering Aspects of Nuclear Structure and Nuclear Dynamics*, edited by M. Korojila, Z. Basrak, and R. Caplar (World Scientific, Singapore, 2000), p. 271.

[5] M. Freer *et al.*, Phys. Rev. C **76**, 034320 (2007).

[6] O. S. Kirsebom *et al.*, Phys. Rev. C **81**, 064313 (2010).

[7] F. Iachello, Phys. Rev. C **23**, 2778(R) (1981).

[8] M. Gai, M. Ruscev, A. C. Hayes, J. F. Ennis, R. Keddy, E. C. Schloemer, S. M. Sterbenz, and D. A. Bromley, Phys. Rev. Lett. **50**, 239 (1983).

[9] R. Bijker and F. Iachello, Phys. Rev. Lett. **112**, 152501 (2014).

[10] R. Roth, J. Langhammer, A. Calci, S. Binder, and P. Navratil, Phys. Rev. Lett. **107**, 072501 (2011).

[11] A. C. Dreyfuss, K. D. Launey, T. Dytrych, J. P. Draayer, and C.Bahri, Phys. Lett. B **727**, 511 (2013).

[12] E. Epelbaum, H. Krebs, D. Lee, and U.-G. Meissner, Phys. Rev. Lett. **106**, 192501 (2011); E. Epelbaum, H. Krebs, T. A. Lahde, D. Lee, and U.-G. Meissner, Phys. Rev. Lett. **109**, 252501 (2012).

[13] M. Kamimura, Nucl. Phys. **A351**, 456 (1981).

[14] Y. Kanada-Enyo, Prog. Theor. Phys. **117**, 655 (2007).

[15] M. Chernykh, H. Feldmeier, T. Neff, P. von Neumann-Cosel, and A. Richter, Phys. Rev. Lett. **98**, 032501 (2007).

[16] Y. Funaki, H. Horiuchi, W. von Oertzen, G. Ropke, P. Schuck, A. Tohsaki, and T. Yamada, Phys. Rev. C **80**, 064326 (2009) and references therein.

[17] M. Itoh *et al.*, Nucl. Phys. **A738**, 268 (2004); Phys. Rev. C **84**, 054308 (2011); M. Freer *et al.*, Phys. Rev. C **80**, 041303 (R) (2009); W. R. Zimmerman, N. E. Destefano, M. Freer, M. Gai, and F. D. Smit, Phys. Rev. C **84**, 027304(BR) (2011); W. R. Zimmerman *et al.*, Phys. Rev. Lett. **110**, 152502 (2013).

[18] M. Freer *et al.*, Phys. Rev. C **83**, 034314 (2011).

[19] M. Freer, Nucl. Instrum. Methods Phys. Res., Sect. A **383**, 463 (1996).

[20] P. von Neumann-Cosel, A $^{12}\mathrm{C}(e, e')$ experiment in progress at Darmstadt (private communication).

[21] H. O. U. Fynbo and M. Freer, Physics **4**, 94 (2011).

APPENDIX B

PROCEEDINGS: A NEWLY OBSERVED STATE IN CARBON-12 – CHARACTERISATION AND CONSEQUENSES.

A newly observed state in ^{12}C – characterisation and consequences

D J Marín-Lámbarri[1], M Freer[1], Tz Kokalova[1], C Wheldon[1], D J Parker[1]

[1]School of Physics and Astronomy, University of Birmingham, Birmingham, B15 2TT, UK.

E-mail: `djm179@bham.ac.uk`

Abstract. Measurements of the ^{12}C(^{4}He,^{4}He)^{12}C* reaction at 40 MeV were performed using a charged-particle detector array composed of four double-sided silicon strip detectors. Resonances in ^{12}C were reconstructed with the requirement that the α-decay proceeded first via the ^{8}Be ground state. Of primary significance was the population of the 13.3 and 22.4 MeV resonances, the latter, observed for the first time in this measurement. By using the angular correlation technique the spins of the resonances, have been established as J^{π}=4^{+} and J^{π}=5^{-} respectively.

1. Introduction

Despite all the knowledge acquired over several decades, there are still important details that remain unexplained regarding the nature of the ^{12}C nucleus. Its second excited state at 7.654 MeV (0^{+}) was first proposed 61 years ago by Fred Hoyle in order to explain the abundance of ^{12}C in the universe [1]. Carbon-12 is of great importance for the creation of the elements key to organic life, as well as being the primary step in the synthesis of heavier nuclei in stars. The structure of the Hoyle state is a significant open question. It is known to be composed of three α-particles, but the precise arrangement remains unclear. *Ab initio* calculations suggest the state is configured as a bent-arm [2], in which the three α-particles are located at the vertices of an open triangle. The measurement reported here was motivated by the idea of measuring and characterising the 13.3 MeV excited state in ^{12}C which had previously been observed by members of the Charissa collaboration [3, 4], and which is thought to be a candidate member of the Hoyle-state band. Recent investigations show the existence of a 2^{+} resonance, which could be a collective rotation or vibration of the Hoyle-state [5, 6]. The 13.3 MeV resonance may be one of these collective resonances. Ultimately, by making evermore precise measurements, the data may be sufficiently discriminating to refine current nuclear models. Some results from the present study have been published in [7].

2. Experimental Details

The measurements were performed at the University of Birmingham's MC40 cyclotron with a ^{4}He beam at an energy of 40 MeV incident on a 100 μgcm^{-2} ^{12}C target. The reaction of interest was ^{12}C(^{4}He,^{4}He+^{4}He+^{4}He)^{4}He which corresponds to the inelastic excitation of ^{12}C above the three α-decay threshold at 7.275 MeV. A bespoke charged-particle detector array of four double-sided silicon strip detectors (DSSSDs) was used. Each detector is subdivided by 16 vertical and 16 horizontal strips on the front and back faces respectively giving a 5 × 5 cm^{2} surface with

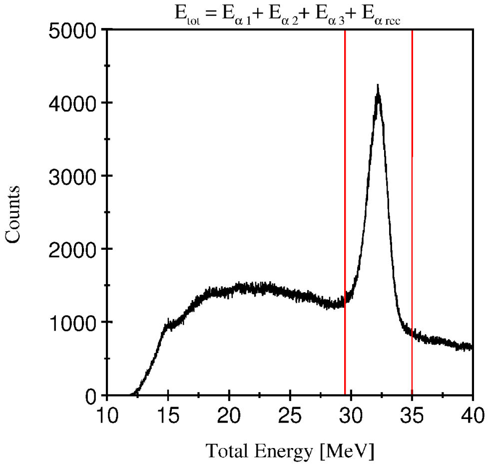

Figure 1. Total energy spectrum. The region between the two red lines was selected, as this corresponds to events proceeding from the ^{12}C(^{4}He,^{4}He+^{4}He+^{4}He)^{4}He reaction (Q=−7.275 MeV).

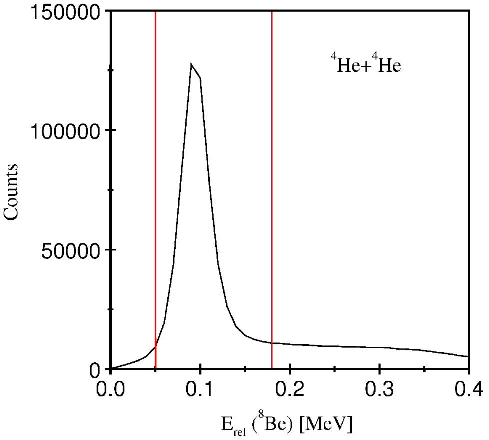

Figure 2. Peak associated with the decay from the ^{8}Be ground state at 92 keV. Data between the two red vertical lines were selected for further analysis.

a thickness of 500 μm. The master trigger was such that at least three of the four final-state particles were recorded via detectors placed at distances 13.0, 11.0, 11.0, 13.0 cm from the target at in-plane angles 62.0°, 32.0°, −32.0°, −62.0°, respectively (positive and negative values indicate opposite sides of the beam axis). The array covered an angular range of θ_{lab} = 20° to 75°. The detectors were calibrated with a triple α-particle source.

3. Analysis and Results

The DSSSDs do not have explicit particle identification so event selection was achieved through the full kinematic reconstruction allowing the energy and scattering angle of each particle to be determined and, therefore, the momentum. By conservation of momentum and energy the fourth, undetected α-particle was reconstructed. Using the information from all the products and the beam energy it was then possible to create the total energy spectrum for the reaction, as shown in figure 1. This allowed events from the reaction of interest to be selected, with Q= −7.275 MeV. A second filter, which gives an additional level of selectivity, required events originating only from the decay of the ^{8}Be nucleus in its ground state, reconstructed from pairs of detected α-particles for events within the peak of figure 1. The centroid of the peak of figure 2, at a relative energy, E_{rel} = 92 keV, clearly identifies the decay of the ^{8}Be ground state.

To visualise the event energy landscape, a Dalitz plot was generated as shown in figure 3. Excitation energies in ^{12}C were calculated for the case in which three α-particles from the decay from ^{12}C were detected (horizontal axis). For the vertical axis the excitation energies were calculated for events in which one of the ^{12}C break-up α-particles was undetected, *i.e.* the reconstructed particle; the scattered beam particle being one of the three hits. It is possible to observe features running parallel to the horizontal and the vertical axes, as well as diagonal ridges (with a gradient equal to -1). The horizontal and vertical features correspond to resonances in ^{12}C and the diagonal lines to states in ^{8}Be (from right to left the ground state is the first diagonal

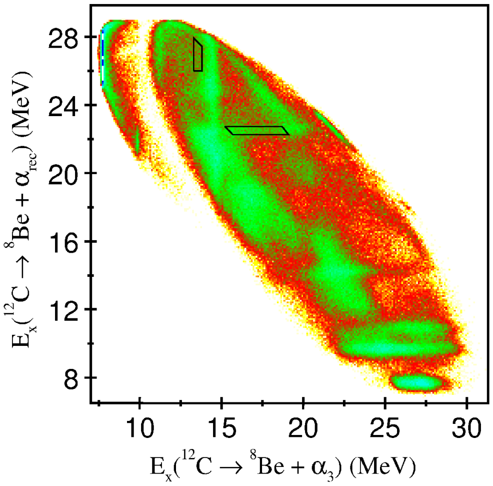

Figure 3. Dalitz plot of the $^{12}C(^4He,^4He)^{12}C^*$ reaction measured at a beam energy of 40 MeV. The solid boxes shows the region selected for the angular correlation analysis.

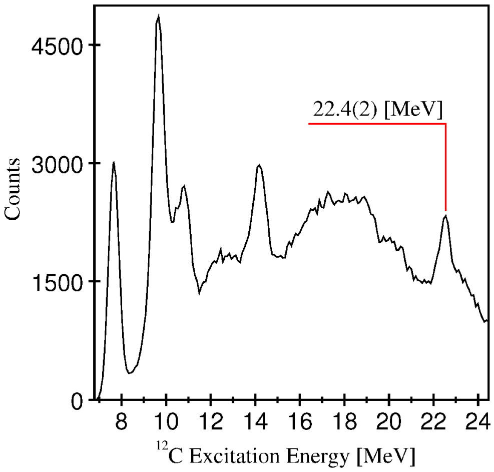

Figure 4. Projection onto the vertical axis of the Dalitz plot of figure 3. Different known resonances are shown as well as the newly observed state at a 22.4(2) MeV.

line). The projection of the Dalitz plot is shown in figure 4, in which excited states at 7.654 (0^+), 9.641 (3^-), 10.844 (1^-), 14.083 (4^+) MeV are observed. Additionally, the presence of a resonance at 22.4(2) MeV is observed for the first time.

3.1. Angular Correlations

With the aim of gaining an insight into the nature of the newly observed state in ^{12}C the distribution pattern of the final products (α-particles) in the decay has been analysed. This analysis method is formally known as angular correlations and is model independent when the initial and final particles all have spin zero, as here. A more detailed explanation of this method can be found in [8]. For this correlation analysis it is necessary to define the centre-of-mass emission angle θ^* of the ^{12}C nucleus with respect to the beam axis, and the emission angle Ψ of the first α-particle from the decay of the resonance in ^{12}C, also with respect with the beam axis, and within the ^{12}C centre-of-mass frame. Using the Dalitz plot of figure 3 it was possible to select a specific excitation energy to be examined. The event selection windows are shown by the solid rectangular boxes in figure 3, for the 13.3 and 22.4 MeV states, determining both the excitation energy and the origin of the particles detected, and therefore, enabling the angular correlation plots for the selected data to be produced. This procedure was first applied to well known resonances, 7.654 (0^+), 9.641 (3^-), 10.844 (1^-) and 14.083 (4^+) MeV, with the aim of demonstrating the effectiveness of the procedure. Subsequently, this method was applied to the 13.3 MeV and the newly observed 22.4 MeV states. The angular correlation plots for the 13.3 MeV and the newly observed resonance are shown in figure 5, demonstrating the key features in which the structure in the θ^*-Ψ plane are dependent on

$$W(\theta^*, \Psi) \propto | \, P_J[\cos(\Psi + \Delta\Psi)] \, |^2, \tag{1}$$

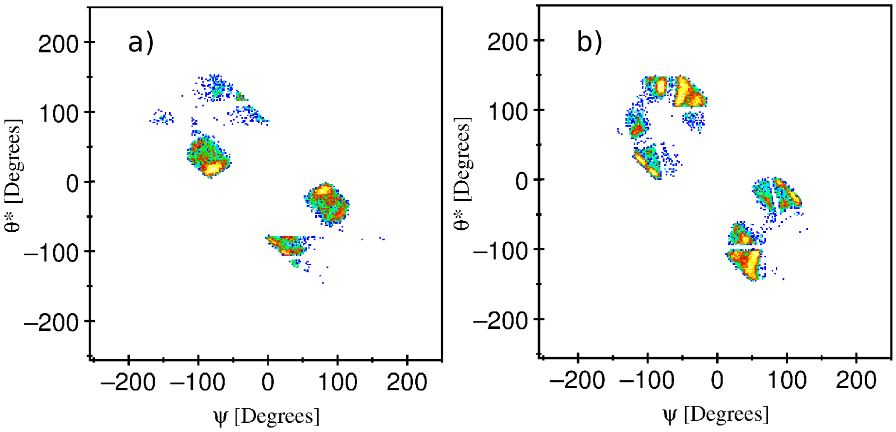

Figure 5. Angular correlation plot a) for the 13.3 MeV resonance and b) for the 22.4 MeV resonance in ^{12}C. The gradient of the angular correlation features increases as the spin increases.

to first order. A small change in Ψ, $\Delta\Psi$, is related to a small change in θ^*, $\Delta\theta^*$, through

$$\frac{\Delta\theta^*}{\Delta\Psi} = \frac{J}{l_{gr} - J}, \tag{2}$$

where l_{gr} is the grazing angular momentum J is the spin of the state and P_J are the Legendre polynomial of order J. Within the θ^*-Ψ plane, the formation of sloped features will appear with a specific gradient $\Delta\theta^*/\Delta\Psi$, given by equation 2 for which the periodicity reveals the spin of the resonance under analysis [8]. For the case of a spin-zero state the gradient will be zero, increasing as the spin increases, as shown in figure 5. In order to analyse the periodicity, the angular correlation plot is projected onto the Ψ axis at a specific angle $\Delta\theta^*/\Delta\Psi$, determined by the spin of the state. For the present reaction, the grazing angular momentum was estimated to be 9.8 $\hbar$ using r_0=1.2 fm, for which the optimum angles for the projection of the data for the 9.641 (3^-), 10.844 (1^-) and 14.083 (4^+) were found to be $\Delta\theta^*/\Delta\Psi$= 6.5°, 25.3° and 39.7° respectively. The known states all exhibit the correct periodicity for the published spin value. From figure 6 it is possible to observe that the 13.3 MeV data appear to best match the periodicity of the Legendre polynomial J=4 and for the case of figure 7 (22.4 MeV) the periodicity corresponds to order J=5. The associated angles are $\Delta\theta^*/\Delta\Psi$= 39.7° and 60.0° for 13.3 MeV and 22.4 MeV respectively. Recent measurements using ^{3}He projectiles observed a peak at 22.2(3) MeV, confirming this state [9].

4. Conclusions

The 13.3 MeV state must have natural parity as the decay involves only spin-zero nuclei, yielding a spin and parity of J^π= 4^+. Similarly for the 22.4 MeV level, the spin and parity are found to be J^π=5^-. The observation of a 5^- resonance at 22.4 MeV is strong evidence for triangular $\mathcal{D}_{3h}$ symmetry [10], based on the pattern of excited states 0^+, 2^+, 3^-, $4^\pm$ and 5^-, predicted by the algebraic cluster model [10], for an equilateral triangle structure. As a result, this symmetry is now established in nuclear physics [7]. The model also predicts additional states such as the 4^- state, degenerate with the 4^+ level; a strong signature of $\mathcal{D}_{3h}$ symmetry [3, 10]. The significance of this result is that the algebraic model also predicts the structure of the Hoyle

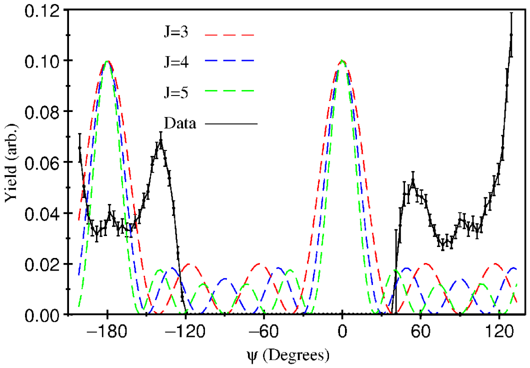

Figure 6. Projection of the angular correlation data for the 13.3 MeV resonance onto the Ψ axis at an angle of 39.7° (black line). The Legendre polynomials of order J=3, 4 and 5 are plotted for comparison (red, blue and green respectively).

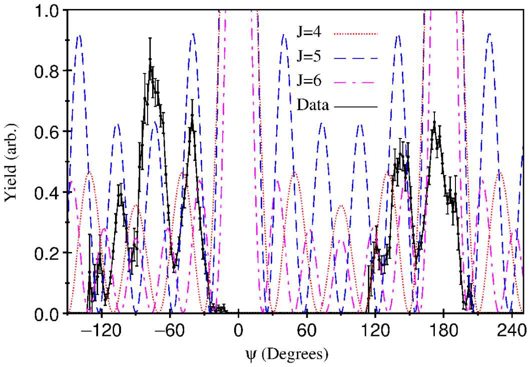

Figure 7. Projection of the angular correlation data for the 22.4 MeV resonance onto the Ψ axis at an angle of 60.0° (black line). The Legendre polynomials of order J=4, 5 and 6 are plotted for comparison (red, blue and magenta respectively), generated from [7].

state to correspond to an expanded equilateral triangle, the excitations of which are calculated to be 0^+, 2^+, 3^-, $4^{\pm}$, 5^-. The expanded structure means that the energy range is more compact, placing the calculated 5^- Hoyle resonance at around 17 MeV. Such concrete predictions offer a tangible challenge for future experiments.

5. Summary

A measurement of the ^{12}C(^{4}He,^{4}He)^{12}C* reaction establishes evidence for a newly observed resonance at 22.4(2) MeV for which an angular correlation analysis was performed. The spin and parity of the state was found to be J^π=5^- confirming the observation of a triangular oblate spinning top with $\mathcal{D}_{3h}$ symmetry for the first time in nuclear physics. The spin and parity of the 13.3 MeV Hoyle-band candidate has been measured unambiguously as $J^\pi = 4^+$.

This work is supported in part by the University of Birmingham and in part from CONACyT, Mexico.

References

[1] Hoyle F 1954 *Astro. Phys. J. (Suppl.)* **1**
[2] Epelbaum E *et al.* 2011 *Phys. Rev. Lett.* **106**
[3] Freer M *et al.* 2011 *Phys. Rev. C* **83**
[4] Kirsebom O *et al.* 2010 *Phys. Rev. C* **81**
[5] Freer M *et al.* 2009 *Phys. Rev. C* **80**
[6] Hyldegaard S *et al.* 2010 *Phys. Rev. C* **81**
[7] Marín-Lámbarri D J *et al.* 2014 *Phys. Rev. Lett.* **113**
[8] Freer M 1996 *Nucl. Instr. and Meth. A* **383** 463–472
[9] Wheldon C *et al.* 2014 *Phys. Rev. C* **90**
[10] Bijker R *et al.* 2000 *Phys. Rev. C* **61**

BIBLIOGRAPHY

[1] K. Ikeda, N. Tagikawa, and H. Horiuchi *Prog. Theor. Phys. Suppl.*, vol. **464**, (1968).

[2] “MIT open course ware: http://ocw.mit.edu,” (accessed 19/06/14).

[3] K. Krane, *Introductory Nuclear Physics.* Wiley & Sons, (1988).

[4] P. Navrátil, J. Vary, and B. Barrett *Phys. Rev. Lett.*, vol. **84**, no. 25, (2000).

[5] M. Freer *et al. Journal Physics G*, vol. **23**, (1997).

[6] D. Brink and J. Castro *Nuc. Phys. A*, vol. **91**, (1967).

[7] Y. K. En’yo and H. Horiuchi *Progr. Theoret. Phys.*, vol. **142**, no. 205, (2001).

[8] M. Chernykh, H. Feldmeier, T. Neff, P. von Neumann-Cosel, and A. Richter *Phys. Rev. Lett.*, vol. **98**, no. 032501, (2007).

[9] “Nuclear Physics Birmingham: http://www.np.ph.bham.ac.uk/pic/cyclotron,” (accessed 27/01/14).

[10] MICRONSEMICONDUCTOR, “: http://www.micronsemiconductor.co.uk/pdf/w1.pdf,” (15/02/14).

[11] C. Wheldon, “http://www.wheldon.talktalk.net/,” (accessed 20/07/14).

[12] D. Marín-Lámbarri, R. Bijker, M. Freer, M. Gai, D. Parker, T. Kokalova, and C. Wheldon *Phys. Rev. Lett.*, vol. **113**, no. 012502, (2014).

[13] J. Lilley, *Nuclear Physics, Principles and Applications.* Wiley & Sons, 2nd ed., (2004).

[14] E. Öpic *Proc. R. Ir. Acad. A*, vol. **54**, no. 49, (1951).

[15] F. H. and *Astrophysics J (Suppl.)*, vol. **1**, no. 12, (1954).

[16] D. Dunbar, R. Pixley, W. Wenzel, and W. Whaling *Phys. Rev.*, vol. **92**, no. 649, (1953).

[17] W. Fowler *Reviews of Modern Physics*, vol. **56**, no. 2, (1984).

[18] M. Freer and H. Fynbo *Prog. Part. Nuc. Phys.*, vol. **78**, pp. 1–23, (2014).

[19] O. Kirsebom, M. Alcorta, M. Borge, M. Cubero, C. Diget, L. Fraile, B. Fulton, H. Fynbo, D. Galavitz, B. Jonson, M. Madurga, T. Nilsson, G. Nyman, K. Riisager, and M. Turrión *Phys. Rev. Lett.*, vol. **108**, no. 202501, (2012).

[20] M. Itoh, S. Ando, T. Aoki, H. Arikawa, S. Ezure, K. Harada, T. Hayamizu, T. Inoue, T. Ishikawa, K. Kato, H. Kawamura, Y. Sakemi, and A. Uchiyama *Phys. Rev. Lett.*, vol. **113**, no. 102501, (2014).

[21] E. Epelbaum, H. Krebs, D. Lee, and U. Meißner *Phys. Rev. Lett.*, vol. **106**, no. 192501, (2011).

[22] E. Epelbaum *et al. Phys. Rev. Lett.*, vol. **109**, no. 252501, (2012).

[23] A. Toshaki, H. Horiuchi, P. Schuck, and G. Röpke *Phys. Rev. Lett.*, vol. **87**, no. 192501, (2001).

[24] Y. Funaki, H. Horiuchi, W. von Oertzen, G. Roepke, P. Schuck, A. Toshaki, and T. Yamada *Phys. Rev. C*, vol. **80**, no. 064326, (2009).

[25] M. Freer, S. Almaraz-Calderon, A. Aprahamian, N. Ashwood, M. Barr, B. Bucher, P. Copp, M. Couder, N. Curtis, X. Fang, F. Jung, S. Lesher, W. Lu, J. Malcom, A. Roberts, W. Tan, C. Wheldon, and V. Ziman *Phys. Rev. C*, vol. **83**, no. 034314, (2011).

[26] O. Kirsebom, M. Alcorta, M. Borge, M. Cubero, C. Diget, R. Dominguez-Reyes, L. Fraile, B. Fulton, H. Fynbo, S. Hyldegaard, M. Madurga, A. M. Martin, T. Nilsson, G. Nyman, A. Perea, K. Riisager, and O. Tengblad *Phys. Rev. C*, vol. **81**, no. 064313, (2010).

[27] S. Hyldegaard *et al. Phys. Rev. C*, vol. **81**, no. 024303, (2010).

[28] M. Freer, H. Fujita, Z. Buthelezi, J. Carter, R. Fearick, S. Förtsch, R. Neveling, S. Perez, P. Papka, F. Smit, J. Swartz, and I. Usman *Phys. Rev. C*, vol. **80**, no. 041303, (2009).

[29] L. Hafstad and E. Teller *Phys. Rev.*, vol. **54**, p. 681, (1938).

[30] H. Morinaga *et al. Phys. Rev.*, vol. **101**, no. 1, pp. 254–258, (1961).

[31] M. Mayer *Phys. Rev.*, vol. **78**, no. 1, (1950).

[32] O. Haxel, J. Jensen, and H. Suess *Phys. Rev.*, vol. **75**, no. 1766, (1949).

[33] R. Machleidt, F. Sammarruca, and Y. Song *Phys. Rev. C*, vol. **53**, no. 1483, (1996).

[34] B. Pudliner *et al. Phys. Rev. C*, vol. **56**, no. 1720, (1998).

[35] S. Karataglidis *et al. Phys. Rev. C*, vol. **52**, no. 861, (1995).

[36] M. Freer, R. Betts, and A. Wuosmaa *Nuc. Phys. A*, vol. **587**, pp. 36–54, (1995).

[37] H. Margenau *Phys. Rev.*, vol. **59**, (1941).

[38] Y. K. En'yo *Progr. Theoret. Phys.*, vol. **117**, no. 655, (2007).

[39] R. Roth, T. Neff, H. Hergert, and H. Feldmeier *Nuc. Phys. A*, vol. **745**, no. 3, (2004).

[40] R. Bijker, F. Iachello, and A. Leviatan *Annals of Physics*, vol. **236**, pp. 69–116, (1994).

[41] R. Bijker, A. Dieperink, and A. Leviatan *Phys. Rev. A*, vol. **52**, no. 2786, (1995).

[42] R. Bijker and F. Iachello *Phys. Rev. C*, vol. **61**, no. 067305, (2000).

[43] G. F. Knoll, *Radiation Detection and Measurement.* Wiley & Sons, 2nd ed., (1989).

[44] M. Freer *Nuclear Instruments and Methods A*, vol. **383**, pp. 463–472, (1996).

[45] T. Muñoz-Britton. PhD thesis, Birmingham, (2011).

[46] E. D. Silviera *Proc. 14th Winter Meeting on Nuclear Physics (Borneo)*, (1976).

[47] N. Curtis. PhD thesis, Birmingham, (1991).

[48] "MIDAS: http://npg.dl.ac.uk/midas/," (accessed 23/07/14).

[49] S. Singer, "Daresbury NPG: http://npg.dl.ac.uk/midas/manual/sunsort/," (accessed 13/03/14).

[50] N. Curtis, N. Clarke, B. Fulton, S. Hall, M. Leddy, A. Murphy, J. Pople, R. Ward, W. Catford, G. Gyapong, S. Singer, S. Chappell, S. Fox, C. Jones, D. Watson, W. Rae, and P. Simmons *Phys. Rev. C*, vol. **51**, no. 1554, (1995).

[51] N. Curtis, A. Murphy, N. Clarke, M. Freer, B. Fulton, S. Hall, M. Leddy, J. Pople, G. Tungate, R. Ward, W. Catford, G. Gyapong, S. Singer, S. Chappell, S. Fox, C. Jones, D. Watson, W. Rae, P. Simmons, and P. Regan *Phys. Rev. C*, vol. **53**, no. 1804, (1996).

[52] N. Curtis, "University of birmingham, unpublished.".

[53] "TUNL: http://www.tunl.duke.edu/," (accessed 4/04/14).

[54] M. Freer, I. Boztosun, C. Bremner, S. Chappell, R. Cowin, G. Dillon, B. Fulton, B. Greenhalgh, T. Munoz-Britton, M. Nicoli, W. Rae, S. Singer, N. Sparks, D. Watson, and D. Weisser *Phys. Rev. C*, vol. **76**, no. 034320, (2007).

[55] R. Bijker *Annals of Physics*, vol. **298**, no. 334, (2002).

[56] D. Eck, “http://math.hws.edu/eck/,” (accessed 02/11/14).

[57] R. Bijker and F. Iachello *Phys. Rev. Lett.*, vol. **112**, no. 152501, (2014).

[58] C. Wheldon, T. Kokalova, M. Freer, A. Glenn, D. Parker, T. Roberts, and I. Walmsley *Phys. Rev. C*, vol. **90**, no. 014319, (2014).

[59] T. Kokalova, M. Freer, Z. Buthelezi, J. Carter, R. Fearick, S. Förtsch, H. Fujita, R. Neveling, P. Papka, F. Smit, J. Swartz, and I. Usman *Phys. Rev. C*, vol. **87**, no. 057307, (2013).

[60] V. Datar *et al. Phys. Rev. Lett.*, vol. **111**, no. 062502, (2013).

[61] J. Templon, B. Raue, K. Murphy, D. Millener, D. Carman, G. Huber, B. Markham, D. Miller, P. Schwandt, and L. Bland *Phys. Lett. B*, vol. **413**, no. 253, (1997).